ACTIVE VIBRATION CONTROL AND STRUCTURAL ACOUSTIC CONTROL FOR SIMPLE AND COMPLEX STRUCTURES

By

Serkan Külah

A Thesis Submitted to the
Graduate School of Engineering
in Partial Fulfillment of the Requirements for
the Degree of

Master of Science
in
Mechanical Engineering

Koc University

June 2012
Koc University
Graduate School of Sciences and Engineering

This is to certify that I have examined this copy of a master's thesis by

Serkan Külah

and have found that it is complete and satisfactory in all respects,
and that any and all revisions required by the final
examining committee have been made.

Committee Members:

_____

İpek Başdoğan, Ph. D. (Advisor)

_____

Çağatay Başdoğan, Ph. D.

_____

Polat Şendur, Ph. D.

Date: _____

ABSTRACT

ACTIVE VIBRATION CONTROL AND STRUCTURAL ACOUSTIC CONTROL FOR SIMPLE AND COMPLEX STRUCTURES

In this thesis, a novel methodology is developed for active vibration control and structural acoustic control of simple and complex structures. In the first section, optimal positioning of collocated sensor/actuator pairs for vibration control of plate-like structures are investigated and performance of an active vibration controller is studied numerically and experimentally. In the second part of the thesis, a new design methodology for local and global vibration control system is developed for a 3D shell structure with complex geometry and complex boundary conditions. The objective of the local vibration control is to reduce vibration energy at the sensor location whereas the objective of the global vibration control is to reduce vibration over the entire structure. In order to achieve, effective vibration suppression of the structure, local and global performance indices are defined and used for the optimization of sensor/actuator pair position as well as the controller parameters. The methodology is applied to suppress vibrations on the front panel of a vehicle as a case study. A finite element model of the vehicle is built and used for the frequency response analysis in the presence of engine disturbances. Then, local and global optimization studies are carried out for positioning the sensor/actuator pair and parameter tuning of the controller. By comparing controller active and inactive cases, the vibration suppression performance of the controller is demonstrated locally and globally.

In the final part of the thesis, a novel methodology is presented for design of an active structural acoustic control (ASAC) system on a complex 3D shell structure with complex geometry and complex boundary conditions. The actuator/sensor position and

control parameters are optimized based on acoustic performance indices. As a case study, a vibro-acoustic model of a vehicle is used to present the developed methodology. It is shown that on a complex 3D surface, a well-positioned collocated sensor and actuator pair with optimized design parameters can suppress the vibration spatially on a complex shaped panel and therefore it can reduce the sound pressure level inside the passenger cabin. It is shown that the proposed methodology can be successfully applied for the structures that have complex shape and boundary conditions for noise suppression

Keywords : Active vibration control, Active Structural Acoustic control, Vibro-acoustics, Electro-mechanics, Piezoelectric patches, Velocity feedback control, Finite element modeling, Optimization

ÖZET

BASİT VE KARMAŞIK YAPILAR İÇİN AKTİF TİTREŞİM KONTROLÜ VE AKTİF YAPISAL AKUSTİK KONTROL

Bu tezde, aktif titreşim kontrolü ve basit ve kompleks yapıların yapısal akustik kontrolü için yeni bir metodoloji geliştirilmiştir. Tezin ilk bölümünde, plaka benzeri yapılar üstünde sensör/actuator çiftlerinin, titreşim kontrolü için en optimal şekilde konumlandırılması üstüne çalışılmış ve aktif titreşim control performansı deneysel ve sayısal olarak incelenmiştir. Tezin ikinci bölümünde, yerel ve global titreşim kontrolü için yeni bir tasarım metodolojisi karmaşık geometrili ve karmaşık sınır koşullarına sahip üç boyutlu geometriye sahip bir yapı için geliştirilmiştir. . Yapının üzernde etkili bir titreşim sönümleme elde etmek için, yerel ve global performans kriterleri tanımlanmış ve sensör / aktüatör çifti pozisyonu ve kontrol parametreleri bir algorithma yaratılarak performans kriterleri çerçevesinde bulunmuştur. Örnek bir çalışma olarak, geliştirilen metodoloji motor montaj uzantılarının bağlandığı bir aracın ön panelindeki yapısal titreşimleri bastırmak için kullanılmıştır. Araç modeli, gerçek-boyutlu bir aracın sonlu eleman modeli kullanılarak oluşturulmuş ve yapısal frekans yanıtı analizleri, motor kaynaklı titreşimler varlığında elde edilmiştir. Elde edilen yapısal frekans cevapları sensör / aktüatör çiftinin yerleşiminin, yapının yerel ve küresel titreşimin sönümlemesi için optimizasyon çalışmalarında kullanılmış ve denetleyici parametrelerin optimal değerleri elde edilmiştir.Kontrolörcünün aktif ve inaktif durumlarında yapının frekans cevapları karşılaştırarak kontrolcünün titreşim sönümleme performansı yerel ve küresel durumlar için olarak gösterilmiştir.

Bu tezin son bölümünde, karmaşık geometrisi ve karmaşık sınır koşulları bulunan üç boyutlu geometriye sahip bir yapı üstünde akti yapısal akustik kontrolcü sistem tasarımı için yeni bir yöntem sunulmuştur. Aktüatör / sensör'ün yapı üstündeki konumu ve

kontrolcü parametreleri, kapalı bir akustik boşluk içerisindeki, gürültü bastırma performansını göz önünde tutan bir performans endeksi kullanılarak optimize edilmiştir. Aktivatör ve sensör konumu ile denetleyici parametre optimizasyonu seçilen frekans bantları içindeki gürültü azaltma seviyeleri göz önünde tutularak bulunmuştur. Örnek bir çalışma olarak, geliştirilmiş methodoloji, gerçek boyutlu bir aracın vibro-akustik simulasyon modeli üstünde gösterilmiştir.Analizler sonucunda karmaşık üç boyutlu yüzey üzerinde, optimize edilmiş kontrolcü parametreleri ve iyi bir konuma yerleştirilmiş sensör ve aktüatör çifti ile Panel üstündeki mekansal titreşimler sönümlenmiş,bu sayede kabin içine yayılan gürültü azaltılmış ve araç içindeki ses basıncı düzeylerinin azaltabildiği gösterilmiştir. Analizler ve simulasyonlar sonucunda, önerilen yöntemin karmaşık şekil ve sınır koşullarına sahip bir yapı üstünde aktif yapısal gürültü kontrolü tasarımı için uygulanabilir olduğu gösterilmiştir

Anahtar Kelimler : Aktif titreşim sönümlemesi, Aktif yapısal akustik kontrolcü, titreşim ve akustik , Elektro-mekanik, Piezoelektrik yama, Geri besleme titreşim kontrolü, Sonlu eleman modelleme, Optimizasyon

ACKNOWLEDGEMENTS

I would like to express my gratitude to my supervisor Assoc. Prof. İpek Başdoğan for her guidance and encouragements throughout this work. Her professional view and proficiency always guided me during my research studies and I want to thank her for revealing me as a researcher. I also thank thesis committee members Assoc. Prof Çağatay Başdoğan and Polat Şendur for their valuable support and critical reading of my work.

I would like to thank Ugur Arıdoğan for his companionship and guidance. He guided and supported me during my studies and without his brilliant ideas and kind assistance, the achievements of this work would not have been possible.

My gratitude also goes to my colleagues Utku Boz and Hakan Uçar for their contributions to my research with their invaluable knowledge, moral support and friendship. Without their support, it would not be possible to overcome the difficulties that I encountered during my research studies.

I thank my dearest, Ayten Bilgin for being the meaning of life, for her support and above all for her desire to be in my life from now on.

I thank, Arda Aytekin, Mehmet Ayyıldız, Denizhan Edeer, Gökalp Gürsel, Buket Baylan, Bige Deniz, Bircan Buğdaycı for their companionship and support as entrusted friends and making off-work time funny and entertaining.

Without, Berkay Yarpuzlu, Reşit Haboğlu, Barış Çağlar, Talha Akyol, Emre Ayaroğlu, Emre Ölçeroğlu, Hasan Sinan Bank and Fatma Virdil my spare times in Koç university would not be enjoyable and motivating.

I am most grateful to my mother Ülkiye and my father Samin. Without their wisdom, love and unconditional support to my decisions I would not have become the person who I am today.

TABLE OF CONTENTS

LIST OF FIGURES

LIST OF TABLES

Chapter 1

INTRODUCTION

Shell structures are commonly used in automotive, aerospace and marine applications and vibrations occurring on these structures can cause malfunction of the whole system or failure of certain components. Today, trend in engineering, is to create lighter and stronger ground, air and naval vehicles. With this approach, for instance, in aerospace applications, fuel consumption levels are decreased and flight performances are improved. However, frequent use of lightweight structures caused vibration problems become more and more severe, due increase in vibration amplitudes and vibration decay times. To cope with vibration problems, several methodologies are being developed in the past few decades. Passive treatments are one of these methods, in which, absorptive materials are utilized to damp unwanted vibrations. Passive treatments are frequently used in industry and in commercial products. However, passive treatments are not very effective for low frequency vibrations and for systems with varying dynamics during operation. Also, in applications, where weight is important, passive treatments are not suitable, because of additional mass due absorptive materials. In these cases, active methods are desirable especially for ground and air vehicles, where total weight is a primary concern. Therefore, in this thesis, new design methodologies for local and global active vibration control and active structural acoustic control are developed for 3D shell structures. The methodology is developed on a simple plate-like structure, and then it is improved to make the methodology applicable on complex 3D structures with complex boundary conditions.

In ground, air and naval vehicles, engine induced and environmentally induced vibrations (due road, aerodynamics, fluid structure interactions etc.) are the main results that reduce travel comfort, safety and performance. Therefore, many researchers are

focused to develop solutions to reduce structural vibrations occurring on vehicle bodies. For instance, Kozek et al. [1] tried to overcome road induced structural vibrations occurring on railway cars. In this study, an active system is designed to reduce unwanted low frequency vibrations occurring on railway car in order to increase riding comfort. In another study, Bohn et al.[2] focused on engine induced vibrations and developed a solution to reduce transmitted vibration from engine to vehicle body. In vehicles, engine induced vibrations are transmitted by vehicle structure and excite flexible, lightweight parts of vehicle body and therefore generate noise due coupling of acoustic medium and structure. As a result, several researchers studied active controllers for suppression of noise. For instance, Song et al. [3] and Oliveira et al. [4] developed active vibration controllers to reduce noise using mechanical and piezoelectric actuators for vibration suppression of thin flexible structures. In another study by Gonzales et al. [5], active sound sources are used to modify sound field of a vehicle compartment to reduce the cabin noise.

In conclusion, structural vibrations occurring on ground, air and naval vehicles is an important topic, resulting in comfort, maintenance and operational problems and suppression of unwanted mechanical vibrations is a major and hot research topic in the field of engineering. To gain more knowledge and necessary information about active vibration control, active acoustic control and optimization topics next section is devoted to literature review. In the following literature review section, actuator/sensor location optimization, active vibration control and active structural acoustic control topics are reviewed briefly.

1.1. Literature Review

1.1.1. Optimization of the Actuator/Sensor Locations in Active Control Design

The undesired mechanical vibrations and noise can be avoided or minimized by active vibration and noise control systems. The design of such systems starts with the dynamic characterization of target structure that is called host structure for embedding or bonding the actuators. The dynamic characterization procedure can be carried out numerically and/or experimentally by investigating the vibration characteristics of the host structure. By utilizing sensors and actuators, system identification methods can be applied for modeling the whole system.

The next step in the active control design is the optimization of the sensor/actuator locations. Improper placement of an actuator and sensor may result a low controllability and/or may lead to an uncontrollable system [6]. Moreover, consider the design of a broadband MIMO controller where multiple modes are controlled. In that case, in addition to the actuator and sensor positions, number of actuators that should be used will become an optimization criterion. With careful planning, performance of the controller can be increased and even a stable system can be obtained with multiple sensors and actuators [7].

Many studies in the literature are related to the optimization problem of sensor/actuator locations on the host structure. Hamdan and Nayfeht [8] determined measures of modal controllability and observability for the first time in the literature. In their paper, for first and second order systems they proposed measures for modal optimization criteria which is utilized to determine suitable locations for actuator on host structure. Bin et al.[9] presented an optimization procedure, based on modal control theory. In this study, it is shown that, for a piezoelectric actuator, the optimum position is the location where the

highest strains occurring in x and y directions, parallel to plate surface. To obtain this result, the modal space representation of the system equations is used and finite element model of a cantilever beam is utilized. According to this study, for each mode of interest, the optimum position for actuator is found as the high strain region of each mode when modal control theory is considered.

Jingjun et al. [10] used the modal controllability concept with the truncation criterion of modal cost to obtain optimal location for piezoelectric actuators. Modal cost is defined as the contribution of each mode of the host structure to the response subjected to a particular input. In their study, the modal cost is based on unit impulse disturbance only. Modal cost is depended on the disturbance location. As a result, during optimization procedure disturbance location is taken into account. Truncation of modal cost is the determination of each modes contribution to the total cost. It is a weighting process for the modes that contribute to the system response. Positions of the actuators are determined by modal controllability concept, taking truncated modal costs into account. Also they cited that, for a collocated system, modal controllability is equal to the modal observability at any location on the structure. In their paper, they used finite element formulations with ANSYS FE package and conducted simulations for a simply supported beam equipped with piezoelectric actuators.

Quek et al. [11] used a pattern search method to find optimal locations on a plate for actuator/sensor pairs taking modal and system controllability as performance criteria. To increase solution performance and faster convergence, they implemented a start point algorithm, which is based on maximizing virtual work done by finding the maximum strain region on the host structure and taking this location as the initial location for search algorithm. They used finite element methodology to implement their algorithm and showed performance of their work by conducting numerical experiments on a clamped-clamped and cantilever plate.

Halim and Moheimani [12] also used modal controllability and observability as their performance indices for their work. In order to reduce control spillover effects, they used spatial controllability. They used H_2 norm of transfer functions to obtain characteristics of responses only specific to a location. By this way, they eliminate information from transfer functions about other parts of the host structure. In their study, they defined modal controllability as the measure of authority of actuator on a certain mode and spatial controllability as the measure of authority on the entire structure. They combined these two criteria as performance measures for their optimization procedure and tried to maximize spatial controllability over multiple modes, while maintaining modal controllability on every single mode. They performed the optimization procedure on a plate and they used finite element techniques and conducted experiments.

Yaowen and Lei [13] used an analytical solutions to conduct optimization studies by using maximum host structure displacement as their optimization criteria. They obtained an analytical solution for steady-state plate deflections depending on actuator location and time. By using the solution for different vibration frequencies of the host structure, they optimized the actuator locations. Optimal locations are obtained as the regions, where high displacement values for the host structure are obtained. In their work, they showed that if driving frequencies for PZT actuators is close to the first natural frequencies of the host structure, distinct regions for actuator placement can be obtained, but for frequencies lower that first natural frequency, all actuator orientations on the plate results in almost same amount of maximum plate deflection. Also, they determined optimum location patterns for a PZT actuator for the case of driving frequencies not close to natural frequency of the host structure. They showed that, optimal locations can be determined for actuator, independent of the driving frequency of the actuator by using combined position mode function (CPMF). Also, they showed that actuator geometry has an effect on suppressing certain vibration modes.

In another study, Demetriou [14] used optimal control law for the optimization procedure. In this work, he tried to minimize optimal value of performance index rather than just taking observability and controllability into account. During calculations of optimal value of the cost function, actuator position is also used as a variable and location optimization is conducted by solving Ricatti equation. In this paper, for a cantilever beam a numerical optimization example is also given and performance comparison between an optimal and non-optimal actuator is shown. Also in the numerical example, the control signals for optimal and non-optimal cases are presented and reduction of control effort by conducting optimization procedure is given. Fahroo et al.[15] also used LQR and Ricatti solution based optimization procedure. In this paper, dependence on initial conditions and elimination of them for optimal solution is investigated. From formulations, it is shown that, cost function is depended on both sizes, location and initial conditions of the problem and to overcome the problem two approaches were developed; first solution is to model initial conditions as random unit vector with uniform distribution and second solution is to eliminate initial conditions in cost function.

Li et al. [16] also proposed a procedure that is independent from initial conditions of the flexible structure. They take the change in mass and stiffness of the host structure into account, as a result of actuator and sensor addition during derivation of design objective function. They used dissipated energy maximization as performance criteria, while putting restriction on sizes of actuators and sensor. Tae-woo and Ji-hwan [17], as a different approach, used system energy as their design criteria and by employing input-output optimal cost functions they conducted an optimization procedure for distribution of an active damping layer by taking into account of system output as performance criteria.

Kumar and Narayanan [18] take LQR performance as the optimization criteria and utilized finite element methods to formulate the problem. To obtain optimum sensor actuator locations on the host structure, they used Genetic algorithm and zero-one

optimization procedure to solve the problem. Zero-one procedure is referring to presence of an actuator at a location or not. In this paper, Genetic algorithms validity and effectiveness is showed by using numerical examples. They also determined that optimal locations are found near high modal strain energy regions consistent with the previous works.

1.1.2. Active Vibration Control

In this section, the literature related to the active vibration control of beams and plate-like structures with Piezo actuators are reviewed. Aoki et al. [19], focused on modeling of a smart plate structure with square piezoelectric actuators. They introduced three analytical solutions to model the piezoelectric patch dynamics. Using these models, they predicted the open loop behavior of the piezoelectric actuator on the system. In order to validate obtained results, they used an experimental setup which consists of a flexible clamped plate and collocated sensor - actuator pairs. The active damping system ensures stability when collocated sensor and actuator pairs are used on the host structure. The effect of collocated sensor actuator pair is also addressed in the work of Baudry et al. [20]. In this paper, decentralized active control of periodic vibrations on a flexible plate is investigated and global stability problems are addressed. It is also shown that collocation of sensor actuator pairs results in a strictly positive real open loop response at any frequency while non-collocated pairs results in a non-positive real response which results in stability problems. In this study, global stability conditions for non-collocated sensor–actuator pairs and decentralized controller are driven from plant matrix. Decentralized adaptive controller, using frequency domain gradient and newton-raphson adaptation method, is designed and implemented by using PZT actuators and PVDF sensors in non-collocated orientation. Periodic vibrations are suppressed on a simply supported plate. PZT and PVDF are acronyms for Lead Ziconate Titanate (ceramic structure) and Polyvinylidene Fluoride

(polymer structure) which are two most common active piezoelectric layer classes [21, 22] and used by many researchers [23-28]

Active control of plate vibrations was also studies in the paper of Chantalakhana and Stanway [29]. In this study, they modeled a clamped-clamped plate and gave a complete modeling procedure including finite-element formulation, model reduction and model updating procedures. They added viscoelastic and metallic constraining layers to the plate surface and obtained good vibration suppression levels for a broad frequency band except the first two modes. The first two modes are found at low frequency domain and it is not suitable to suppress these vibrations with passive damping. Passive damping is to modify the material properties of the structure, such as damping and stiffness by using additional materials or geometrical changes, to change the response of the structure [30]. Passive damping is a simple solution and can be very effective but have some limitations. First of all, performance of passive damping applications vanishes at low frequencies because low frequency vibration suppression requires lots of damping material to absorb the vibration energy and as a result passive applications becomes not applicable for most situations. Also, once designed the damping solutions like passive dampers or damping layers cannot be adjusted, and they fail to adapt to the changing environment. This problem is also addressed in the work of Chantalakhana and Stanway [29]. As a result, they implemented an active modal controller to suppress low frequency vibrations occurring on the plate and reduced the high vibrations amplitudes of the low frequency modes which could not be suppressed with the passive damping layers. This type of approach is named as ACLD (Active constrained layer damping). It is a method combining advantages of both active and passive damping [31].

An active/passive treatment for vibration suppression of non-linear panel flutter is investigated in the paper of Moon and Kim [32]. As active treatment, they used an optimal controller by using optimal control theory. They also used cost functions to calculate

optimal piezoelectric actuator positions to maximize modal piezoelectric forces. As passive treatment technique, they used L–R series shunt circuits. These are electro-mechanical simple circuits, which simply feedback the electrical sensor signals generated by the piezoelectric actuators. These electrical signals are generated due to the self-sensing nature of the piezoelectric materials. Shunt circuit approach is also a common approach used by other researches like Makiharak [33] and Zhao [34]. The self-sensing nature of the piezoelectric materials is also a commonly used technique in the literature. A self-sensing actuator is simply a piezoelectric patch, acting as an actuator and sensor at the same time. In the paper, Qui and Haraquchi [35], Qui used a bridge circuit to use a single patch as both sensor and actuator at the same time and combined this system with an adaptive controller to suppress vibrations occurring on the plate. He also showed a method to balance the bridge circuit.

Moon and Kim [32] used finite element techniques to conduct numerical solutions. Finite element techniques are also used by Young-hun [36] to simulate controller performance. In this study, the modeling procedure for the simulation of an active modal controller on a square plate is shown. For actuator position optimization, Young-hun used modal analysis results of the plate, strain information and piezoelectric actuator dynamics. He maximized effectiveness of the actuators by placing them near to high strain regions which is also a consistent choice when compared with the literature.

Active vibration suppression is also used to reduce noise levels by reducing radiation from thin flexible elements. A lot of research is being carried out on this subject [37-39], since all commercial vehicles like airplanes, cars and ships involve thin structural elements. Radiating noise from thin, flexible elements results in high acoustic pressures inside the coupled acoustic fields. An effective control approach to suppress radiated noise from vibrating structures is named as active structural acoustic control (ASAC) [37] . In an ASAC, in addition to structural sensors like acceleration and velocity, microphones are

used as sensors to detect variations in acoustic pressure. In the study, Dozio et al.[37] presented a predictive controller and used it to control structural vibrations on a thin clamped-clamped plate to reduce radiating noise from plate surface. They succeeded in achieving broadband noise reduction. Elliot et al. [38] showed the initial simulation work of an ASA controller using local feedback loops and an array of sensor actuator pairs. He also showed that, with usage of perfectly collocated sensor actuator pairs by assuming point force actuators and point velocity sensor the systems becomes unconditionally stable. In the study, Ma et al.[40], used embedded piezoelectric patch actuator to suppress vibrations of a carbon fiber reinforced carbon plate to control structural acoustics. They used both adaptive feedback, feed forward controllers and a hybrid controller that combines both feedback and feed forward control loops. Filtered x-LMS algorithm is used for adaptation of the controller. By using a low-cost digital signal processing board, they managed to obtain noticeable reductions in sound pressures levels with constant, swept frequency and varying amplitude disturbance conditions.

1.1.3. Active Structural Control System Design

In order to reduce vibration levels in automotive, marine and aerospace applications, active vibration controller methodologies are being developed and their performances are being investigated by various researchers [3, 4, 27, 39, 41-47] in the past.

The selection and implementation of controller algorithms, the placement of sensors and actuators are well documented for thin-flexible structures [7]. Yet, those applications are still limited to beam-like and plate-like structures with properly defined boundary conditions [7]. For example, for fully-clamped plate structures, the design and gain tuning of velocity feedback controllers are studied in all its aspects [12, 39, 42, 43, 48, 49]. It is shown that, with automatic tuning of multiple-velocity feedback controller, total energy

absorption can be maximized while the energy of the structure is minimized at the sensor location [48, 49]. However, in case of complex structures, especially for large and flexible ones, reduction of vibration levels around sensor locations will not guarantee energy reduction over the entire structure. To overcome this problem and improve overall dynamics of complex structures with active treatments, the design and performance evaluation must be carried out spatially. In literature, the spatial controllers with model based algorithms (such as H∞ and LQR) are designed for simple beam-like and plate-like structures using analytical models [50-53]. However, in reality, complete and accurate analytical models of 3D complex structures are practically impossible so it may be not a feasible approach to design a model-based controller. In these conditions, the model independent controller algorithms (velocity and position feedback controllers etc.) can be preferred. These algorithms are practical and efficient for reducing the vibration energy if the parameters are properly tuned [48, 49]. However, in order to achieve a spatial control of flexible complex structures with multiple feedback loops, infinite number of sensors and actuators may be required [48]. This requirement can be satisfied with finite number of sensors and actuators by conducting tradeoffs and optimization studies.

1.1.4. Active Structural Acoustic Control (ASAC) System Design

Automobile industry is forced to produce more comfortable and quieter vehicles because of high competition in the market. Comfort, safety and performance are three major customer's selection criteria that make significant differences in sales performance of automobiles. Considering these customers' expectations, noise, vibration and harshness (NVH) has been a research topic for automobile manufacturers in the last decades [1, 2, 54]. One of the fundamental problems in NVH is the low frequency vibration on vehicle bodies and structure-borne noise in the passenger cabin. The passive treatments do not

provide effective solutions to suppress sound pressure levels at these low frequencies. For that reason, effective and alternative solutions are required to reduce noise and increase comfort inside the passenger cabins. Active structural acoustic control is an alternative solution to suppress noise due low-frequency vibration. In the last three decades, in order to reduce noise levels in automotive, marine and aerospace applications, active vibration controller methodologies are being developed and their performances are being investigated by various researchers [27, 44, 46].

The selection and implementation of controller algorithms and the placement of sensors and actuators have been addressed by various research studies for effective noise reduction using active structural acoustic control (ASAC) methodology. ASAC systems in literature, involve feedback and feed forward algorithms with structural sensors and actuators. These types of controller systems suppress structural vibrations while considering acoustic response. For instance, Song et al. [3] investigated both structural and acoustic aspects for a ASAC system on a cabin mock-up model. Panel selection was conducted based on acoustic contribution analysis and actuators were placed on the most contributing panel considering noise levels inside the cabin. Similar to this study, de Oliveira et al. [41] used vehicle mock-up model to design and validate active and passive noise treatments. They used velocity feedback controller for collocated sensor and actuator pair and a satisfactory noise reduction is achieved in the experimental setup for two microphone positions. In a further study, de Oliveira et al. [55] designed and implemented adaptive feed forward controller algorithm for the same vehicle mock-up model that they used in reference [3]. They modified filtered x-LMS algorithm to deal with varying disturbances and built an adaptation scheme for improvement of convergence rate of the algorithm. They stated that a combination of feedback and feed-forward controllers should be used to improve vibration and noise suppression around lightly damped resonances of the vibro-acoustic system. In a recent study, Misol et al. [56] applied ASAC scheme to a

real vehicle's windshield. They used Piezo ceramic patch transducers as actuators to reduce the interior noise inside an automobile passenger cabin. Their experimental results show that a local reduction up to 15 dB in the acoustic response can be achieved. These experimental studies show that the reduction of noise radiation from vibrating surfaces requires a feed forward or spatial feedback controller, since all wetted areas contribute energy transfer from structure to fluid medium. The general feedback control systems use local sensor information for generation of drive signal for actuators to suppress vibrations. Therefore, in order to achieve spatial control of a structure, infinite numbers of sensors and actuators are required. This is not a practical and efficient solution, especially for complex structures. To overcome this problem, model-based controllers and identification techniques are developed for computation of unmeasured plant response to achieve spatial control effect on beam-like and plate-like structures [50, 57]. However, for a complex shaped structure with complex boundary conditions, under random disturbances and operational conditions, it is not a feasible and possible approach to obtain accurate plant model and design model-based controller [58]. In these cases, implementation of model-independent controller is preferred. In the study, Zilletti et al. [48] used velocity feedback controller, which is a robust model-independent controller with collocated sensor and actuator pair to reduce total vibration energy and to improve panel sound transmissibility on plate-like structure. It is shown that with proper tuning of velocity feedback controller, reduction in total vibration energy can be achieved with a single control loop [48, 49].

However, the total energy reduction in any panel does not guarantee reduction in sound pressure level inside an enclosure because each surface's contribution to sound pressure level is different. Therefore, acoustic contribution assessment is required to determine most influential radiating surface to acoustics when an enclosure is considered. After determination of most influential radiating surface, actuator/sensor positioning and gain tuning for a feedback control loop can be conducted by considering several factors, such as

frequency bandwidth, disturbance type and acoustic response. In the literature, for plate-like and beam-like structures actuator/sensor positioning is well-studied to improve closed loop performance of controller when structural vibrations are considered [6, 7, 9, 12]. When acoustics is considered to increase control authority on the system, actuator positions on the controlled surfaces can be determined by considering coupling of structural and acoustic modes [3]. But when complex radiating geometry is considered, determination of coupled modes with the acoustic medium becomes a difficult task because of the dominant local modal behaviors on the structure. In another approach, decentralized control strategy is utilized with multiple actuators on the surface to limit noise transmissibility of controlled surface [38]. But also for a complex geometry and boundary conditions this approach will lead to high number of control loops to guarantee spatial reduction and will not be practical due to the complexity of the surface.

1.2. Contribution of This Thesis

Considering all of the advancements in the previous studies, the main contribution of this thesis is to develop design methodologies for local and global vibration control and active structural acoustic control for 3D shell structures. The methodology is presented on a simple plate-like structure then it is developed to make the methodology applicable on complex 3D structures with complex boundary conditions.

The presented methodologies include optimal positioning of actuator/sensor pairs and finding optimal design parameters for the controller. The following procedures are followed in designing the controller methodologies:

- A finite element model of the structure is created together with the piezo actuator electro-mechanical properties.
- Frequency response analysis results are verified by experimental measurements.

- Modal controllability measure is investigated for optimum positioning of the sensor/actuator pair for suppression of the flexible modes of the plate structure.
- Once the optimal positions are determined, a controller is designed to attenuate each structural mode.
- A new vibration control methodology is developed for a complex structure with complex boundary conditions.
- Local and global optimization studies are carried out for positioning the sensor/actuator pair and parameter tuning of the controller.
- By comparing controller active and inactive cases, the vibration suppression performance of the controller is demonstrated locally and globally.
- A new structural acoustic control methodology is developed for a complex structure with complex boundary conditions.
- Local and global optimization studies are carried out for positioning the sensor/actuator pair and parameter tuning of the controller.
- By comparing controller active and inactive cases, the vibration suppression performance of the controller is demonstrated locally and globally.

1.3. Outline

In chapter 2, modeling procedure for a fully clamped plate with attached piezoelectric patches is presented. Finite element model of the flexible plate, together with the piezoelectric patches is built. The optimal position of piezoelectric actuator is determined using frequency responses of the flexible plate for different locations of collocated sensor/actuator pairs. Having found the optimal positions for each structural vibration mode, velocity feedback controller is designed using simulated frequency response functions for various feedback gains in the presence of forced vibrations. In chapter 3, a

new design methodology for local and global active vibration controller for a complex geometry structure is given. Developed methodology is used to determine optimal actuator/sensor positions and controller parameters for vibration suppression. A case study is presented to show applicability of the developed method on a complex structure. In chapter 4, a new design methodology for an active structural acoustic controller is given for a complex structure is given. Developed methodology is used to determine optimal actuator/sensor positions and controller parameters for noise suppression. A case study is presented to show applicability of the developed methodology on a complex structure. In Chapter 5, the discussion and conclusion of the thesis is given.

Chapter 2

ACTIVE VIBRATION CONTROL SYSTEM DESIGN FOR SIMPLE GEOMETRY STRUCTURE

2.1. Introduction

In this section, theoretical information used for modeling procedure of piezoelectric patch attached plate system and position optimization studies for actuator/sensor location is given. The created model is used for design of the control system and estimation of controller performance. In the first section of this chapter, piezoelectricity theory and piezoelectric patch dynamics are explained. In the following section, finite element modeling theory for coupled electro-mechanical system is given, involving steel plate and piezoelectric patches as actuators. After this section, modal controllability theory is explained and its implementation to the existing system using finite element modeling methods is presented. The chapter is finalized with the simulation and experimental active vibration control case studies and the obtained results are compared. The obtained results for position optimization of actuator/sensor pair are evaluated by considering several actuator/sensor locations on the plate for simulations and experimental studies.

2.2. Simple Plate-Like System

2.2.1. Experimental Setup

In this study, for active control experiments, a box structure is build which represents a real vehicle's acoustic environment and is used for simulations. Experimental setup and a CAD drawing of the structure and separation plate are shown in Fig.2.1. The structure is a rectangular cavity with dimensions $2000 \times 1000 \times 1000\ mm$ and separated into two rooms by a thin steel plate. One room is called engine compartment and the other is called passenger compartment to simulate the real vehicle interior noise environment. The steel plate has a thickness of 1.8mm and clamped along on all four edges by using rigid aluminum frames. The cavity walls are constructed using wood filled concrete with a thickness of *10mm*. In the construction of the experimental setup, as connection equipment $45 \times 45\ mm$ aluminum square profiles are used with corresponding connection parts. In experiments, disturbance generators (e.g. electromechanical shaker) are placed inside the engine compartment which is the left compartment in Fig.2.1 and actuators are placed from the passenger side compartment which is the right compartment in Fig.2.1. For optimization analysis, ABAQUS FEM software is used and modeling procedure in only considered for the separation panel. Following assumptions are made for modeling procedure; For the finite element modeling of the smart plate: (i) the material of the host structure is assumed to be isotropic, (ii) the bonding of piezoelectric patch on host structure is perfect, (iii) the host structure is fully-clamped to rigid support, (iv) the distribution of electrical charge on piezoelectric patch is homogenous, (v) gradient of the electrical field of piezoelectric patch is normal to the host structure.

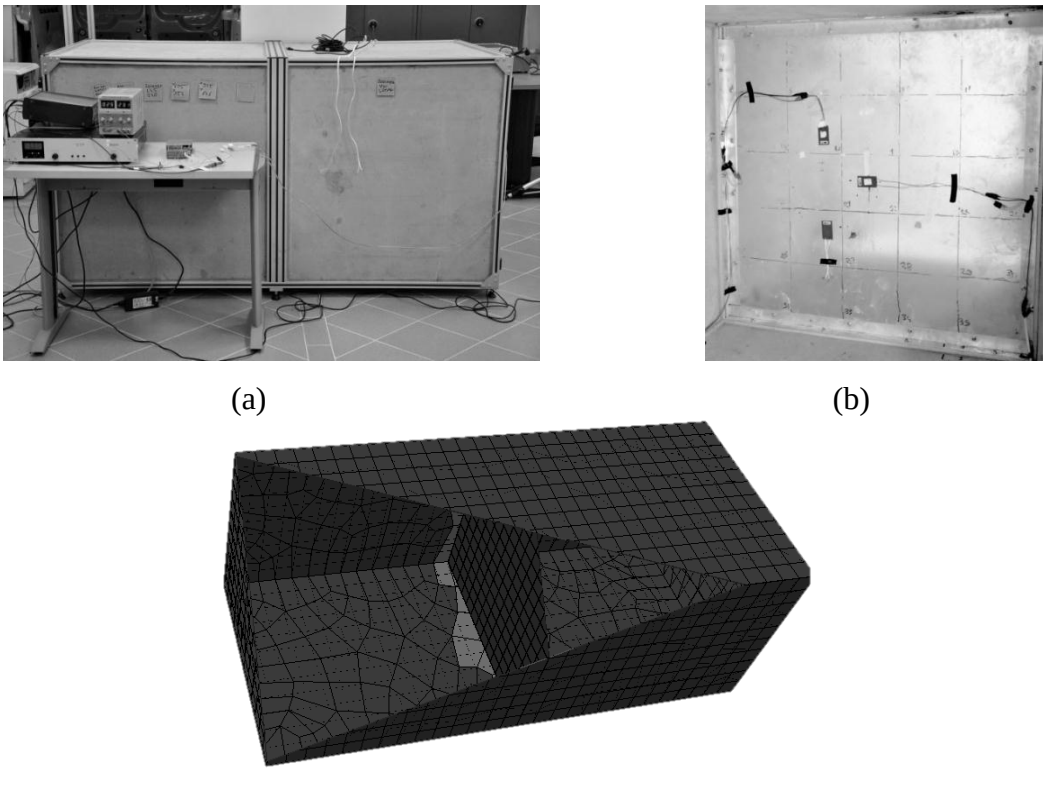

(a) (b)

(c)

Figure 2.1 Experimental setup. a) Exterior view of the experimental setup showing the whole box system. b) Separation plate (smart plate) with attached active piezoelectric patches for experiments. c) CAD drawing of box-plate system.

The steel separation plate is made from commercial standard material (AISI 1040 Steel) and therefore its properties are taken as isotropic. Piezoelectric patches are bonded to the surface using Cyanoacrylate Adhesive (i.e. super glue) and therefore, perfect bonding assumption is made during modeling the interaction between the Piezo and the host structure. For finite element simulations, only separation plate is modeled and it is assumed fully clamped to the rigid support because the box structure is very heavy and rigid because of the surrounding wood-filled concrete walls. Also separation plate is connected to box

structure using M5 bolts (*5 mm*) in all four corners at 16 points and fixed with L shaped connection equipment in both faces on all corners (Fig.2.1.b).

2.3. Modeling the Smart Plate System

2.3.1. Theory of Piezoelectricity

Piezoelectric materials have a special characteristic to convert mechanical energy into electrical energy or vice versa. When mechanical disturbance is applied onto piezoelectric materials, they react to the disturbance by means of physical deformation and accumulation of electrical charges inside the material body. For a linear system, like a piezoelectric material, mechanical energy and electrical energy are linearly coupled. Constitutive relations are, therefore, used to represent the linear coupled behavior of the piezoelectric materials which are derived from thermo dynamical relations [59].

Constitutive relations are equations that use the physical considerations to define the relations between two physical quantities. Suppose a system defined as F and depended on two state variables x and y. Then one can write the expression for F using the homogeneous quadratic expression

$$F(x,y) = \frac{1}{2}a_{11}x^2 + a_{12}xy + \frac{1}{2}a_{22}y^2 \quad \textbf{(2.1)}$$

In the above expression for x and y equal to zero, system is assumed to be zero (F (0, 0) = 0) and for the system F, the rate of change of system δF is equal to the linear addition of the rate of change of x and y:

$$\delta F = H\delta x + G\delta y \tag{2.2}$$

where H and G are donated as intensive variables. Using relation one and two, constitutive relations in the form of two linear equations can be obtained as:

$$H = \frac{\delta F}{\delta x} \qquad G = \frac{\delta F}{\delta y} \tag{2.3}$$

$$H = a_{11}x + a_{12}y \qquad G = a_{12}x + a_{22}y \tag{2.4}$$

In the Eq.2.4, a_{11} and a_{22} are the principle constants of the x and y systems [59]. a_{12} is the coupling term that relates two depended variables x and y and a_{12} is equal to a_{21}. The condition $a_{12} = 0$ represents the no coupling case between x and y. In Eq.2.3, the terms a_{11} and a_{22} are determined for constant x and constant y conditions.

Constitutive relations for piezoelectric materials can be derived by using various thermo dynamical relations and different set of independent variables. In the Standard defined for piezoelectricity by IEEE in 1987 [60], equation for electrical enthalpy density is used to derive constitutive relations. Electrical enthalpy density is, as given in the standard

$$H = \frac{1}{2}c^{e}_{ijkl}S_{ij}S_{kl} - e_{kij}E_kS_{ij} - \frac{1}{2}\varepsilon^{S}_{ij}E_iE_j \tag{2.5}$$

Where c^{e}_{ijkl} is the elastic constant matrix, e_{kij} is the piezoelectric constant matrix and ε^{S}_{ij} is the dielectric constant matrix S is the deformation vector, E is the electric field vector. The subscripts are the notations that used to define principle directions.

The differential of H or the energy enthalpy density is given by

$$dH = T \times dS + D \times dE \tag{2.6}$$

Assuming that

$$T = \left[\frac{\delta H}{\delta S}\right]_E \qquad D = \left[\frac{\delta H}{\delta E}\right]_S \tag{2.7}$$

using equations 2.5,2.6 and 2.7 constitutive relations for piezoelectric materials in the form of coupled equations is found as

$$T = c^T \times S - e^{-1} \times E \tag{2.8}$$

$$D = e \times S + \varepsilon \times E \tag{2.9}$$

where T is the deformation vector, c is the piezoelectric matrix, S is the electric field vector, e is the elasticity matrix, E is the stress vector, D is the electrical displacement, and e is the piezoelectric stress matrix. Eq.2.8 is the strain form of the piezoelectric constitutive equation. This relations are expressed in terms of independent variables, electrical field vector S and the elasticity matrix E.

2.4. Finite Element Theory and Modeling

2.4.1. Finite Element Theory

In this thesis, finite element modeling is used to model the smart plate. A smart plate is a system, which consists of active parts or materials that cause actuation on the host structure. Piezoelectric patches are used as actuators in this study and they are attached on the face of a plate. Finite element modeling theory is explained according to the modeled system dynamics and properties. During the vibratory motion, any point on a smart plate follows a displacement path which is depended on time and space. This path can be represented with a relation as u = (x, y, z, t) where x, y and z are the global coordinates of

the smart plate and t is the time variable. By using virtual work principle and defining a small variation of this displacement path as δu for a time interval between t_1 and t_2, eq. of motion of a smart plate can be obtained by the Hamilton's principle [22, 61]

$$\delta \int_{t1}^{t2} (T - U - W) dt = 0 \quad \textbf{(2.10)}$$

where T and U are kinetic and strain energies of the body and W denotes the work done by external forces onto the smart plate.

The kinetic energy of the smart plate is described by with a volume integral

$$T = \frac{1}{2} \int \rho \dot{u}^T \dot{u} dV \quad \textbf{(2.11)}$$

where ρ is the mass density, $\dot{u}$ is the velocity in the global coordinates and dV is the elemental volume of the smart plate.

The strain energy of the smart plate is

$$U = \frac{1}{2} [\epsilon^T \sigma - E^T D] \quad \textbf{(2.12)}$$

where ϵ^T is the transpose strain, σ is stress, E^T is transpose electrical field component and D is the electrical displacement. This strain energy relation of the smart plate can be derived by using the constitutive relations given in Eq.2.8 and 2.9 with the electrical enthalpy density given in IEEE standards on piezoelectricity shown in Eq.2.5

The smart plate's damping, in-plane forces and piezoelectric actuator's forces are include in the work equation. The piezoelectric materials are deformed according to the given constitutive equations under the effect of electrical or physical loads. For actuation or sensing purposes, the piezoelectric materials are attached to the host structure. In case of electrical load application, piezoelectric materials undergo volume change and in the case

of attachment to another structure they generate forces on the bonding surface which causes strain on the host structure. Work done onto a smart plate with included piezoelectric effect is as follows: [22, 59, 61]

$$W = \int (\delta u F_V) dV + \int \delta u^T F_S dS_1 + \delta u^T F_P - \int \varrho \delta \phi \mathrm{d}S_2 - \delta \phi \mathrm{Q} \tag{2.13}$$

where F_v, F_s, F_p denotes the body, surface and point forces respectively for the area element dS and the volume element dV . The electrical charge ϱ is used for the charge on the piezoelectric patch surface, the applied concentrated charge is denoted by Q and $\delta\phi$ presents the variation of electrical potential.S_1 denotes the smart plate's surface area whereas S_2 is the area of piezoelectric patch actuator surface.

By collecting kinetic and potential energy equation of the system, Electrical enthalpy density relation, work equation and substituting these equations into Hamiltonian of the system in Eq.2.10 general representation of system's equation of motion can be obtained as:

$$\begin{aligned} 0 = \int [\rho \delta u^T \ddot{u} - \delta \epsilon^T c^E \epsilon + \delta \epsilon^T e^E E + \delta E^T e \epsilon + \delta E^T \varepsilon^S E + \delta u^T F_v] dV \\ + \int \delta u^T F_s \, dS_1 + \delta u^T F_p - \int \delta \phi \varrho dS_2 - \delta \phi Q \end{aligned} \tag{2.14}$$

thereafter, by supposing zero virtual displacement (δu = 0) at time steps t_1 and t_2 , using finite element theory and applying the variation methods of calculus, the equation of the motion for the system can be expressed in terms of mass, damping and stiffness matrices as :

$$\mathbf{M}\ddot{\mathrm{q}} + \mathbf{C_d}\dot{\mathrm{q}} + \mathbf{K}\mathrm{q} = \mathbf{T}_{\mathrm{cf}}\mathrm{Q} \tag{2.15}$$

where **M** presents the mass matrix, $\mathbf{C_d}$ is the damping and **K** is the stiffness matrix for the smart plate. The response of the smart plate is presented with q where $\mathbf{T}_{cf}$ is the transformation vector from applied charge-to-force and **Q** is the applied charge. The formulations for these matrixes are as follows:

$$M = \sum_i {L_{ui}}^T \left[\int \rho {N_u}^T N_u dV\right] L_{ui} \quad \textbf{(2.16)}$$

$$C_d = \sum_i {L_{ui}}^T \left[\int {N_u}^T \mu N_u dV\right] L_{ui} \quad \textbf{(2.17)}$$

$$K = \sum_i {L_{ui}}^T \left[\int {N_u}^T c^E N_u dV\right] L_{ui} \quad \textbf{(2.18)}$$

$$T_{cf} = \sum_i {L_{ui}}^T \left[\int {N_u}^T e \mathrm{N}_{\emptyset} \emptyset_i\right] L_{\phi i} \quad \textbf{(2.19)}$$

in these equations $\boldsymbol{\mu}$ is the viscous matrix, subscript u is used for elemental displacements and ϕ is used for electrical potentials. $\mathbf{L}_{ui}$ is the localization matrix for i_{th} element relating local elemental displacements to global values and N_u is the shape function for non-electrical finite elements that converts nodal displacements and to elemental strain field and. $\mathbf{L}_{\phi i}$ is the localization matrix for i_{th} element relating local elemental electrical potential to global values and $N_{\emptyset}$ is the shape function for electrical finite elements that converts nodal electrical potential to elemental electrical potential.

By applying harmonic external electrical charge to electrical elements $\mathbf{Q}(\omega) = \mathbf{Q}e^{j\omega t}$, the steady-state response of the smart plate is in the same form as $\mathbf{q}(\omega) = \mathbf{q}e^{j\omega t}$. So that, the following form for is obtained

$$\mathbf{q}(\omega) = [-\omega^2\mathbf{M} + j\omega\mathbf{C_d} + \mathbf{K}]^{-1}\mathbf{T}_{cf}Q(\omega) \quad \textbf{(2.20)}$$

or in short notation

$$\mathbf{q}(\omega) = \mathbf{H}(\omega)\mathbf{T}_{cf}\mathbf{Q}(\omega) \quad \textbf{(2.21)}$$

where $\mathbf{H}(\omega)$ the transfer is function between the applied charges to the piezoelectric elements and $\mathbf{q}(\omega)$ is the displacement field. The solution of this formula enables the calculation of frequency response of the smart plate when the piezoelectric patch is employed as actuator. Similar modeling approaches are also applied to the finite element modeling of smart materials with flexible structures. In the purpose of finding optimal location of piezoelectric patch on the flexible plate, precise estimate of frequency response of the smart plate is directly related with the accuracy of the finite element model. In the following section, first, information about the plate-box experimental system and finite element modeling procedures using ABAQUS software are given. In the following section, verification of finite element model with experimental results is presented. After this section optimization procedures and modal controllability theory are given and conclusions are presented.

2.4.2. Finite Element Modeling

Finite element model of the smart plate is created in ABAQUS software. Host plate structure is made from industrial steel and isotropic properties of steel are used. In this study, commercially available piezoelectric actuator patch (PI Dura-act 876.A12) is used on a square fully-clamped steel plate. This type of piezoelectric patches are compact, lightweight and insulated so the attachment on host structure is easy and additional weight is negligible considering the weight of the steel plate. The material properties of the steel plate and the piezoelectric actuator patch are presented in Table.2.1. Material properties of piezoelectric patch are provided by the manufacturer for the used material (PIC 255)

Piezoelectric coefficients with double subscripts link electrical and mechanical quantities. The first subscript gives the direction of the electrical field associated with the voltage applied or the charge or the voltage produced. The second subscript gives the

direction of mechanical stress or the strain. The principle directions for piezoelectric materials are shown in (Fig.2.2)

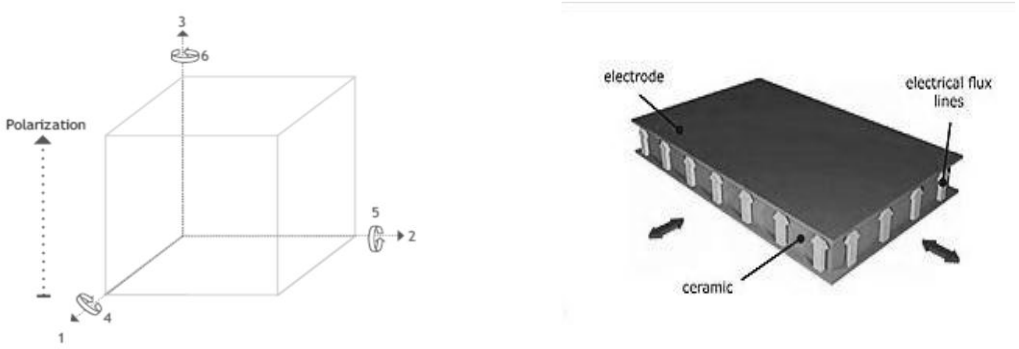

(a) (b)

Figure 2.2 Designation of principle aces in piezoelectric materials. Polarization arrow shows the d31 effect, which is the induced strain in direction 1, per unit electric field applied in direction 3 b) d31 effect on the used PI Dura-act 876.A12 piezoelectric patches, light arrows shows the charging direction normal to the attached surface. Dark arrows shows the strain direction occurring due charging. [62]

Table 2-1 Material properties of the host structure and piezoelectric patch

Property	**Steel**	**Piezoelectric Patch (PIC255)**
Length (mm)	*1000*	*65*
Width (mm)	*1000*	*31*
Depth (mm)	*1.8*	*0.5*
Elastic modulus (GPA)	*190*	*70.2*
Poisson's ratio	*0.33*	*0.36*
Density (kg/m^3)	*6305*	*7800*

Piezoelectric Constant d_{31} (10^{-10} m/V)	-	*-1.74*
Piezoelectric Constant d_{33} (10^{-10} m/V)	-	*3.94*
Piezoelectric Constant d_{15} (10^{-10} m/V)	-	*5.35*
Piezoelectric Elastic Constant c_{11} (10^{11} N/m^2)	-	*1.230*
Piezoelectric Elastic Constant c_{33} (10^{10} N/m^2)	-	*9.711*
Piezoelectric Elastic Constant c_{55} (10^{10} N/m^2)	-	*2.226*
Piezoelectric Elastic Constant c_{12} (10^{10} N/m^2)	-	*7.670*
Piezoelectric Elastic Constant c_{13} (10^{10} N/m^2)	-	*7.025*
Piezoelectric Elastic Constant c_{44} (10^{10} N/m^2)	-	*2.226*
Piezoelectric Elastic Constant c_{66} (10^{10} N/m^2)	-	*2.315*
Piezoelectric Dielectric Constant $\boldsymbol{\varepsilon_{11}}$ (10^{-12})	-	*1649*
Piezoelectric Dielectric Constant $\boldsymbol{\varepsilon_{33}}$ (10^{-12})	-	*1750*

Piezoelectric patch material properties are assumed as isotropic but the electrical properties are taken anisotropic to reflect dynamic behavior of the piezoelectric material. To define material properties, matrix calculations are required and piezoelectric stress matrix should be calculated. In Eq.2.8 the stress form of piezoelectric constitutive equation is given as;

$$\mathbf{T} = \mathbf{c}^{\mathrm{T}} \times \mathbf{S} - \mathbf{e}^{-1} \times \mathbf{E} \tag{2.22}$$

where **e** is the piezoelectric stress matrix. But in material properties, this matrix is not provided directly and need to be calculated. Equation 2.22 can be written in the form of piezoelectric constant matrix **d,** and elastic constant matrix **c,** as follows:

$$\mathbf{T} = \mathbf{c}^{\mathbf{T}} \times \mathbf{S} - \mathbf{c} \times \mathbf{d}^{\mathbf{T}} \times \mathbf{E} \tag{2.23}$$

So **e** is the piezoelectric stress matrix and its equation is

$$\mathbf{e} = \mathbf{c} \times \mathbf{d^T} = \begin{bmatrix} c_{11} & c_{12} & c_{13} & 0 & 0 & 0 \\ c_{12} & c_{22} & c_{23} & 0 & 0 & 0 \\ c_{13} & c_{23} & c_{33} & 0 & 0 & 0 \\ 0 & 0 & 0 & c_{44} & 0 & 0 \\ 0 & 0 & 0 & 0 & c_{55} & 0 \\ 0 & 0 & 0 & 0 & 0 & c_{66} \end{bmatrix} \times \begin{bmatrix} 0 & 0 & d_{31} \\ 0 & 0 & d_{31} \\ 0 & 0 & d_{33} \\ 0 & d_{15} & 0 \\ d_{15} & 0 & 0 \\ 0 & 0 & 0 \end{bmatrix} \quad \textbf{(2.24)}$$

in elasticity matrix **c**, the independent terms are; c_{11}, c_{33}, c_{44}, c_{12}, c_{13} and dependent terms are $c_{22}=c_{11}$, $c_{55}=c_{44}$, $c_{66} = 2 \times (c_{11} - c_{12})$ and $c_{23} = c_{13}$. In piezoelectricity matrix **d**, the independent terms are; d_{33}, d_{31}, d_{15} and the dependent terms are $d_{32}=d_{31}$ and $d_{24}=d_{15}$[63]. The piezoelectric stress matrix **e** is calculated for the selected piezoelectric patch and after matrix multiplication and taking transpose of result, the piezoelectric stress matrix for the selected commercial product PI Dura-act 876.A12 is found as:

$$\mathbf{e^T} = \begin{bmatrix} 0 & 0 & 0 & 0 & 11.9091 & 0 \\ 0 & 0 & 0 & 11.9091 & 0 & 0 \\ -7.0693 & -7.0793 & 13.81434 & 0 & 0 & 0 \end{bmatrix} \frac{NV}{m} \quad \textbf{(2.25)}$$

Stress matrix used by ABAQUS is the transpose of the calculated e matrix. As a result, during material definition, the obtained result in Eq.2.25 is used. The piezoelectric dielectric matrix is also required for piezoelectric material definition and is taken as follows;

$$\varepsilon = \begin{bmatrix} 1649 & 0 & 0 \\ 0 & 1649 & 0 \\ 0 & 0 & 1750 \end{bmatrix} \times 10^{-12} \quad \textbf{(2.26)}$$

in Table.2.1 dielectric (permittivity) matrix values are given relative to ε_0 which is permittivity of vacuum. The standard value of ε_0 is approximately $8.854187817620 \times 10^{-12}$ $\mathrm{F} \times \mathrm{m}^{-1}$ according to ISO 31.5 [64] standard and in simulations to use absolute

dielectric values, dielectric matrix is multiplied with 10^{-12} to achieve absolute value of permittivity for piezoelectric material.

Finite element modeling procedure has been carried out, after defining material properties for the host structure and piezoelectric material. The system, which includes fully clamped host structure with surface bonded piezoelectric actuator, will be referred as "*smart plate"* in the rest of this study. Modeling is started with the host structure. The smart plate ($1 \times 1m \times 0.0018\, mm$) is modeled as a rectangular prism with the given side dimensions. As element type for finite element modeling *C2D20*, *20*-node quadratic brick element is used for the host structure. This element type can be found under the three-dimensional solid element library of ABAQUS and is suggested for standard analysis. *0.05 m* is used for element global size. Element size is determined by considering simulation times. In the experimental setup, the smart plate is clamped to the box structure using very rigid connection elements, as a result in the finite element model; plate is fixed using encastre boundary conditions at all edges. By applying boundary condition all translational and rotational degree of freedoms for the smart plate edges are set to zero resulting in fixed support condition. As material, steel is used with given properties in Table.2.1 and distributed homogeneously onto the structure. The build finite model for plate is shown in Fig.2.3

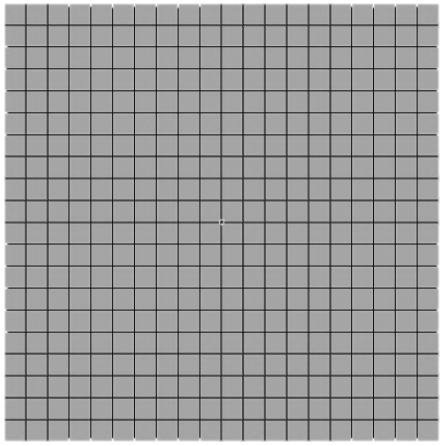

Figure 2.3 Finite element model of the steel plate (host structure)

Finite element modeling procedure for piezoelectric patch performed after modeling the smart plate. Technical information about both material properties of active piezoelectric material and patch system including the electrical connections and insulation layer are taken from the manufacturer. In this project PI P-876 DuraAct™ P-876.A12 are used as actuator surfaces. These transducers are selected because of their lightweight design, high flexibility and quick response characteristics and insulated structure. DuraAct™ patch transducers are compact units based on a thin piezoelectric ceramic foil between two conductive films, all embedded in a ductile composite-polymer structure. This design makes the brittle piezoelectric material both pre-stressed and insulated. Detailed schematic design of the piezoelectric patch is shown in Fig.2.4 [65]

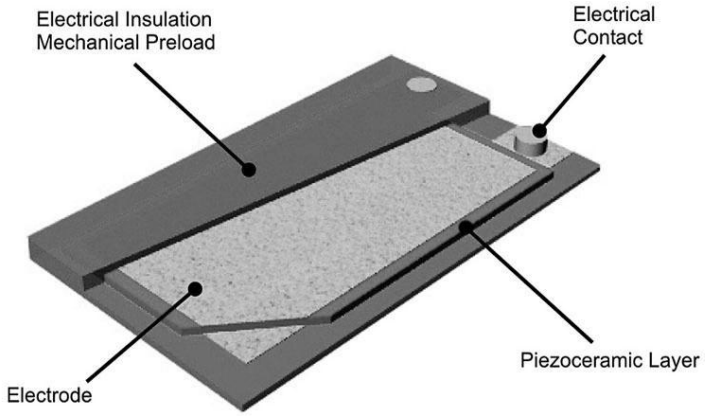

Figure 2.4 DuraAct™ transducer design[65]

Finite element model of the patch is prepared according to the design aspects shown in Fig.2.4. In the model, piezoelectric active layer is modeled with an insulation layer to separate it with the host structure. Also on the patch there are two pins found for electrical connections. One pin is for the positive pole connection and one pin is for the ground connection. The ground connection pin shows the ground surface of the patch which is important because electrical flux lines occurring normal to the ground plane creating a potential between positive and ground faces. As a result, patch is bended towards to the ground plane during operation. Grounded face of the piezoelectric patch is therefore important and is modeled as a boundary condition during model creation.

Patch is modeled as two separate blocks, which are connected at the ground plane. One block is for modeling the active Lead Ziconate Titanate (PZT) piezoelectric material and other block is used as a non-active insulation layer between the host structure and patch. Patch dimensions are taken from the manufacturer and are as follows $0.061 \times 0.035 \times 0.0005\, m$. The active piezoelectric layer thickness is given as *0.0002 m* and other remaining *0.0003 m* is the insulation layer on the patch. The manufacturer could not be able to supply mechanical properties for the insulation layer and its coupled properties with the

active piezoelectric layer for that reason in the model all mechanical properties of the patch is taken as given properties for PIC 255 PZT material in Table.2.1.

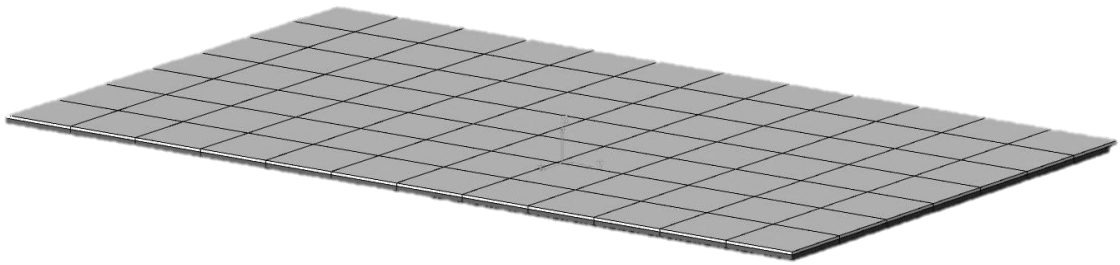

Figure 2.5 Finite element model of the piezoelectric patch. Active piezoelectric layer is the top layer, insulation layer is the bottom layer.

Build model is shown in Fig.2.5. The element type used for meshing host structure (C320) is again used for meshing of the insulation layer. For piezoelectric layer mesh, another element type should be used. ABAQUS have piezoelectric element type family for modeling of active piezoelectric materials. *C320E* is the used as the electrical mesh element found under this family. The notation *"E"* represents electrical degree of freedom supported by this element. For both insulation layer and piezoelectric layer a global element size of *0.0005 m* is used for meshing. This value is again selected by trial and errors considering both simulation accuracy and simulation time. The insulation layer and piezoelectric layer are coupled at the intersection region found between by using Tie command. This command couples the rotational and translational degrees of freedom at intersecting nodes found between the selected surfaces and also as stated before, this intersection plane also used as ground pole for electrical analysis. Grounding of this plane

is done by applying “0” (zero) electrical potential to this surface as boundary condition. In simulations, top surface (Fig.2.5) is used as charging surface and by applying surface charge to this plane, electrical potential is created between top and bottom layers of piezoelectric material. By this way, dynamic behavior of actual patch is simulated. The prepared piezoelectric model is assembled with the host plate structure for electro-mechanical structures. This model is used to predict piezoelectric actuator and plate responses during operation. For simulations, the prepared piezoelectric patch model is coupled at the bottom surface of the insulation layer shown in Fig.2.5 to the plate structure by using tie command in ABAQUS.

2.5. Validation of the Finite element model

In previous section, modeling procedure for coupled system is presented. In this section, the numerical and experimental frequency responses will be compared for verification of the finite element model. In numerical structural analysis, patch is positioned at the center of the plate and the electrical charge is applied to the piezoelectric actuator in accordance with the electrical limitations (provided by the manufacturer) of the piezoelectric material while the velocity of the center position (collocated actuator/sensor pair) of the smart plate is measured. The simulated frequency response is acquired between the applied charge and velocity. For experimental analysis, the smart plate in Fig.2.1 is clamped along on all four edges. The velocity measurement is conducted by Polytech PDV100 laser Doppler vibrometer (LDV) [66]. The target location of the vibrometer is determined as the center of the piezoelectric patch to provide a collocated sensor and actuator pair likewise in the simulation. The actuation signal is generated by signal analyzer and amplified by E-413 DuraAct Piezo Driver and sent to the piezoelectric patches (DuraAct P876.A12). NetdB [67] data acquisition system is used for frequency

domain analysis. Sine sweep signal with frequency components between 2-100 Hz and in accordance with electrical limitations is created to drive the piezoelectric patches. The patches can operate between (+400, -250) voltage range and this limit is taken into account in both simulations and experimental analysis. In experiments one analog output channel of NetdB system is used to generate the signal and it is transmitted to the piezoelectric patches via an amplifier E413.D2 [68] supplied by PI Tech. Setting of the frequency domain analysis is tabulated in Table.2.2

Table 2-2 Settings of the data acquisition system for frequency domain analysis

Analyzer Property	**Value/Type**
Frequency Span	0 Hz - 156 Hz
Sampling rate	51200 Hz
Block size	4096
Number of Averages	50
Averaging mode	Linear
Overlap ratio	50%
Signal Type	Sine Sweep
Frequency component	2 - 100 Hz
Duration of one signal run	50 seconds
Window type	Hanning
Total Duration	300 seconds

In simulations to conduct frequency domain analysis patch is excited by applying surface charge to the top surface of the patch (Fig.2.5 top surface). To obtain transfer functions between applied surface charge to the velocity at the center of the plate , for each frequency between 1 Hz to 100 Hz, unit charge is applied to the piezoelectric patches . Amplitude of the charge is selected as 0.001 for each frequency to stay within the 400-volt

limit of the commercial product. The generated voltage value is checked by measuring generated voltage on the patches during simulations and a potential voltage around 395 volts is generated with these settings on the patches at each frequency. "*Steady-state dynamic, direct"* solver is used to evaluate frequency domain response of the system at the given excitation frequencies. This solver computes response of the system at each frequency increment. In simulations 1 Hz to 100 Hz range is divided linearly into 500 frequency points. The solver computes system response at each 0.2 Hz frequency increment. The increment number and increment size is adjusted by taking into account of both simulation time and accuracy. For each frequency increment, piezoelectric patches' center node's translational and rotational velocities are collected to compare results with the experimental frequency domain analysis.

In addition to the dynamic analysis, modal analysis of the smart plate system is conducted in ABAQUS to conduct model-updating procedure. During model updating procedure corrections are made on steel plate's material properties and damping values. Because in modeling, standard values of material properties are used but in experiment a real steel plate is used and small deviations from standard values are expected. As objective of model updating, modal frequencies and their consistency between simulation and experiment is taken into account. In Table.2.3 obtained modal frequencies in experiment and in simulation are compared.

Table 2-3 Modal frequencies

	Experiment	Simulation	Difference
Mode 1	13.67 Hz	13.190 Hz	% 3.5
Mode 2	27.05 Hz	26.975 Hz	% 0.2
Mode 3	30.08 Hz	26.975 Hz	%10.32

For the first and second mode, very close frequency values are obtained between simulation and experiments, but third mode is found at a higher frequency in experiments and also second and third mode is found at the same frequency in simulations. This is because of the plate geometry and simulation environment. Square geometry is used in simulations and as a result, second and third modes are found at the same frequency. This behavior is not observed in experiments because of not perfect boundary conditions and small geometrical deviations from perfect square shape of the plate. As a result, third mode is found at a higher frequency in experiments. But still close modal frequencies are obtained. Therefore plate model and modified steel properties can be taken as adequate for dynamic analysis.

For electro-mechanical model verification (dynamic analysis), one piezoelectric patch is attached to the center and one is attached to the northwest regions of the plate with respect to the center in both simulations and experimental setup (same geometrical position). In both test environments, frequency response of the system between applied volts (V) to velocity (m/s) is obtained. In experiments, frequency response between applied patch voltage to velocity and in simulation, frequency response between applied patch charges to velocity is obtained. Velocity response of the system is measured at the center of patch in both environments, in collocated orientation. In simulations, frequency response between applied voltages to velocity cannot be directly obtained because ABAQUS only lets user to apply surface charge as electrical load. This results in dB shifts in obtained frequency responses when response for applied per voltage is required instead per surface charge. To obtain frequency response functions between applied voltage and obtained panel velocities, in simulations in addition to the charge to velocity frequency response, charge to voltage frequency response in obtained. For charge to velocity frequency response, system equation is as follows:

$$D(\omega) = H(\omega)Q(\omega) \quad \textbf{(2.27)}$$

where $D(\omega)$ is the resultant panel velocity at the measurement location, $Q(\omega)$ is the applied surface charge and $H(\omega)$ is the transfer function with the unit $(^{(\mathrm{m/s})}/_{q})$. For charge to generated voltage following system equation can be written

$$V(\omega) = G(\omega)Q(\omega) \quad \textbf{(2.28)}$$

where $V(\omega)$ is the generated voltage on the piezoelectric patch due to the applied surface charge $Q(\omega)$ and $G(\omega)$ is the tranfer function with the unit $(^{\mathrm{V}}/_{q})$. By taking invers of the transfer function $G(\omega)$ and inserting into Eq.2.27 one can obtain the transfer function between applied voltages to panel velocities from simulations

$$D(\omega) = H(\omega)G(\omega)^{-1}V(\omega) \quad \textbf{(2.29)}$$

In Eq.2.29, $H(\omega)G(\omega)^{-1}$ is the transfer function between applied voltages to panel velocities with the unit $(^{(\mathrm{m/s})}/_{V})$ .In Fig.2.6 simulated transfer functions $H(\omega)$ and $G(\omega)$ are shown for the patch located at the center the plate.

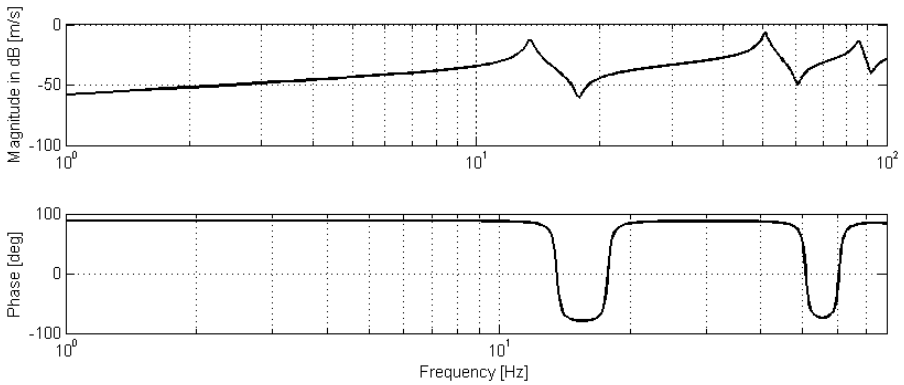

(a)

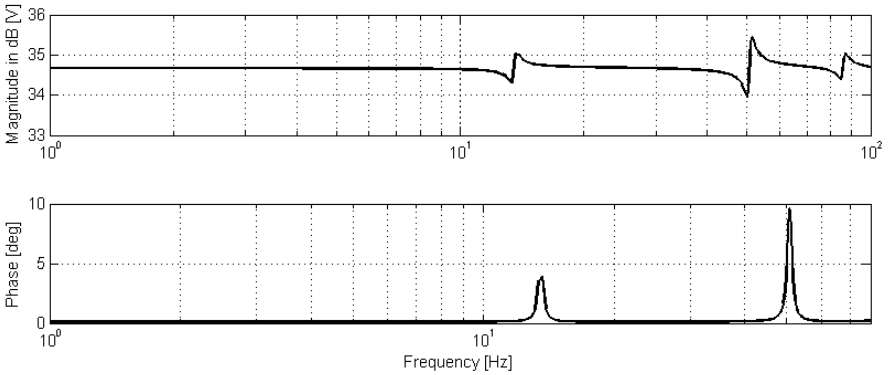

(b)

Figure 2.6 Simulated transfer functions of smart plate system for piezoelectric patch located at center, velocity sensor located at center a) $H(\omega)$ b) $G(\omega)$

Fig.2.7 presents the simulated and experimental frequency responses of the smart plate for the center patch. The simulated response function is calculated by utilizing transfer functions given in Fig.2.6 and using relation in Eq.2.29. In both experiment and simulations, it is observed that the simulated frequency response perfectly fits the experimental response up to the first resonance frequency. Therefore, the simulation model is considered sufficient for investigation of the controller performance at the first resonance frequency.

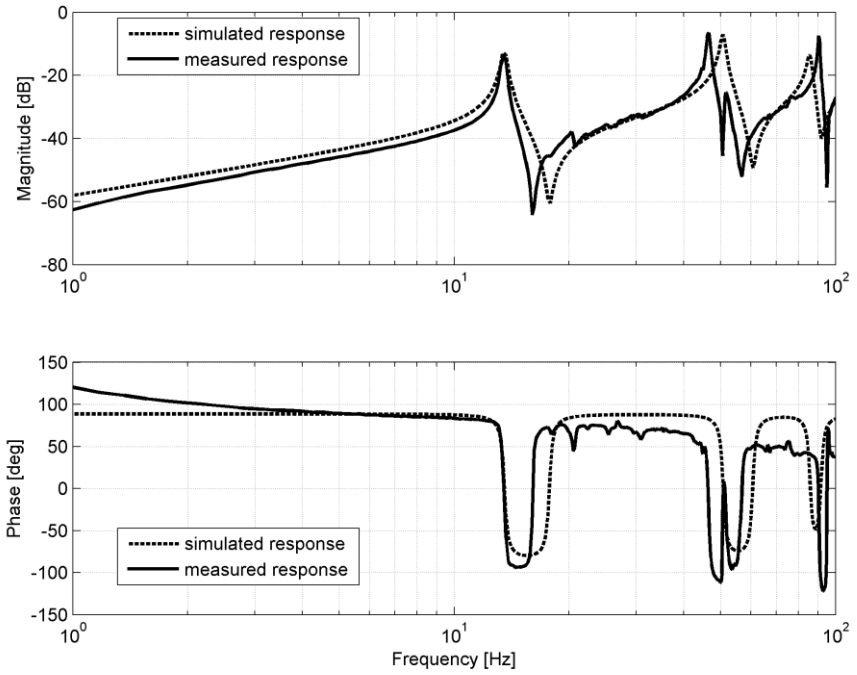

Figure 2.7 Frequency response of smart plate with collocated piezoelectric actuator and velocity sensor at the center section of the plate: simulation (——) and experiment (- - - -)

There is an inconsistency between simulation and experimental results at the higher resonance frequencies. This is because of the not fully-met clamped-clamped boundary conditions assumption in experimental setup and imperfections in steel plate. However, the response magnitudes of these resonance modes and frequency response behavior of both simulations and experiment are quite similar. Because of this similarity, the model can be also used for the optimal positioning investigations in the high frequency range.

This verification procedure is also repeated for a patch placed at the northwest section of the plate. The plate is excited by northwest piezoelectric patch and plate vibrations are measured at the center of the patch. In the experiments, the plate is excited with the patch and velocity of plate is measured with LDV. Again frequency response of the system is

collected between applied piezoelectric patch voltages to generated velocity. In simulations again transfer functions between applied charge to obtained voltage and panel velocities are obtained and transfer function between applied voltages to panel velocities are calculated. Obtained result is presented in Fig.2.8

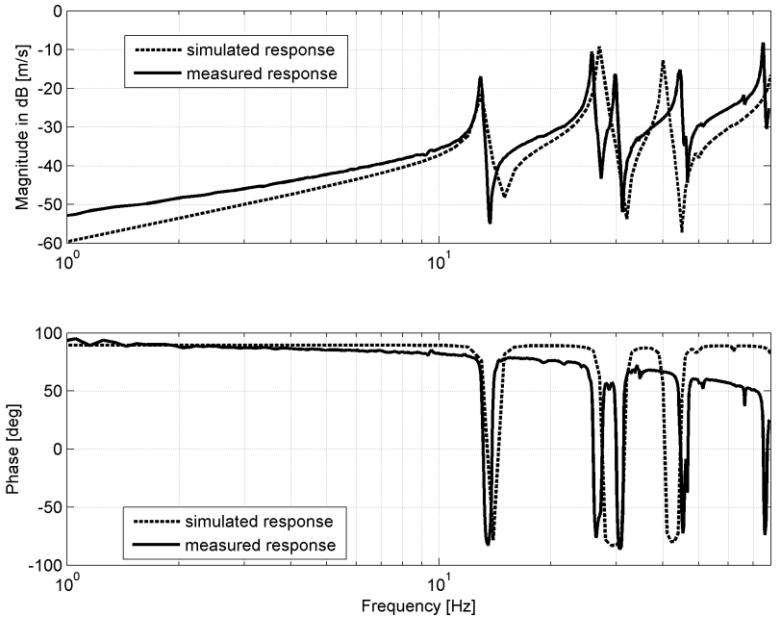

Figure 2.8 Frequency response of smart plate with collocated piezoelectric actuator and velocity sensor at the northwest section of plate: simulation (——) and experiment (- - - -)

Again for experimental and simulation results, it is observed that, up to the first resonance frequency the simulated frequency response is consistent with the experimental response. There is again a shift in higher resonant modes whereas the response magnitudes of these resonance modes and frequency response behavior are quite similar in both simulations and experiment. Because of this similarity, it can be concluded that for different actuator placement locations on the smart plate, simulation model can predict the real experimental response of the smart plate system.

2.6. Optimization for Piezoelectric Patch Locations

The attachment location of piezoelectric actuator patch determines the controller authority of the active vibration system. In this section, the study for determination of optimal locations of piezoelectric actuators on host structure is presented.

2.6.1. Optimization Criteria and Design Variables

To investigate the variation of effectiveness of piezoelectric actuator with attachment locations, two-dimensional grid 11×11 on the surface of the smart plate is defined. The grid points are labeled with numbers between 1 and 121. For an initial study, frequency responses for three different grid points are gathered via attaching the piezoelectric patch over that grid and measuring the velocity of center of the grid point. Fig.2.9.a shows the selected grid points on the smart plate and Fig.2.9.b presents the corresponding measured frequency responses of the smart plate.

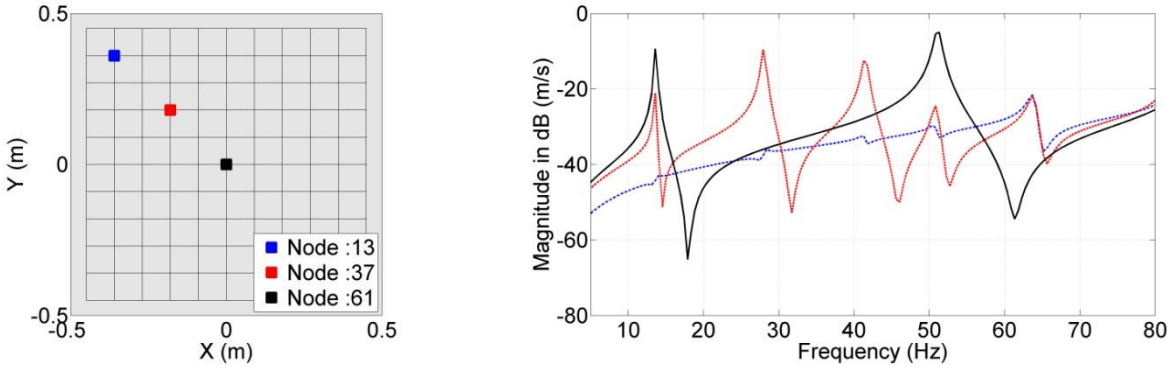

(a) (b)

Figure 2.9 The effect of attachment location on vibration response: (a) The two dimensional grid and selected nodes (b) corresponding frequency responses for node 13 (— _ —), node 37 (- - - -) and node 61 (——)

It is observed that, when the piezoelectric patch is attached at the center (node 61) of the smart plate, the response magnitude of the first resonance mode is maximized as compared to response magnitudes of other attachment nodes. Thus, the maximum curvature of the first mode of a clamped-clamped plate occurs at the center and along the edges, while the center lies on the nodal line for the second and third resonance vibration modes. Because of this fact, the second and third resonance frequencies of the smart plate is not excited when piezoelectric actuator is placed at this center node. These outcomes show that the authority on the certain resonance mode is a measurable quantity or in other words "modal controllability" and it can be considered as the optimization criterion in this thesis.

In section 2.3, the frequency response of the smart plate is formulated in Eq.2.20 and there exists 121 feasible attachment points for the piezoelectric patch on the smart plate. Then, the response of the smart plate for i^{th} actuator location can be obtained from

$$\mathbf{q}_{\mathrm{i}}(\mathrm{j}\omega) = [\,-\omega^2\mathbf{M} + \mathrm{j}\omega\mathbf{C_d} + \mathbf{K}]^{-1}\mathbf{T}_{\mathrm{cf}}\mathbf{Q}(\mathrm{j}\omega) \qquad i \in [\,1{,}121] \tag{2.30}$$

and the relation between the response of the smart plate and applied charge can be represented with a frequency response function $\mathbf{G}_{\mathrm{i}}(\omega)$ where

$$\mathbf{G}_{\mathrm{i}}(\mathrm{j}\omega) = \frac{\mathbf{q}_{\mathrm{i}}(\mathrm{j}\omega)}{\mathbf{Q}(\mathrm{j}\omega)} = [\,-\omega^2\mathbf{M} + \mathrm{j}\omega\mathbf{C_d} + \mathbf{K}]^{-1}\mathbf{T}_{\mathrm{cf}} \tag{2.31}$$

So, the transfer function of the smart plate is $|\mathbf{G}_{\boldsymbol{i}}(\omega_m)|$ at the interested resonance mode m via i^{th} actuator location. By calculating this value for each actuator location, the modal controllability measure λ *is* obtained for each actuator position i and interested mode m as follows

$$\lambda^{\mathrm{i}}{}_{\mathrm{m}} = \frac{\mathbf{G}_{\mathrm{i}}(\mathrm{j}\omega_{\mathrm{m}})}{\max|\mathbf{G}_{\mathrm{i}}(\mathrm{j}\omega_{\mathrm{m}})|} \times 100 \qquad i \in [\,1{,}121] \tag{2.32}$$

The frequency response function for each actuator location is calculated using the finite element model and the optimal location of piezoelectric actuator is found for the vibration modes of interest. In the following section, results of modal controllability analysis are presented.

2.6.2. Optimal Actuator Positions

This section presents the obtained results for optimal location investigation of piezoelectric actuator on the smart plate. Figures 2.10 and 2.11 present the mapping of the modal controllability value over the surface of the smart plate. For instance, for the first resonance mode, optimal location of the piezoelectric patch is the center of the plate, which is presented with 100% modal controllability value in the Figure 2.10a. This result is in accordance with the previous research studies conducted on fully-clamped plate ([22, 23, 78-80]. Fig.2.10.b presents the modal controllability for the second and third resonance modes. Since the smart plate is square, the resonance frequencies of the axis-symmetric modes coincide. As it can be seen from the figure, the centers of quadrants are the most effective positions of actuator for the second and third resonance modes. Fig.2.11.a presents the optimal location for the fourth and fifth resonance modes together and Fig.2.11.b shows the optimal location for the sixth mode.

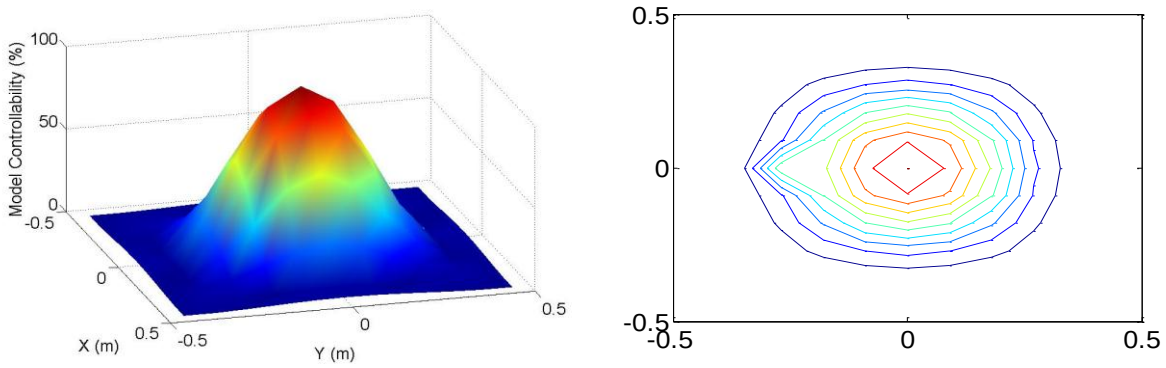

(a) (b)

Figure 2.10.a Piezoelectric actuator patch's control authority for the first resonance mode of the plate: (a) Surface plot (b) contour plot.

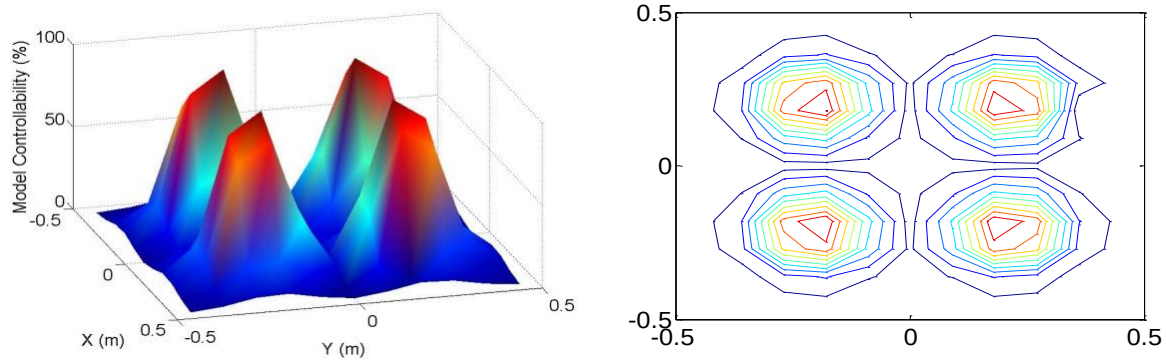

(a) (b)

Figure 2.11.b Piezoelectric actuator patch's control authority for the second and third resonance mode of the plate: (a) Surface plot (b) contour plot.

From Fig.2.10 and Fig.2.11 it can be concluded that modal controllability of piezoelectric patches increases when they are placed on high strain regions on the host structure in the frequency of interest (modal frequency). This result is very clear in second and third mode's modal contribution contour plot. In Fig.2.10.b contribution contour plot highest modal controllability locations are occurred a bit closer to the center of the plate

rather than being exactly at the center of quadrants because fixed boundaries at each side of plate caused high strain regions to shift slightly towards to the center of the plate.

For second and third resonance modes high strains occurred near middle sections of the quadrants because of high displacement amplitudes at these positions during vibration. From Fig.2.10.b it can be concluded that piezoelectric patch actuator has highest control authority on second and third modes when placed near to these regions. From contour plots it can be seen that control authority on these modes diminishes if patch is placed in another position. On the contour plot in Fig.2.10.a and Fig.2.10.b, it is observed that modal controllability is not totally symmetrical on plate surface. This is because of the patch's geometrical shape. Used piezoelectric patches are manufactured in rectangular shapes and patches' dynamic response is not totally identical in all directions. Also patches' anisotropic electro-mechanical properties are not totally symmetrical for each principle coordinates.

From these results it can be concluded that with the used methodology of modal controllability and created FE model; patch locations, geometrical shape and electro-mechanical behaviors are considered in optimization study.

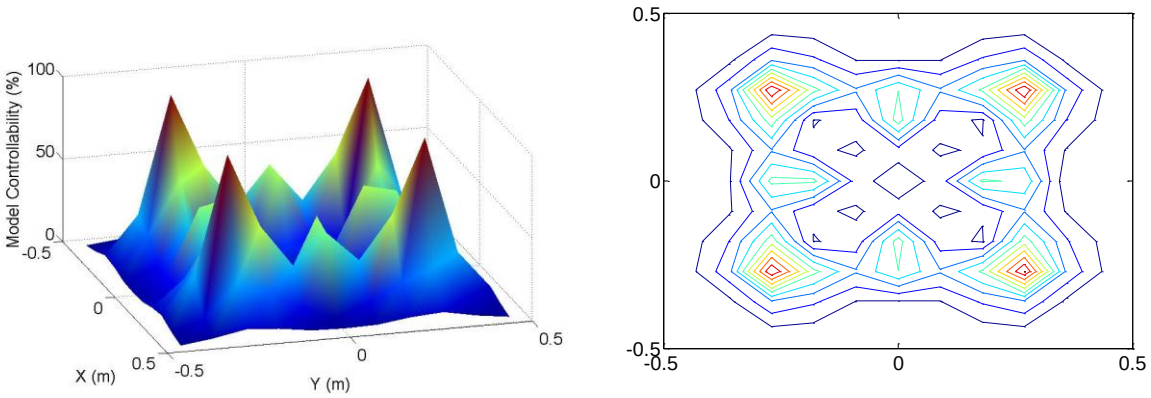

(a) (b)

Figure 2.12.a Piezoelectric actuator patch's control authority for the fourth and fifth resonance modes of the plate: (a) Surface plot (b) contour plot.

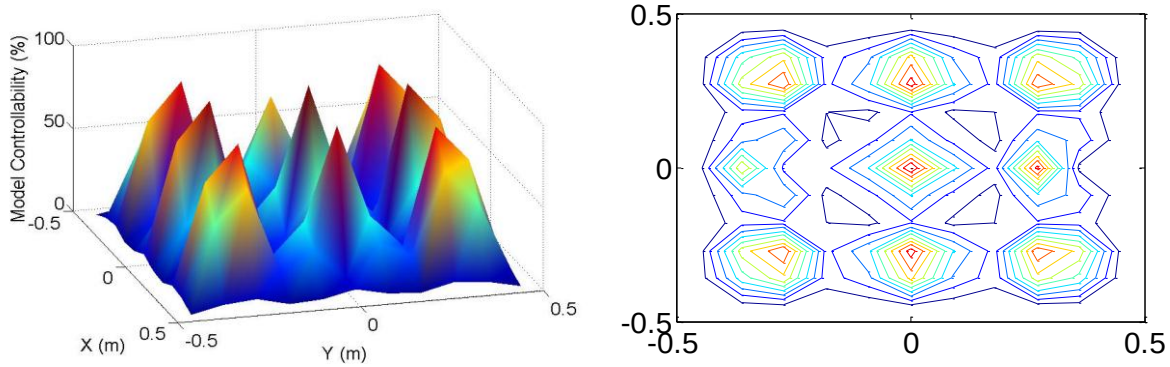

(a) (b)

Figure 2.13.b Piezoelectric actuator patch's control authority for the sixth and seventh resonance modes of the plate: (a) Surface plot (b) contour plot.

2.7. Simulation Studies on Vibration Control

In this section, numerical implementation of velocity feedback controller is presented. The aim of numerical implementation is to investigate the performance of active vibration controller in the design stage. The frequency response functions of the smart plate via piezoelectric actuators are obtained using the finite element model of the smart plate. In the

velocity feedback control simulations, the smart plate system is disturbed from the northwest patch (Fig.2.1.b) and the actuator patch is placed at the center (Fig.2.1.b)

The block diagram in Fig.2.12 shows the implementation in the presence of disturbance. In his block diagram, $\mathbf{D}_i(\omega)$ stands for the frequency response function between the disturbance input (northwest patch) and the velocity of the smart plate at center. The frequency response function for actuator patch (center patch) is shown with $\mathbf{G}_a(\omega)$ for the relation between the actuation signal and velocity at the center of the plate. These disturbance and actuator frequency response functions are summed for the center of the smart plate, since they are in the same-phase for the first resonance mode of the smart plate. Low-pass filter ($\mathbf{G}_f(\omega)$) is included to eliminate the high frequency excitation and it is in the form as follows:

$$\mathbf{G}_f(\omega) = \frac{1}{\sqrt{1 + \left(\omega/\omega_c\right)^{2p}}} \tag{2.33}$$

where p is the filter order, ω_c is the cut of frequency. The general block diagram for the structure and P controller and filter is shown in Fig.2.12.

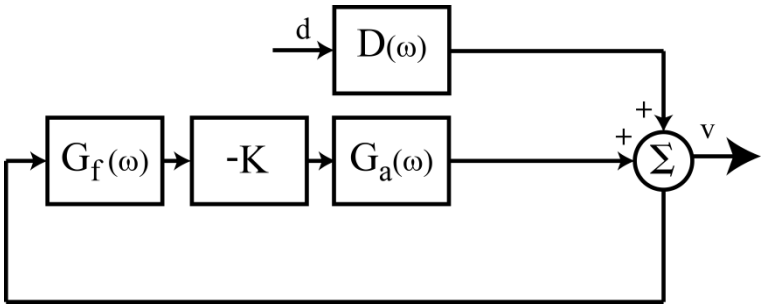

Figure 2.14 Numerical model of velocity feedback controller

From Fig.2.12 the closed-loop frequency response function $G_{cl}(j\omega)$ of the smart plate between the input disturbance d and the velocity *v* of the smart plate is obtained as:

$$G_{cl}(\omega) = \frac{v}{d} = \frac{D_d(\omega)}{1 + KG_f(\omega)G_a(\omega)} \quad \textbf{(2.34)}$$

where *K* is the proportional gain which is the tunable parameter for closed-loop system. To investigate the closed-loop system response at the first resonance mode, closed-loop numerical simulations are conducted and vibration attenuation levels for various velocity feedback controller gains are estimated by using this numerical model. Obtained numerical closed loop simulation results are compared with results obtained from experimental setup. The frequency response function for actuator patch (center patch) shown with $\mathbf{G_a}(\omega)$ is shown in Fig.2.7. The frequency response function for disturbance patch is obtained via applying voltage to the northwest patch and measuring plate response at the center of the plate. The measured and simulated frequency responses are shown in Fig.2.13

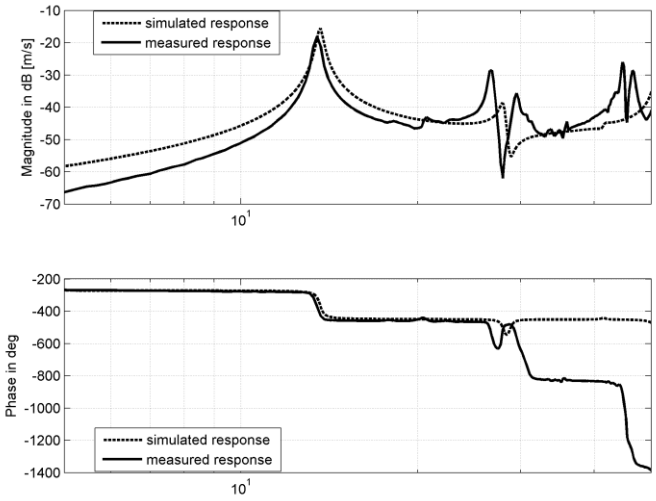

Figure 2.15 Frequency response of smart plate with piezoelectric actuator at the northwest and velocity sensor at the center section of the plate: simulation (——) and experiment (- - - -) ($D_i(\omega)$)

2.8. Experimental Studies on Vibration Control

This section presents experimental implementation of the velocity feedback controller. The experimental set-up for active vibration control system for the smart plate is presented in Figure 2.14. In this set-up, the signal generator stands as the source of disturbance signal. The programmable controller (NI-PCI-6229 Data Acquisition System [69]) is included for digital controller implementation and signal analyzer is used to calculate and record response of the smart plate. Smart plate has two piezoelectric patches, which are named as disturbance patch at the northwest (-0.35m, 0.35m from the left upper corner) and actuator patch at the center. High voltage amplifiers are also included in experimental set-up to amplify and drive the piezoelectric patches. Laser Doppler Vibrometer is the vibration sensor and connected to programmable controller and signal analyzer for creation of controller output signal and record. This set-up will be used for first resonance forced vibration suppression and the results are compared with simulation results.

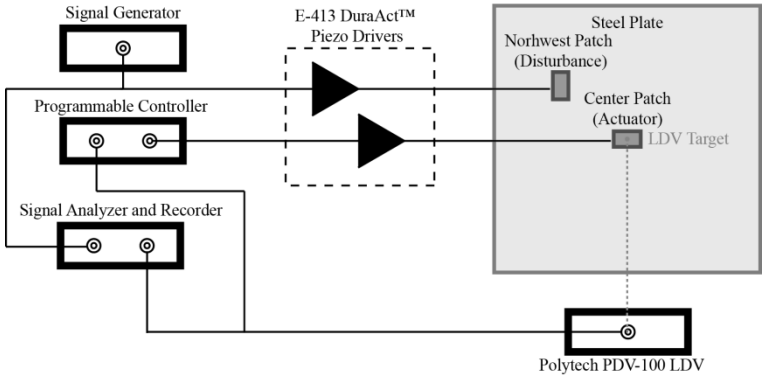

Figure 2.16 Experimental Setup

2.9. Results

The simulations are conducted for the smart plate in the presence of disturbance. Surface charge load applied to the disturbance in the bandwidth of 2 *Hz* to 100 *Hz* and the vibration of the smart plate is measured at the center of the plate. Monitoring the open loop and closed-loop response of the plate, vibration attenuation levels are determined for the first resonance mode (13.65*Hz*). The open loop corresponds to the case where the controller is inactive and the actuator patch is passive whereas the closed-loop indicates the condition where the controller is active and the measured velocity is fed back to the actuator patch after multiplication and filtering.

For simulations, frequency response functions for the disturbance and actuator patches are utilized. These frequency response functions are gathered using finite element model as described (Fig.2.7- actuator model, Fig.2.13- disturbance model). By defining the cut-off frequency of the low pass filter is 30.78 *Hz*, the closed-loop frequency response function of the smart plate is estimated via the formulation given in Eq.2.34. The proportional gain *K* is selected as 3, 5 and 7 respectively. As can be seen from Fig.2.15, the open-loop response of the smart plate is -15*dB* at the first resonance frequency. In the closed-loop case, this response magnitude is attenuated to -20, -22 and -24 *dB* for each controller gain.

In addition to first mode vibration suppression is also achieved for sixth resonance frequency. The open loop response of the smart plate is -30dB at the sixth resonance frequency. In the closed-loop case, this response magnitude is also attenuated to -34, -36, -38, dB for each controller gain. However, for second and third resonance frequencies center position has very low control authority which is also suggested in modal controllability results in Fig.2.10.b and in numerical simulations this result also proven. In Fig.2.15, it can be seen that no suppression is achieved around second and third resonance frequencies with the actuator located at the center of the plate consistent with the obtained results using modal controllability theory.

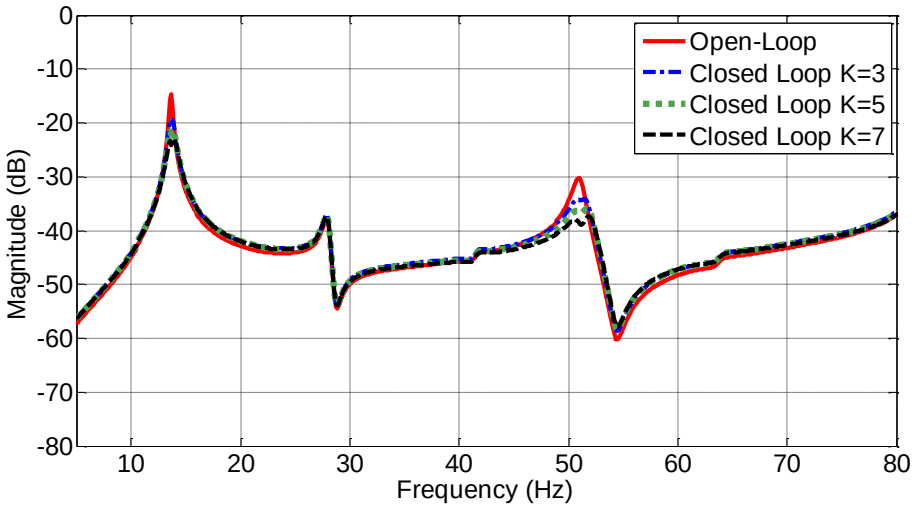

Figure 2.17 Open and closed loop simulated responses of smart plate.

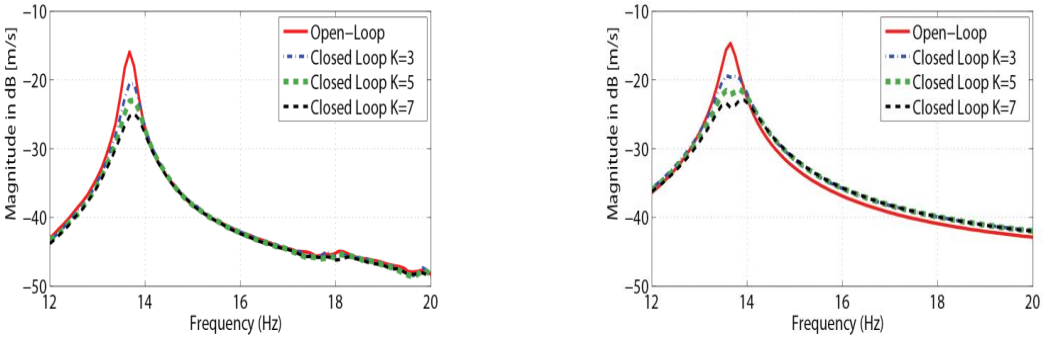

(a) (b)

Figure 2.18 Open and closed loop responses of the smart plate (a) the simulated first resonance frequency (b) the experimental first resonance frequency. The legends are as follows: open-loop (——), closed-loop with K=3 (-.-), closed-loop with K=5 (……..),closed-loop with K=7 (– – –).

Obtained suppression levels for the first resonance frequency for various controller gains are compared with experimental results. Comparison is only conducted for this frequency because simulated frequency responses are consistent with the actual response

up to first resonance frequency, for higher frequencies there are shifts in the response (Fig.2.7, Fig.2.8 and Fig.2.13). In Fig.2.16 for the first resonance mode open and closed loop response of the plate for numerical and experimental simulations are presented.

The simulation and experimental results of vibration suppression of the smart plate are provided in Table.2.4. From obtained results it can be concluded that the closed-loop simulation and experimental results are very similar. Therefore, the closed-loop simulation results are accurate to verify the simulation model since the experimental vibration suppression results are precisely estimated for various velocity feedback gains.

Table 2-4 Vibration suppression results

	Simulations		Experiments	
Feedback Gain (K)	In dB	In Percentage	In dB	In Percentage
3.00	4.94	43.83%	4.60	41.12%
5.00	7.45	57.59%	7.17	56.20%
7.00	9.40	66.12%	9.37	66.00%

2.10. Conclusion

In this chapter, Finite element methods are utilized to generate an accurate model of a smart plate system. For the smart plate system, piezoelectric patches are used as actuator. To model the system, an electro-mechanical coupled FE model is build. The model is verified by comparing obtained panel response from simulations and experiments for two different patch attachment locations (northwest, center). Using FE model, plate response is successfully estimated and simulated frequency responses fit perfectly to the actual response up to first resonance frequency. A shift between simulation and experimental results at the higher resonance frequencies is found and this is because of the imperfections in experiments. However, the response magnitudes of these resonance modes and frequency response behavior of both simulations and experiment are quite similar. Because

of this similarity, the model is used for the optimal positioning investigations. For optimal positioning, modal controllability theory is utilized and for panel resonance frequencies, optimal attachment points for the piezoelectric patches are determined. Obtained results are verified by conducting active vibration control simulations and active vibration control experiments. From simulations and experiments modal controllability results are verified and expected closed-loop behavior for the system is obtained.

Chapter 3

ACTIVE CONTROL OF COMPLEX 3D SHELL STRUCTURE FOR LOCAL AND GLOBAL VIBRATION SUPPRESSION

3.1. Introduction

Shell structures are commonly used in the automotive, aerospace and marine applications and vibrations of these structures can cause malfunction of the whole system or failure of certain components. In this paper, a new design methodology for local and global vibration control is developed for a 3D shell structure with complex geometry and complex boundary conditions. The objective of the local vibration control is to reduce vibration energy at the sensor location whereas the objective of the spatial vibration control is to reduce vibration over the entire structure. In order to achieve effective vibration suppression of the structure, local and global performance indices are defined and used for the optimization of sensor/actuator position as well as the controller parameters. The methodology is applied to suppress vibrations on the front panel of a vehicle as a case study where the engine mount extensions are attached. A finite element model of this the structure is created and used for the frequency response analysis in the presence of operational disturbances. Then, local and global optimization studies are carried out for positioning the sensor/actuator pair and parameter tuning of the controller. By comparing controller active and inactive cases, the vibration suppression performance of the controller is demonstrated locally and globally. This chapter is organized as follows: Section 2 introduces modeling theory and definition of the frequency response functions for the 3D complex panel. Section 3 describes the developed methodology for the local vibration suppression and optimization, Section 4 focuses on global vibration suppression and

optimization. Section 5 presents the case studies, while introducing the finite element model of an example 3D complex panel. At last, Section 6 concludes the chapter.

3.2. Modeling and Controller Design for a Complex Structure:

In this section, finite element theory for modeling the complex structure and derivation of structural frequency response functions are presented. Then the controller design for this type of structure for local and global vibration suppression is explained with the methodology used for optimizing the actuator position and controller parameters.

3.2.1. Modeling Theory

For a linear, elastic, time-invariant complex structure with n degrees of freedom, equation of motion using the finite element modeling theory can be written as

$$\mathbf{M}\ddot{x}(t) + \mathbf{C}\dot{x}(t) + \mathbf{K}x(t) = \mathbf{F}(t) \tag{3.1}$$

where **M**,**C** and **K** are the $n \times n$ mass, damping and stiffness matrices of the structure and **F**(t) is the $n \times 1$ vector of applied external forces on the structure. **x** (t) is the $n \times 1$ vector of the structure's response to the externally applied force.

For a harmonic external input of the form

$$\mathbf{F}(\omega) = \mathbf{f}(\omega)e^{i\omega t} \tag{3.2}$$

displacement of the system has the corresponding form

$$\mathbf{X}(\omega) = \mathbf{x}(\omega)e^{i\omega t} \tag{3.3}$$

where ω is the excitation frequency of the external loading on the structure. By using Eq.3.1, input-output relationship (frequency response representation) of the system is as follows

$$\mathbf{X}(\omega) = \mathbf{H}(\omega)\mathbf{F}(\omega) \tag{3.4}$$

where the transfer function $\mathbf{H}(\omega)$ is

$$\mathbf{H}(\omega) = (-\omega\text{^}2\,\mathbf{M} + i\omega\mathbf{C} + \mathbf{K})^{-1} \tag{3.5}$$

Using the modal coordinate transformation, response of the structure to a unit harmonic load in the frequency domain can be expressed as [70]

$$\mathbf{H}_{k,j}(\omega) = \sum_{r=1}^{n} \frac{\phi_{kr}\phi_{jr}}{{\omega_r}^2 - \omega^2 + i2\zeta_r\omega_r\omega} \tag{3.6}$$

In Eq.3.6, $\mathbf{H}_{k,j}(\omega)$ is the transfer function between the displacements of the k_{th} degree of freedom in response to the applied forces to the j_{th}degree of freedom. ϕ_{kr} is the modal vector corresponding to the measurement points and ϕ_{jr} is the modal vector corresponding to the excitation points. r is the mode shape, ω_r is the mode excitation frequency and ζ_r is the mode's damping factor.

Using the relation in Eq.3.6, complex panel's response in the velocity form is as follows

$$\mathbf{V}_{k,j}(\omega) = \sum_{k=\mathrm{r}}^{n} \left[\frac{\phi_{kr}\phi_{jr}}{{\omega_r}^2 - \omega^2 + i2\zeta_r\omega_r\omega}(i\omega)\right] \tag{3.7}$$

Using Eq.3.7, velocity response at any degree of freedom ($\mathbf{V}_{k,j}(\omega)$) of the complex panel in the presence of any external loading at any degree of freedom, for each frequency ω can be obtained.

3.2.2. Controller Design and Actuation

The implementation of the vibration control system to the complex structure will introduce an additional external force, which is generated by the controller. So, the complex structure will be under the influence of both external disturbances and the controller actuator force. For a complex structure with complex boundary conditions, model-independent controller algorithms can be preferred since these algorithms are well-established, practical and efficient for structural vibration control. In addition, these controllers do not require any plant parameters and can be optimized to maximize the vibration energy reduction. For that reason, proportional-integral (PI) controller is suitable for implementation (Eq.3.8), which simply generates the controller output signal by considering the displacement and velocity response of the structure [71].

$$\mathbf{G_c}(i\omega) = \mathrm{K_p} + \frac{\mathrm{K_i}}{i\omega} \tag{3.8}$$

In Eq.3.8, $\mathbf{G_c}$ is the controller transfer function, K_p is the velocity feedback gain and K_i is the position feedback gain**.** Basically, the velocity feedback adds damping to all modes while displacement feedback provides additional damping in the low frequency range. Besides, it was shown that a collocated sensor/actuator pair and a low pass filter is enough to ensure the robustness of the system [48]. Therefore, in this study a collocated ideal point force actuator and a velocity sensor is used and a low-pass filter is included to confine the sensor signal in the bandwidth of the interested frequency range. The generalized equation for n^{th}order filter is given in Eq.3.9

$$\mathbf{G}_f(\omega) = \frac{1}{\sqrt{1 + \left(\omega/\omega_c\right)^{2p}}} \tag{3.9}$$

where p is the filter order, ω_c is the cut of frequency. The general block diagram for the structure and P-I controller and filter is shown in Fig 3.1.

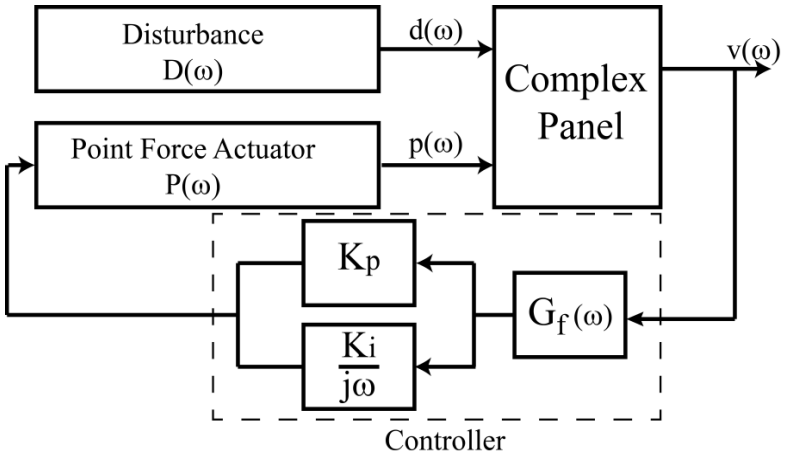

Figure 3.1 General block diagram of the vibration control system for complex structure

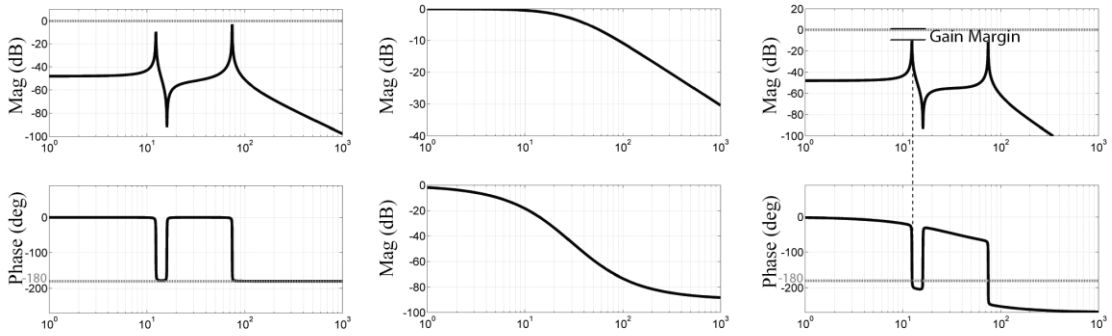

(a) (b) (c)

Figure 3.2 Representative bode plots a) Collocated transfer function b) Low-pass Filter c) Open-loop transfer function

For a collocated actuator and sensor representative transfer function is presented in Fig.3.2.a [72]. In collocated configuration, the phase of the response will be obtained between 0^o and -180^o and system will be unconditionally stable. However, with filter

implementation, (Fig.3.2.b) additional phase is introduced to the system and system phase will no longer be confined between 0^o and -180^o (Fig.3.2.c). This will result a gain margin for the system (Fig.3.2.c) and requires optimization of control gain parameters to guarantee system stability and performance. The selection and optimization of the controller parameters (feedback gains), for local and global vibration suppression is explained in the following sections

3.3. Design Methodology for Local Vibration Suppression

This section presents the design methodology of the feedback controller for suppressing the vibration of the complex panel at the sensor/actuator location. The motivation of the methodology is to optimize the sensor and actuator position on the body and controller parameters for the maximization of local vibration suppression of the complex structure.

3.3.1. Simulation Method for Local Performance Evaluation

The local vibration suppression of the complex structure is performed by the frequency response analysis. Fig. 3 presents the block diagram for the analysis.

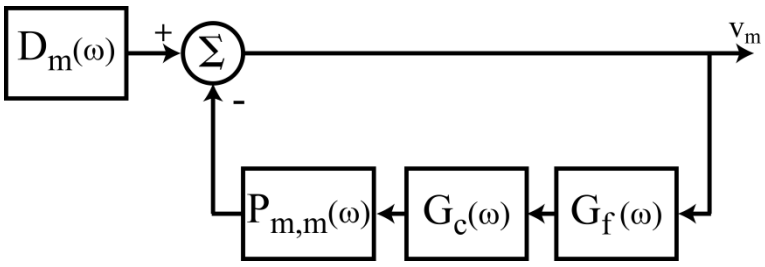

Figure 3.3 Block diagram for the closed-loop frequency response analysis

In this diagram, v_m represents the velocity of the complex structure measured at sensor/actuator (Local) location. The m subscript denotes to the local output degree of freedom. $\mathbf{D_m}(\omega)$ Stands for the open-loop frequency response of the complex panel at the degree of freedom m in the presence of disturbance applied to the external degree of freedom j. Using Eq.3.7, it has the form

$$\mathbf{D}_m(\omega) = \mathbf{V}_{m,j}(\omega)\mathbf{F}_{\mathrm{j}}^{\mathbf{e}}(\omega) \tag{3.10}$$

In Eq.3.10, $m \in \boldsymbol{N_p}$ where $\boldsymbol{N_p}$ is the output degrees of freedom on complex panel and $\mathbf{F}_{\boldsymbol{j}}^{\mathbf{e}}(\omega)$ is applied external disturbances to the degrees of freedom *j*, where $j \in \boldsymbol{N_e}$ and $\boldsymbol{N_e}$ is the degrees of freedom where external disturbance is applied. On the complex panel in addition to the external disturbances, actuator generates external loading effect. Using Eq.3.7, response of the m_{th} degree of freedom with respect to actuator input to the degree of freedom k is derived as

$$\mathbf{P}_{k,m}(\omega) = \mathbf{V}_{k,\mathrm{m}}(\omega)\mathbf{F}_m{}^{\mathbf{a}}(\omega) \tag{3.11}$$

To obtain transfer function between actuator and panel response, unit force at each frequency is applied to complex panel, $\boldsymbol{F_m}^{\boldsymbol{a}}(\omega)$ and response between applied unit forces to complex panel velocities are obtained. For control actuation, notation $\mathbf{P}_{m,m}(\omega)$ is used to represent the transfer function between the collocated sensor and actuator pair at any degree of freedom. $\left(\ k \in \boldsymbol{N_p},\ m \in \boldsymbol{N_p},\ k = m\right)$ $\mathbf{P}_{k,m}(\omega)$ notation is used for other degrees of freedom $\left(\ k \in \boldsymbol{N_p},\ m \in \boldsymbol{N_p},\ k \neq m\right)$

$\mathbf{G_c}$ and $\mathbf{G_f}$ are the controller and band-pass filter frequency responses, respectively. Then, the closed-loop frequency response $\mathbf{G_{cl,k}}(\omega)$ between the velocity v and disturbance input d for each degree of freedom k on the structure can be obtained as:

$$\mathbf{G_{cl,m}}(\omega) = \frac{\mathbf{D_m}(\omega)}{\mathbf{1} + \mathbf{G_c}(\omega)\mathbf{G_f}(\omega)\mathbf{P_{m,m}}(\omega)} \quad \textbf{(3.12)}$$

$\mathbf{G_{cl,m}}(\omega)$ is the closed loop frequency response of complex panel at the local sensor/actuator location m, in the presence of external disturbance $\mathbf{D}_m(\omega)$ and collocated actuator control effect $\mathbf{P}_{m,m}(\omega)$. This equation states that the minimization of the effect of external disturbances on any node of the structure can be achieved by minimizing the closed-loop frequency response at that degree of freedom. This minimization can be achieved by placing the collocated sensor/actuator pair at that location and proper parameter tuning of the controller.

3.3.2. Optimization of Local Vibration Suppression

This section presents the optimization methodology for local vibration suppression whose objective is to minimize vibration energy at the sensor/actuator location. As explained in the former section, the local vibration reduction can be achieved by minimizing the closed-loop frequency response at the sensor location. However, for the optimal suppression value, the difference between the open-loop and close-loop frequency response for a particular frequency is important. The H_2 norm of the open and closed loop transfer functions for the local sensor/actuator point is derived to obtain response characteristics of complex panel at the m^{th}sensor location.

$$\alpha_m{}^L = \left\|\boldsymbol{D_m}(\omega_p)\right\|_2^2 = \left(\frac{1}{2\pi}\right)\int_{-\infty}^{\infty}\left|\boldsymbol{D_m}(\omega_p)\right|^2 d\omega \quad \textbf{(3.13)}$$

$\alpha_m{}^L$ is the H_2 norm of the open-loop transfer function of the system at m^{th}sensor location and includes characteristics of measured response of the complex system.

$$\gamma_m^L = \left\|\mathbf{G_{cl,m}}(\omega_p)\right\|_2^2 = \left(\frac{1}{2\pi}\right)\int_{-\infty}^{\infty}\left|\mathbf{G_{cl,m}}(\omega_p)\right|^2 d\omega \quad \textbf{(3.14)}$$

γ_m^L is the H_2 norm of the closed-loop frequency response of the system measured at m^{th} sensor/actuator location and includes characteristics of measured response of the complex system. By taking difference of the open and closed-loop norms, controller performance characteristics are evaluated for a specific frequency band ω_p. To maximize and determine an optimal value for this difference, we define a local performance index ${\beta_m}^L$ as follows:

$${\beta_m}^L = \frac{\alpha_m^L - \gamma_m^L}{\Gamma_m} \times 100\% \qquad \Gamma_m = max(\alpha_m^L - \gamma_m^L) \quad \textbf{(3.15)}$$

In this equation, Γ_m is the normalization value and used to evaluate the performance of control action on the complex panel for each configuration. The close-loop response of panel is depended on sensor/actuator location m, controller parameters K_p, K_i and frequency band of interest ω_p. Therefore, with an optimization algorithm the most effective sensor/actuator location and control gains can be obtained. The maximization of the local performance index β_m^L, gives the optimal location of the collocated sensor/actuator pair and the optimal parameter setting of the controller.

3.4. Design Methodology for Global Vibration Suppression

In this section, the design methodology of the feedback controller is explained for suppressing vibration over the entire structure. In local performance evaluation section, the local performance index includes the characteristics of the complex panel in close-loop case for the collocated sensor/actuator location. In contrast to the design methodology for

local vibration suppression, the objective in global optimization is to optimize the collocated sensor and actuator position and controller parameters for the maximization of spatial vibration suppression of the complex structure. First, the simulation model for the spatial performance evaluation is described and then global vibration suppression method is presented.

3.4.1. Simulation Method for Global Performance Evaluation

The frequency response analysis is conducted for performance evaluation of global vibration suppression of the complex structure. In Fig.3.4.a and 3.4.b, block diagrams for the global analysis is presented.

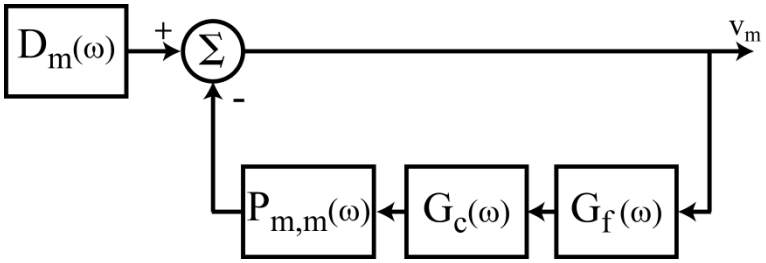

Figure 3.4.a Block diagram for the closed-loop frequency response analysis at the sensor/actuator node

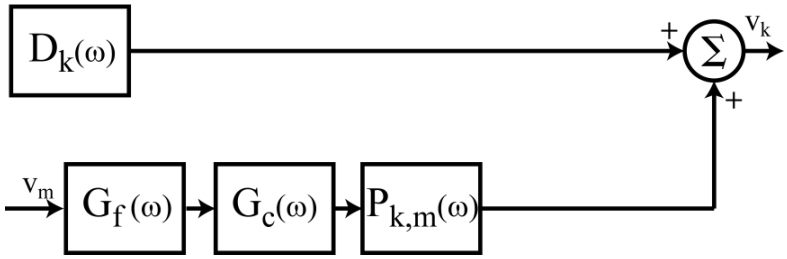

Figure 3.5.b Block-diagram for the closed-loop frequency response analysis at the other nodes (excluding the sensor/actuator node) of the structure

As opposed to local vibration suppression case (Fig.3.3), the block diagram is divided into two parts: the first part (Fig.3.4.a) is used for the simulation of the vibration response at the collocated sensor/actuator degree of freedom, (k=m) and the second part (Fig.3.4.b) is considered for the simulation of the vibration response at other degrees of freedom, ($k \neq m$) on the complex structure. In these diagrams, $\mathbf{D}_k$ is the disturbance frequency response and v_k represents the velocity of the complex structure likewise in the local vibration suppression case. The transfer function $\mathbf{P}_{k,m}$ is between the sensor/actuator node m and other output degrees of freedom k on the complex panel for global evaluation.($k \in \boldsymbol{N_p},\ m \in \boldsymbol{N_p},\ k \neq m$) Refer to section 3.1. Then, the closed-loop global frequency response of complex panel $\widehat{\mathbf{G}}_{\mathbf{cl,k}}(\boldsymbol{\omega})$ between velocity v and disturbance input d can be obtained as:

$$\widehat{\mathbf{G}}_{\mathbf{cl,k}}(\boldsymbol{\omega}) = \begin{cases} \dfrac{\mathbf{D_m}(\omega)}{\mathbf{1} + \mathbf{G_c}(\omega)\mathbf{G_f}(\omega)\mathbf{P_{m,m}}(\omega)} & k = m \\ \mathbf{D_k}(\omega) + \mathbf{v_m}\mathbf{G_c}(\omega)\mathbf{G_f}(\omega)\mathbf{P_{k,m}}(\omega) & k \neq m \end{cases} \quad \textbf{(3.16)}$$

In this equation, subscript m denotes the degree of freedom on the complex panel where sensor/actuator pair is positioned and k is the output degrees of freedom on complex panel for global behavior. For the collocated sensor/actuator arrangement, Eq.3.12 is used to obtain response of the panel at the local sensor/actuator location. However, local information does not include global response. For other degrees of freedom on the complex panel($k \neq m$), close-loop behavior of system is determined by using the system model in Fig.3.4.b. With this approach, Eq.3.12 is extended and close-loop equation of the global response $\widehat{\mathbf{G}}_{\mathbf{cl,k}}(\omega)$ is obtained as in Eq.3.16. This equation states that the minimization of the effect of external disturbances at any node of the structure (where the sensor/actuator pair is placed) can be achieved by minimizing the local closed-loop frequency response (Eq.3.12). However, the closed-loop frequency responses at the other nodes of the structure

are directly affected by the control actuation due to the local vibration suppression (Eq.3.16). Therefore, in order to achieve a global vibration suppression of the structure, the minimization of both local and global closed-loop responses is required. This optimization can be achieved by placing the collocated sensor/actuator pair at the optimum location and parameter tuning of the controller by defining a global performance index.

3.4.2. Optimization of Global Vibration Suppression

In this section, the optimization methodology for global vibration suppression is presented. The objective of global suppression is to reduce vibration energy over the entire structure. As explained in the former sections, the local vibration reduction can be achieved by minimizing the closed-loop frequency response at the sensor/actuator location, however for global vibration suppression, it is not sufficient. The closed-loop frequency response at the other degrees of freedom (excluding the sensor/actuator node) must be also considered in the optimization algorithm. So, to achieve an optimal suppression value over the entire structure, the difference between the open-loop and closed-loop frequency response for a particular frequency at all nodes is required. To satisfy this requirement, a global performance is defined index ${\beta_k}^G$ as follows:

$$\alpha_k = \left\|\boldsymbol{D_k}(\omega_p)\right\|_2^2 = \left(\frac{1}{2\pi}\right)\int_{-\infty}^{\infty}\left|\boldsymbol{D_k}(\omega_p)\right|^2 d\omega \qquad \textbf{(3.17)}$$

$${\gamma_k}^G = \left\|\widehat{\boldsymbol{G}}_{\boldsymbol{cl_k}}(\omega_p)\right\|_2^2 = \left(\frac{1}{2\pi}\right)\int_{-\infty}^{\infty}\left|\widehat{\boldsymbol{G}}_{\boldsymbol{cl_k}}(\omega_p)\right|^2 d\omega \qquad \textbf{(3.18)}$$

$${\beta_k}^G = \frac{\alpha_k - {\gamma_k}^G}{max(\alpha_k - {\gamma_k}^G)} \qquad \textbf{(3.19)}$$

In the equations, k is the output degree of freedom on the structure, ω_p is the particular frequency range and $\|\cdot\|_2$ denotes the two-norm of the frequency response vectors for the frequency range selected. The global performance index differs from the local performance index in the calculation of the closed-loop response. For the global vibration suppression, Eq.3.12 is used for calculation of the closed-loop response at the sensor/actuator node ($k = m$), and Eq.3.16 is used for closed-loop response analysis at the other nodes ($k \neq m$). The maximization of the global performance index (Eq.3.19) provides the optimal location for the collocated sensor/actuator pair and optimal parameter setting of the controller for the entire vibration suppression of the complex panel. The optimization algorithm is summarized with a flow chart in Fig.3.5.

The optimization algorithm (Fig.3.5) evaluates all configurations on the complex panel and determines the best configuration based on the defined performance indexes. The algorithm uses extended close-loop response equation to include global behavior of the complex structure.

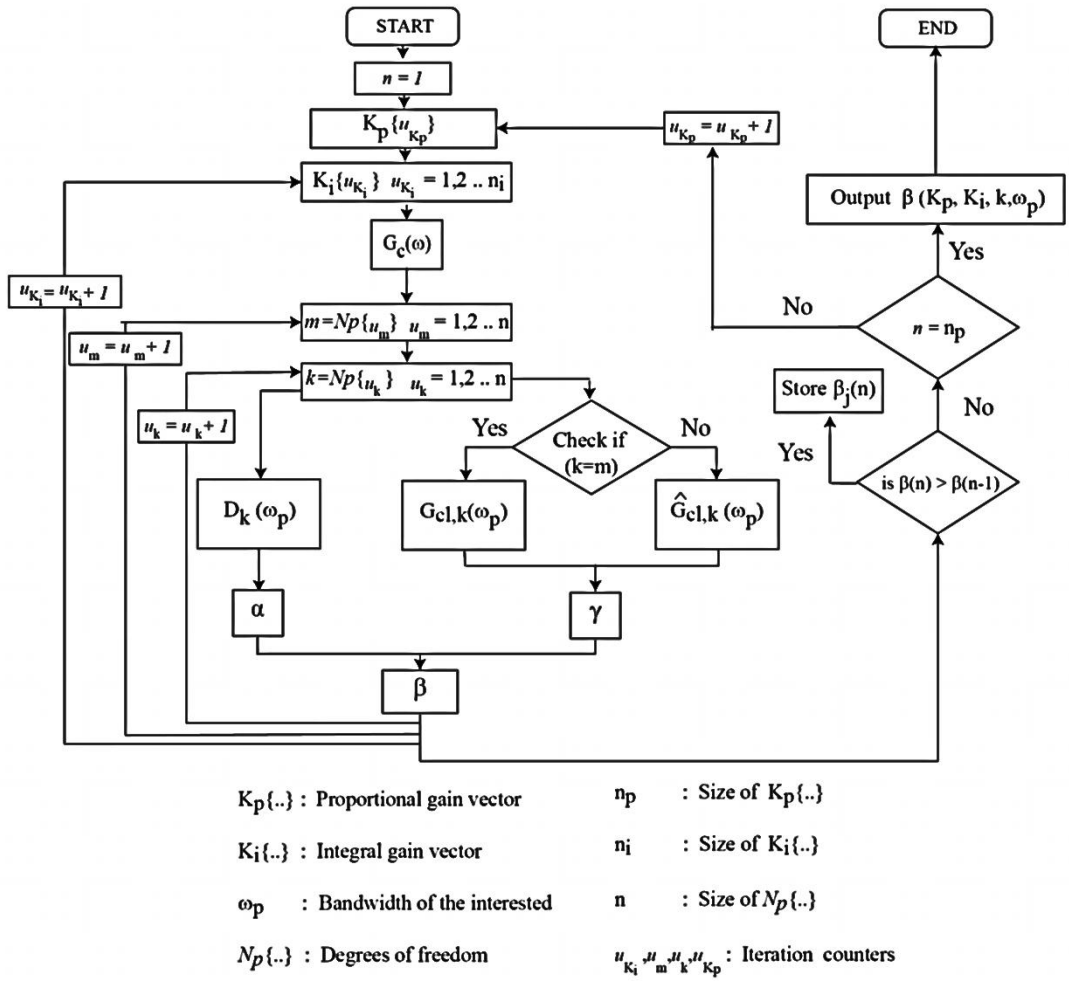

Figure 3.6 Flow-chart for determination of the control gains and actuator location for local and global vibration control

For a particular frequency of interest ω_p, the algorithm determines the optimal degree of freedom for collocated actuator/sensor pair from the defined degrees of freedom, $\mathbf{N_p}$ on the complex panel and the controller parameters; K_p proportional gain and K_i integral gain. With the optimization procedure also system stability is ensured for the determined gains. For unstable cases, performance index will return a very low value and would not be stored by the algorithm.

3.5. Active Vibration Control Case Study

This section presents the case studies to demonstrate the applicability of the methodology for a complex panel. At first, finite element model of the complex panel system and external disturbance model are presented. Design study for local vibration suppression is carried out and the optimal placement of sensor/actuator pair is investigated. Then, the methodology for the global vibration suppression is utilized for optimal placement of sensor/actuator pair and parameter tuning of the controller.

3.5.1. Modeling and Controller Design for a Complex Structure:

In this section, first, the finite element model of the complex structure is presented. Then, the frequency response analysis results in the presence of external disturbance are explained and the controller design for this type of structure is presented.

3.5.1.1. Finite Element Model:

The complex structure considered in this study is a chassis panel of a real-sized vehicle (Fig. 3.6). The vibration suppression of this panel is aimed because it is directly connected to the engine extensions of vehicle and standing between the passenger cabin and the engine compartment. In the presence of mechanical and acoustical excitation in the engine compartment, the front panel transmits the vibration and noise to the passenger cabin. Therefore, by attenuating the vibration of the front panel, the transmission of the vibration energy to the other panels can be decreased. However, the front panel has geometrical variations in all directions with complex boundary conditions, so it cannot be simplified as a simple plate-like structure for design of active treatments.

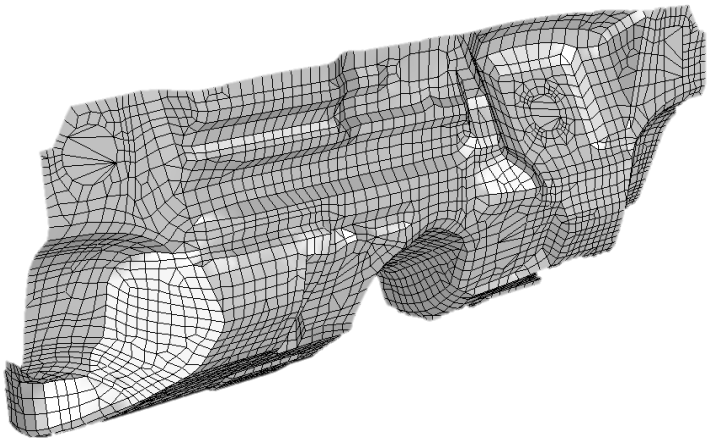

Figure 3.7 Finite element model of the complex panel structure

To investigate the vibration characteristics of the complex structure for the controller design and analysis, the finite element model is built for NASTRAN environment. The dynamic characterization is carried out with frequency response analysis for distributed locations ($\mathbf{N_p}\{..\}$ *see* 3.1) presented with a two-dimensional grid (19 X 7 points) on the complex structure (Fig.3.7.b). The distributed array is utilized to obtain spatial response characteristic of complex panel.

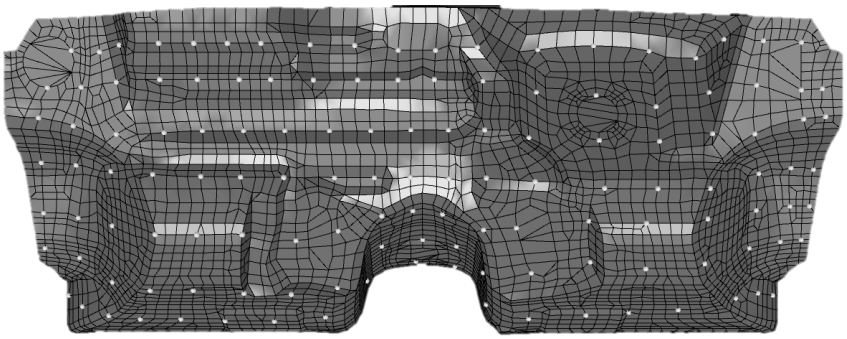

Figure 3.8.a Corresponding position of output degrees of freedom on the complex structure

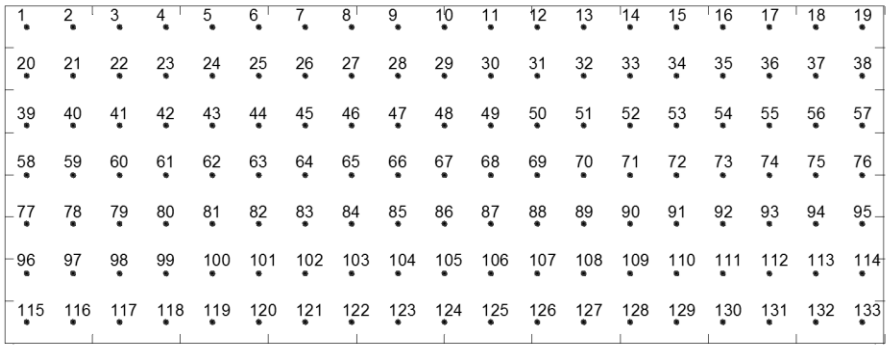

Figure 3.9.b Labeling of the set of considered degrees of freedom selected on the complex structure for the case study

3.5.1.2. External Disturbance Model

The vibration of the complex structure is caused by the disturbance loads generated by the engine. The engine forces are transferred to the complex structure through the engine mount extensions and the structure vibrates at its resonance frequencies. Each engine mount (right, left and transmission) disturbance is modeled with three degrees of freedom (x, y, and z) where amplitudes of these forces vary with frequency. In Fig.3.3, the force

data for each mount is presented for each degree of freedom. This data is experimentally measured and representative.

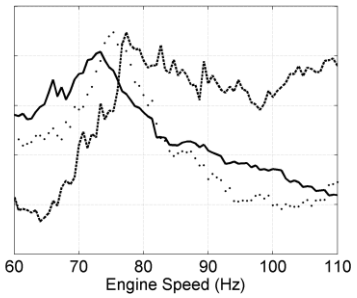

Figure 3.10.a Engine-force on left mount

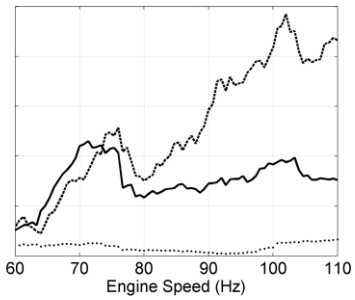

Figure 3.11.b Engine-force on right mount

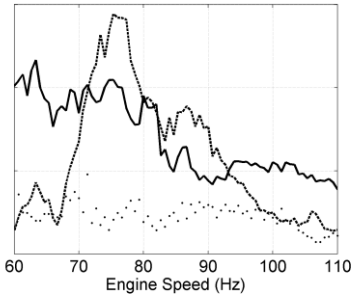

Figure 3.12.c Engine-force on transmission mount

The frequency response analysis of the structure is performed using the finite element model. The engine forces are applied to the complex structure at mount locations and the frequency response of the structure is obtained at the each considered degree of freedom on the measurement grid (Fig.3.7). In Fig.3.9, the predicted frequency responses for four different nodes are given. By analyzing the structural responses, it can be observed that the vibration characteristics vary over the entire structure and the highest vibration amplitude occurs within the bandwidth of the 70 Hz and 80 Hz.

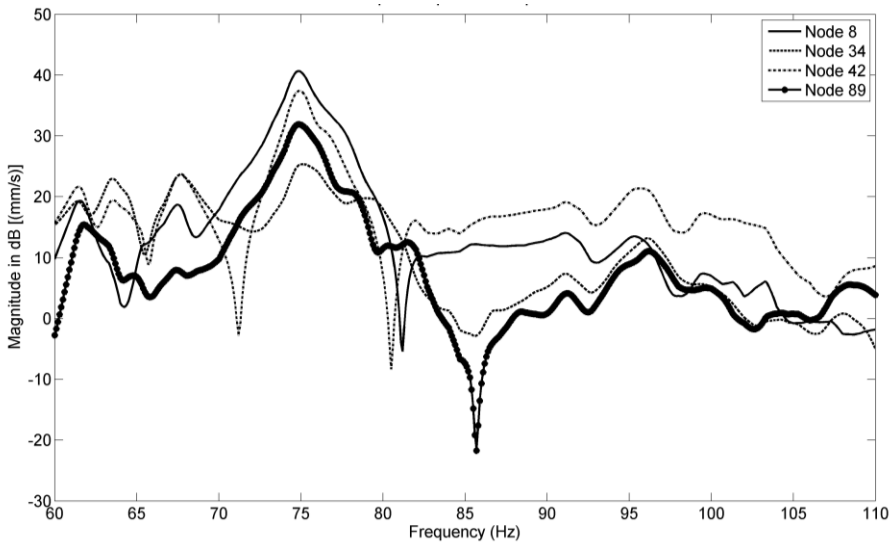

Figure 3.13 Open-loop frequency response at different nodes of the complex structure in the presence of external disturbance ($\mathbf{D}_{k,j}(\omega)$ $k \in N_p, j \in N_e$ *see* 3.3.1)

3.5.2. Design Study for Local Vibration Suppression

The design methodology of the feedback controller for suppressing vibration at the sensor/actuator location is implemented for the complex panel. The motivation of the methodology is to optimize the sensor and actuator position and controller parameters for the maximization of local vibration suppression. To achieve this objective, the local performance index (Eq.3.15) is maximized. This can be accomplished via the optimal location of the collocated sensor/actuator pair and optimal parameter settings of the controller. The controller parameters, proportional and integral gain are taken as unity and optimal placement of the sensor/actuator position is investigated for obtaining maximum local performance index. As described in Section 3.5.1, the complex structure has the highest amplitude around *75* Hz, so in performance index calculation, the particular frequency range is selected as *67* Hz to *85* Hz. Then, for each node on the structure,

closed-loop response using the frequency response analysis (as explained in Section 3.3) is obtained and the performance index is calculated. Fig.3.10 presents the closed-loop frequency response functions for four different nodes *(41, 55, 79* and *89)* on the structure. The corresponding local performance indices for these nodes are calculated as *23.0%, 4.7%, 100%,* and *11.0%* respectively. The values of local performance index provide the optimum location as node *79* for the collocated sensor and actuator pair.

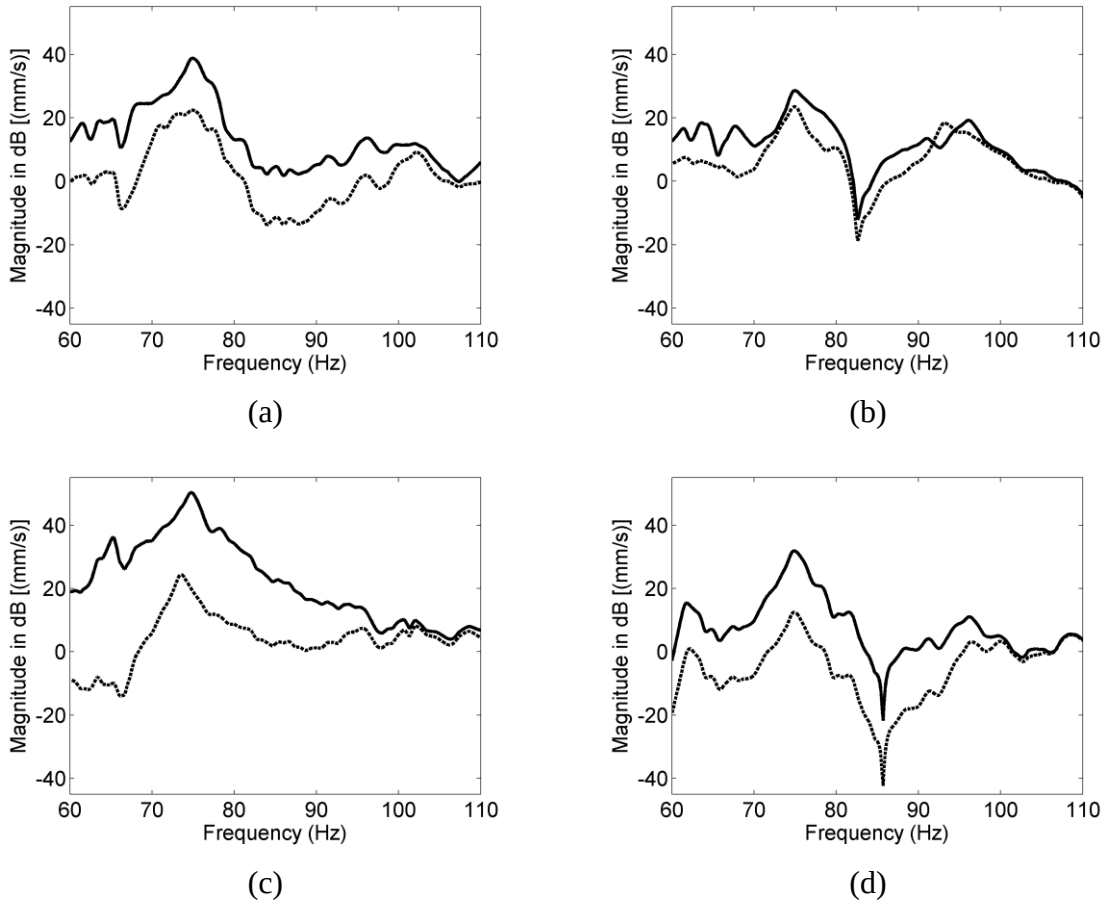

Figure 3.14 Open-loop (solid line) and close-loop (dashed line) frequency response for collocated sensor/actuator pair nodes **a)** 41 **b)** 55 **c)** 79 **d)** 89

Fig.3.11 presents the color contour plot for the local performance index variation over the entire structure. It is obvious that, two points, node *27*, located at the upper section of the front panel and node *79*, located at the right engine mount are found to be most suitable candidates for collocated sensor/actuator placement by applying local vibration suppression methodology. Between these points, point *79* is selected as the collocated sensor/actuator location for local vibration suppression since the local vibration performance metric is calculated as *100%*.

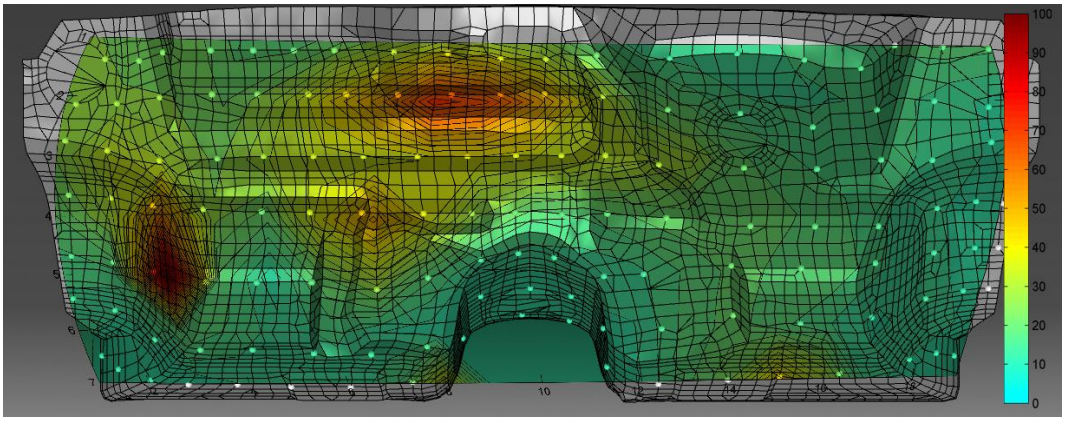

Figure 3.15 Contour plot of local performance index parameter over the entire structure for optimal placement of the sensor/actuator pair

3.5.3. Design Study for Global Vibration Suppression

In this section, the global vibration suppression methodology is applied to the complex structure for optimal placement of the sensor/actuator pair and parameter tuning of the controller. The objective of the global methodology is the maximization of spatial vibration suppression over the entire structure. For this purpose, global performance index (Eq.3.18) is calculated and optimized for various controller parameters and sensor/actuator locations. At the end of the optimization procedure, the maximum value of this global performance

index is achieved for node *79* with proportional gain 2.7826×10^{-5} and integral gain 3.8312×10^{-1} for the particular frequency region *67* Hz to *85* Hz.

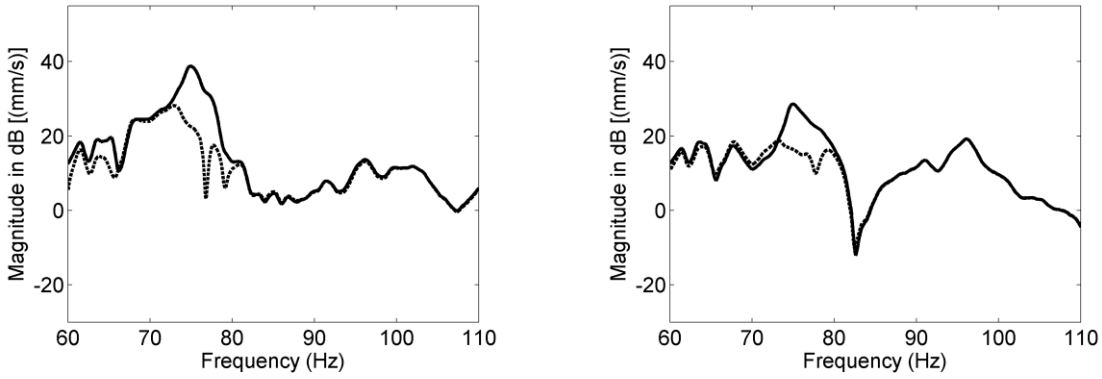

(a) (b)

Figure 3.16.a Open-loop (solid line) and closed-loop (dashed line) frequency response for different nodes **a)** 41 **b)** 55 (sensor/actuator node)

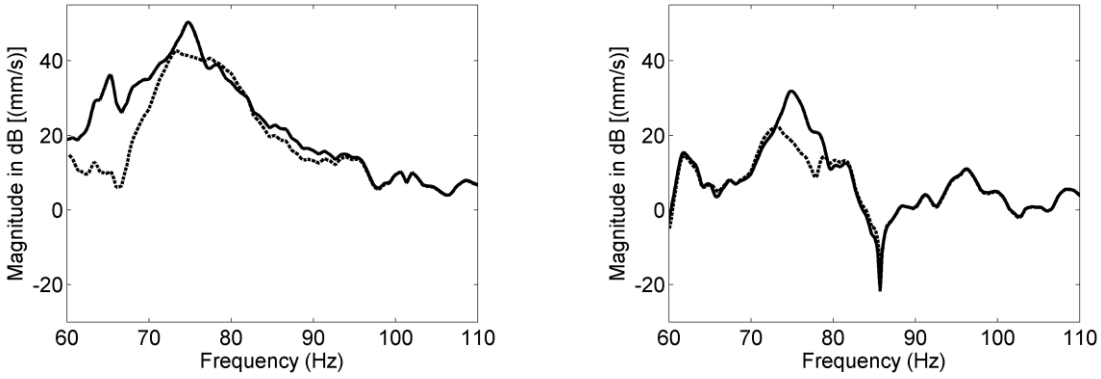

(a) (b)

Figure 3.17.b Open-loop (solid line) and closed-loop (dashed line) frequency response for different nodes **a)** 79 **b)** 89 (sensor/actuator node)

In Fig.3.12, the spatial behavior of the complex structure (at the nodes *41, 55, 79* and *89*) is presented for the controller active and inactive cases. For the controller active case,

the collocated sensor/actuator is placed at the optimal position (node *79*) and the controller parameters are set to the optimum values. As it can be observed from the figure, the vibration of the complex structure is attenuated between *67* Hz to *85* Hz over the entire complex structure. This shows that the global performance index is an applicable and efficient tool to optimize the location of controller actuator and parameters.

The vibration of the entire structure is attenuated by the global vibration suppression methodology. In other words, the total kinetic energy of the complex structure is reduced. The formula for the calculation of total kinetic energy density of the complex structure is [48]

$$\boldsymbol{\eta_{oL}(\omega_p)_k = \frac{1}{2}\rho \sum_{k=1}^{n} \left[\mathbf{D}(\omega_p)_k\right]^2}$$

$$\boldsymbol{\eta_{cL}(\omega_p)_k = \frac{1}{2}\rho \sum_{k=1}^{n} \left[\widehat{\mathbf{G}}_{cl}(\omega)_k\right]^2} \qquad \textbf{(3.20)}$$

In this equation, $\boldsymbol{\eta}$ is the total kinetic energy density, k is the degree of freedom on the structure, ω_p is the particular frequency range selected for the suppression study and $\mathbf{D_k(\omega_p)}$ and $\widehat{\mathbf{G}}_{\mathbf{cl,k}}(\boldsymbol{\omega})$ are the open and close-loop velocities of the structure. Once more, Eq.3.12 is used for calculation of the closed-loop response at the sensor/actuator node ($k = m$), and Eq.3.16 is used for closed-loop response analysis at the other nodes ($k \neq m$).

Utilizing Eq.3.20, the total kinetic energy density of the complex structure is calculated for open-loop and closed-loop cases in the frequency range *60* Hz to *110* Hz. Fig.3.13 presents the kinetic energy densities. As can be seen from the figure, the total kinetic energy density is reduced by an amount of *91.34%* at the *75* Hz without exciting any higher structural modes.

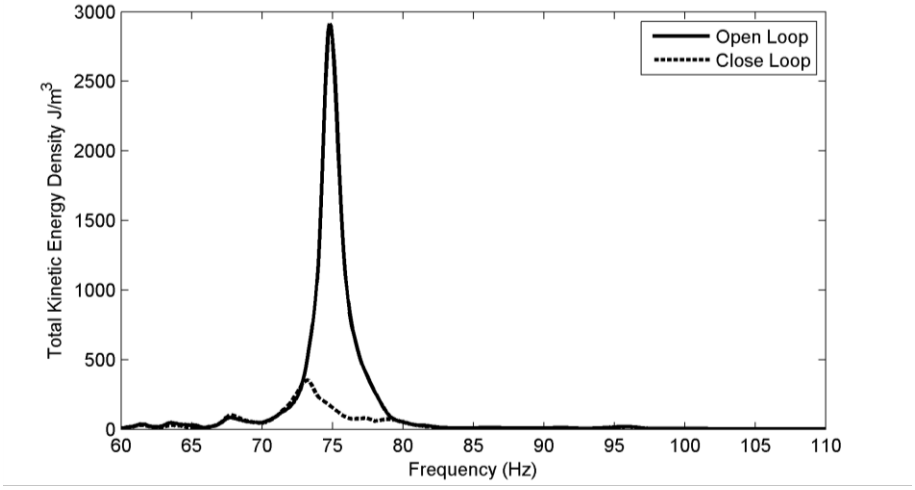

Figure 3.18 Open loop (solid line) and closed-loop (dashed line) total kinetic energy of the complex structure

In a final complementary analysis, the global performance index is evaluated at each node and presented with a color contour plot in Fig.3.14 for optimum controller parameter settings. This figure points out the globally effective and ineffective regions of the structure for active treatment implementations in the particular frequency range (*67* Hz to *85* Hz). As can be noticed from the figure, the nodes *79* and *27* are globally effective for vibration suppression while the nodes 1-5 are effective for vibration augmentation.

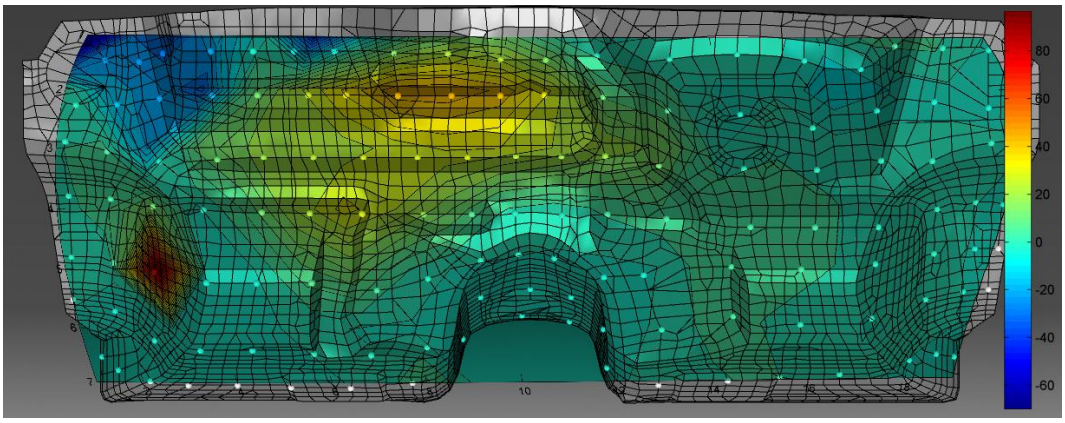

Figure 3.19 Global performance index over the entire structure for optimum controller settings

To evaluate distribution of control effect over the entire complex panel structure, the distribution of change in plate kinetic energies are evaluated at the output degrees of freedom *k*. Using Eq.3.18, each nodes open and closed loop kinetic energy density levels are obtained. Difference between open and closed loop energies shows the control effect generated by actuator over the complex panel surface. By using H_2 norm of differences between open and closed loop cases, for each configuration, control authority is obtained. Therefore, distribution of control effect over the surface at the desired frequency is guaranteed by utilizing optimization algorithm. In Fig.3.15.a, for local optimization case, kinetic energy reduction distribution over complex panel is presented for a certain frequency. At the collocated actuator/sensor location, highest reduction in kinetic energy levels is obtained but at the other locations suppression is not achieved. Also at some locations structural vibrations are augmented because optimization algorithm for local case does not consider any location's response other than sensor/actuator pair location. In Fig.3.15.b, distribution results for global case are presented for the same frequency. Again, for the actuator placement node, high reduction in kinetic energy level is obtained. But, in addition to the controlled node, kinetic energy density levels are reduced at considerable

levels at the upper mid-section of the complex panel and plate vibrations do not augmented. By implementing global considerations into the optimization algorithm, controller authority over the complex panel is maintained. For the local case, total energy of complex panel is reduced around *10%* with augmentation in plate vibrations (black colored regions), but for the global case the total energy is reduced around *91%* without any augmentation over the panel surface. (Fig.3.15)

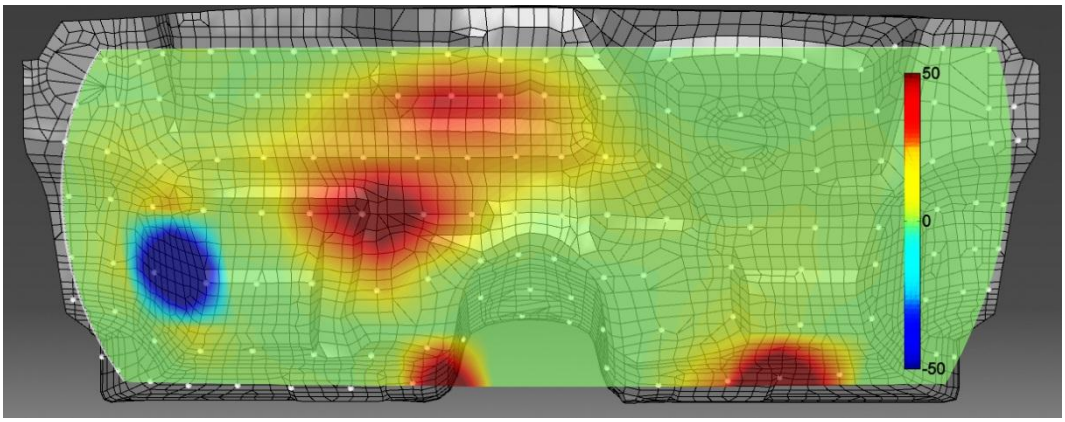

Figure 3.20.a Global energy change over the complex panel surface for optimum **local** controller settings

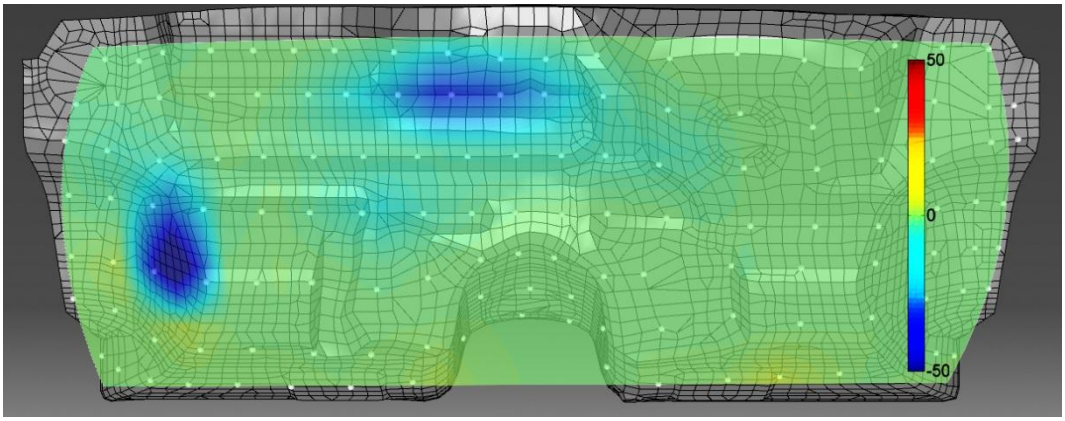

Figure 3.21.b Global energy change over the complex panel surface for optimum **global** controller settings

3.6. Conclusion

In this study, we developed a novel methodology for optimal placement of sensors/actuators and parameter tuning of the controllers. The applicability and effectiveness of the methodology is demonstrated with a complex structure which is a part of a real-sized vehicle model. The finite element model of the structure is used for frequency response analysis. In order to achieve effective vibration suppression of the structure, local and global performance indices are defined and used for the optimization of sensor/actuator position as well as controller parameters. By comparing controller active and inactive cases, the vibration suppression performance of the controller and the effectiveness of the developed methodology is demonstrated locally and globally.

3.7. Acknowledgement

This work is supported by Scientific and Technological Research Council of Turkey (TUBITAK).

Chapter 4

ACTIVE STRUCTURAL ACOUSTIC CONTROL SYSTEM DESIGN FOR COMPLEX 3D GEOMETRY STRUCTURE

4.1. Introduction

In this chapter, a novel methodology is presented for design of an active structural acoustic control scheme on a complex 3D geometry. The actuator/sensor position and control parameters are optimized based on defined performance indices that include noise suppression performance inside an enclosed cavity. Position and controller parameter optimization are based on the noise reduction levels for a selected frequency bands. As a case study, a vibro-acoustic model of a real-sized vehicle is used to present developed methodology. Vibro-acoustic simulations are conducted to build vibro-acoustic system model and the most influential panel for the sound pressure level inside the passenger cabin is identified. This panel is determined by conducting panel acoustic contribution analysis (PACA) based on the acoustic transfer vector (ATV) methodology. After determining the most influential panel, active vibration control system is designed and performance evaluation of the controller and system behavior is evaluated by comparing the open and closed loop response of local and zonal sound pressure levels. It is shown that on a complex 3D surface, a well -placed collocated sensor and actuator pair with optimized tuning can suppress the vibration spatially on a complex shaped panel and therefore it can reduce the sound pressure level inside the enclosure. The proposed methodology can be successfully applied for the structures that have complex shape and boundary conditions

for noise suppression. This chapter is organized as follows: Section 2 introduces modeling theory and definition of the frequency response functions for the vibro-acoustic system and 3D complex panel. Section 3 describes the developed methodology for the active structural acoustic controller and optimization, Section 4 presents the case studies, while introducing the finite element model of an example vibro-acoustic system and 3D complex panel. At last, Section 5 concludes the chapter.

4.2. Nomenclature:

$\boldsymbol{k}$	:	Measurement degrees of freedom on complex surface
$\boldsymbol{j}$	:	Structural degrees of freedom where external disturbance applied
$\boldsymbol{n}$	:	Acoustic degrees of freedom where SPL is measured
$\boldsymbol{m}$	:	Structural degrees of freedom on complex surface where actuator is positioned
$\boldsymbol{K_s}$	:	Structural stiffness matrix
$\boldsymbol{C_s}$	:	Structural damping matrix
$\boldsymbol{M_s}$	:	Structural mass matrix
$\boldsymbol{X_k(\omega)}$	:	Displacement vector at the degrees of freedom "*k*"
$\boldsymbol{F_j(\omega)}$	:	External loading at the node "*j*"
$\boldsymbol{K_a}$	:	Acoustic stiffness matrix
$\boldsymbol{C_a}$	:	Acoustic damping matrix
$\boldsymbol{M_a}$	:	Acoustic mass matrix
$\boldsymbol{P_n(\omega)}$	:	Acoustic pressure at the node "*n*"
$\boldsymbol{P_l}$	:	Nodal pressure vector applied to the coupled degrees of freedom "*l*".
$\boldsymbol{F_l^a(\omega)}$	:	Displacement vector acting on acoustic fluid at the coupling boundary at node "*l*"
$\boldsymbol{F(\omega)}$	:	Harmonic external force input
$\boldsymbol{v(\omega)}$	:	Velocity response
$\boldsymbol{V_{k,j}(\omega)}$	:	Mobility transfer function relating input to j^{th} degree of freedom to output at k^{th} degree of freedom
$\boldsymbol{V_k(\omega)}$	:	Velocity at the degree of freedom *"k"*

$\boldsymbol{ATV_{n,k}(\omega)}$	:	Acoustic transfer vector relating acoustic degree of freedom "*n"* to structural degree of freedom "*k"*
$\boldsymbol{G_c(\omega)}$	:	Controller transfer function
$\boldsymbol{K_p}$	:	Proportional gain
$\boldsymbol{K_i}$	:	Integral gain
$\boldsymbol{D_k(\omega)}$	:	Disturbance frequency response
$\boldsymbol{F_j{}^e(\omega)}$	:	External loading applied to degree of freedom "*j"*
$\boldsymbol{A_{k,m}(\omega)}$	:	Actuator transfer function between actuator at the degree of freedom "*m"* and sensor at the degree of freedom "*k"*
$\boldsymbol{A_{m,m}(\omega)}$	:	Actuator transfer function between actuator at the degree of freedom "*m"* and sensor at the degree of freedom "*m"*
$\boldsymbol{F_m{}^a(\omega)}$	:	Actuator loading applied to degree of freedom "*m"*
$\boldsymbol{k}$	:	Measurement degree of freedom
$\boldsymbol{m}$	:	Actuator degree of freedom
$\boldsymbol{G_f(\omega)}$	:	Band-pass filter transfer function
$\boldsymbol{\alpha_n}$	:	H_2 norm of the open-loop frequency response of the system at the n^{th}acoustic degree of freedom
$\boldsymbol{\gamma_n}$	:	H_2 norm of the closed-loop frequency response of the system at the n^{th}acoustic degree of freedom
$\boldsymbol{\Gamma}$	:	H_2 norm difference
$\boldsymbol{\beta}$	:	Performance index
$\boldsymbol{N}$	:	Vector of output degrees of freedom on complex panel

4.3. Vibro-Acoustic Modeling and Controller Design for a Complex Structure for Noise Reduction

In this section, the theory of vibro-acoustic modeling of the complex structures is described. Then the acoustic transfer vector methodology and controller design theory for the active structural acoustic control is presented.

4.3.1. Modeling the Vibro-Acoustic System

For a vibro-acoustic system, the equations for the structural finite element (FE) model can be written as follows: [70, 73]

$$[\mathbf{K_s} + i\omega\mathbf{C_s} - \omega^2\mathbf{M_s}]\mathbf{X_k}(\omega) = \{\mathbf{F_j}(\omega)\} \tag{4.1}$$

In Eq.4.1, $\mathbf{M_s}$, $\mathbf{K_s}$, $\mathbf{C_s}$ are the $n \times n$ structural mass, stiffness and damping matrices. The subscript "*s*" indicates structural parts. $\mathbf{X_k}(\omega)$ is the displacement vector holding the translational and rotational displacements, occurring at the degree of freedom "*k*" , on the structure due external loading**.** $\mathbf{F_j}(\omega)$ is the force vector applied on the structure externally to the degrees of freedom "*j*". Using the FE formulation for the acoustic domain, acoustic FE model equations are as follows:

$$[\mathbf{K_a} + i\omega\mathbf{C_a} - \omega^2\mathbf{M_a}]\{\mathbf{P_n}(\omega)\} = 0 \tag{4.2}$$

In Eq.4.2, $\mathbf{M_a}$, $\mathbf{K_a}$, $\mathbf{C_a}$ are the $m \times m$ acoustic mass, stiffness and damping matrices. $\mathbf{P_n}(\omega)$ is the pressure vector holding the pressure occurring at the acoustic degree of freedom n **.**

In the contact regions of fluid and structure, acoustic pressure on the structure results in a normal loading on the body. Similarly, structural vibrations occurring on the structure

generates surface velocities and surface velocities result in normal fluid velocities due the coupling effect between the structure and the fluid medium. Adding coupling term and effect of fluid pressure, the structural FE model becomes

$$[\mathbf{K_s} + i\omega\mathbf{C_s} - \omega^2\mathbf{M_s}]\{\mathbf{X_k}(\omega)\} + [\mathbf{K_c}]\{\mathbf{P_l}(\omega)\} = \{\mathbf{F_j}(\omega)\} \quad \textbf{(4.3)}$$

In Eq.4.3, $\mathbf{K_c}$ is the coupling matrix, $\mathbf{P_l}$ is the nodal pressure vector applied to the structure/acoustic coupled degrees of freedom "*l*". Similarly acoustic FE model becomes

$$[\mathbf{K_a} + i\omega\mathbf{C_a} - \omega^2\mathbf{M_a}]\{\mathbf{P_n}(\omega)\} - \omega^2[\mathbf{M_c}]\{\mathbf{X_k}(\omega)\} = \{\mathbf{F}_l{}^a(\omega)\} \quad \textbf{(4.4)}$$

In Eq.4.4, $\mathbf{M_c}$ is the coupling matrix, $\mathbf{X_k}$ is the nodal displacement vector and $\mathbf{F}_l{}^a(\omega)$ is the displacement vector acting on acoustic fluid at the coupling boundary. Combining equations 3 and 4, coupled FE/FE model [24] for the vibro-acoustic system is,

$$\left(\begin{bmatrix}\mathbf{K_s} & \mathbf{K_c}\\ 0 & \mathbf{K_a}\end{bmatrix} + i\omega\begin{bmatrix}\mathbf{C_s} & 0\\ 0 & \mathbf{C_a}\end{bmatrix} - \omega^2\begin{bmatrix}\mathbf{M_s} & 0\\ -\rho_0\mathbf{K_c}^T & \mathbf{M_a}\end{bmatrix}\right) \times \begin{bmatrix}\mathbf{X_k}(\omega)\\ \mathbf{P_n}(\omega)\end{bmatrix} = \begin{bmatrix}\mathbf{F_j}(\omega)\\ \mathbf{F_l}{}^a(\omega)\end{bmatrix} \quad \textbf{(4.5)}$$

Because of coupling terms in Eq.4.5, the FE model becomes non-symmetric and both structural and acoustical parts should be solved simultaneously. By utilizing Eq.4.5, frequency response of sound pressure levels for a node inside an acoustic cavity, $\mathbf{P_n}(\omega)$, due vibrations occurring on the enclosing structure $\mathbf{X_k}(\omega)$ can be obtained.

In this study, active structural acoustic controller is considered to reduce sound pressure levels occurring inside an enclosure. Design of an acoustic structural controller requires frequency responses of the controlled structure under the effects of external loadings and actuator. Utilizing the finite element modeling theory, equation of motion for a complex, linear elastic, time-invariant structure with n degree of freedoms is given in Eq.4.1

For a harmonic external force input of the form

$$\mathbf{F}(\omega) = \mathbf{F}e^{i\omega t} \tag{4.6}$$

And corresponding velocity response of the system is

$$\mathbf{v}(\omega) = \mathbf{v}e^{i\omega t} \tag{4.7}$$

where ω is the excitation frequency of the externally applied loading on the structure. By using Eq.4.1, input-output relationship or the frequency response representation of the system is as follows;

$$\mathbf{v}(\omega) = \mathbf{H}(\omega)\mathbf{F}(\omega) \tag{4.8}$$

Where the mobility transfer function $\mathbf{H}(\omega)$ is

$$\mathbf{H}_{k,j}(\omega) = (-\omega\text{^}2\,\mathbf{M} + i\omega\mathbf{C} + \mathbf{K})^{-1} i\omega \tag{4.9}$$

In Eq.4.9, $\mathbf{H}_{k,j}(\omega)$ is the is the mobility transfer function of the structure and gives the velocity of structure under the influence of external loading and utilized to determine open-loop response of the structure and transfer functions for the actuator.

4.3.2. Acoustic Transfer Vector Method

For evaluation of ASAC, interior sound pressure levels for open-loop and closed-loop cases should be evaluated. Open-loop response of the system can be obtained from vibro-acoustic solution (Eq.4.5). To evaluate closed loop response, the complex panel during control action should be evaluated. For closed-loop frequency response estimation, acoustic transfer vector method is used to obtain sound pressure levels inside the enclosed cavity.

Acoustic transfer vector (ATV) is the set of vectors that relates nodal normal velocities of structure with the resultant acoustic pressure in the coupled acoustic medium. ATVs are

input-output relations between the normal surface velocities of the radiating surface and the sound pressure level at a specific acoustic point. When all structural nodes are considered, ATV can be interpreted as an ensemble of Acoustic Transfer Functions (ATF) from radiating surface nodes to a single field point in the acoustic region [74, 75].

The equation for resultant pressure at a field point in presence of structural vibration of node is as follows

$$\mathbf{P_n}(\omega) = \mathbf{ATV}_{\mathrm{n,k}}(\omega)\mathbf{v_k}(\omega) \tag{4.10}$$

Where $\mathbf{P_n}(\omega)$ the measured sound is pressure level and can be obtained from Eq.4.5. $\mathbf{ATV}_{\mathrm{n,k}}(\omega)$ is the acoustic transfer vector relating structural normal velocities, $\mathbf{v_k}(\omega)$ at the structural degrees of freedom k, to the acoustic pressure measured at acoustic degrees of freedom n, and ω is the frequency. Using Eq.4.9, structural response at the fluid structure interface in the form of surface normal velocities $\mathbf{v}_k(\omega)$, can be obtained due to external loading $\mathbf{F}_j(\omega)$. Having been determined $\mathbf{P_n}(\omega)$ and $\mathbf{v}_k(\omega)$, re-arranging Eq.4.10

$$\left[\boldsymbol{ATV}_{\boldsymbol{n,k,}}(\omega)\right]^{\boldsymbol{T}} = \mathbf{P_n}(\omega)\,[\mathbf{v_k}(\omega)^T]^+ \tag{4.11}$$

Eq.4.11 can be written. Using open-loop values of $\mathbf{P_n}(\omega)$ and $\mathbf{v_k}(\omega)$ in presence of structural loading, acoustic transfer vector, $\mathbf{ATV}_{\mathrm{n,k}}(\omega)$ can be obtained.

Using ATV, it is possible to evaluate closed- loop sound pressure levels inside the acoustic cavity by utilizing closed loop surface velocities of the structure. Eq.4.10 indicates that by reducing panel vibrations ($\mathbf{v_k}(\omega)$) it is possible to reduce pressure levels at an acoustic degree of freedom ($\mathbf{P_n}(\omega)$). However, each degree of freedom on the structure contributes to sound pressure levels inside an acoustic enclosure. As a result, spatial control of structural vibrations is required to reduce sound pressure levels. In the next section, design methodology for a structural acoustic controller for a complex structure in presence

of external disturbances is presented to reduce sound pressure levels inside the coupled acoustic domain.

4.3.3. Controller Design and Actuation

In active structural acoustic control methodology, only structural sensors are implemented and the controller output signal is generated by only considering the structural vibrations. Acoustic reduction is achieved by suppressing acoustic radiation to the fluid medium by reducing structural vibrations. For effective suppression, controller gains should optimized by considering acoustic response of the system. For a complex structure and complex boundary conditions, model-independent controller algorithms are suitable since these algorithms are easy to implement, well established, practical and efficient for structural control and therefore suitable for ASAC application. Moreover, these controllers do not require plant parameters and can be optimized for various design criteria like maximizing the structural vibration reduction or minimizing acoustic radiation and sound pressure levels. Proportional-integral (PI) controller is a model-independent control method for implementation (Eq.4.12) which generates the controller output signal by considering the displacement and velocity response of the structure.

$$\mathbf{G_c}(\omega) = K_p + \frac{K_i}{i\omega} \tag{4.12}$$

In Eq.4.12, $\mathbf{G_c}(\omega)$ is the controller transfer function, K_p is the velocity feedback gain and K_i is the position feedback gain**.** The velocity feedback adds damping to all modes while displacement feedback provides additional damping in the low frequency range thus reduces structural vibrations. To confine the suppressive effect to a selected frequency band, a band-pass filter is implemented to the system. In addition, with filter implementation, augmentation in sound pressure levels in untargeted frequencies is prevented. The general block diagram for the system with P-I controller and filter is shown

in Fig.4.1. In Fig.4.1 $d(\omega)$ is the disturbance input due external loadings, $u(\omega)$ is the suppressive input generated by the controller and $v(\omega)$ is the complex panel surface normal velocity and $G_f(\omega)$ is the band pass filter. By multiplying surface velocities with ATV vector resultant pressure $P(\omega)$ is obtained. In this study, single input single output (SISO) control scheme with collocated sensor and point force actuator is considered. In the next section design methodology of a spatial vibration controller with SISO system for noise suppression is explained.

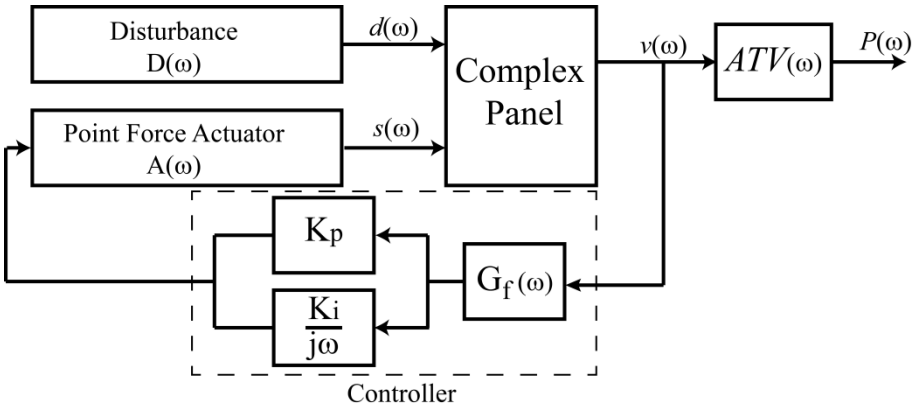

Figure 4.1 General block diagram of the active structural acoustic control system for complex structure

4.4. Design Methodology for Active Structural Acoustic Controller

In this section, the design methodology of the feedback controller for suppressing sound pressure levels inside an enclosure is explained. The motivation of the methodology is to optimize the sensor and actuator location and controller parameters for the maximization of noise suppression by suppressing structural vibrations on a complex structure. Reduction in sound pressure levels is achieved by reducing structural vibrations on the surface. In a SISO active feedback controller only response of the region around sensor considered. But

to achieve reduction in noise levels, the controlled structure should be considered globally. All degrees of freedom on a complex structure contribute to resultant noise at different levels. In this section, first the simulation model for the spatial acoustic controller is explained and then active structural acoustic control method is presented.

4.4.1. Simulation Method for Noise Reduction Performance Evaluation

The frequency response analysis is conducted for performance evaluation of noise suppression, which is achieved by suppressing spatial vibrations of the complex structure. In Fig.4.2.a and Fig.4.2.b block diagrams for spatial evaluation of complex panel vibrations and noise suppression is presented.

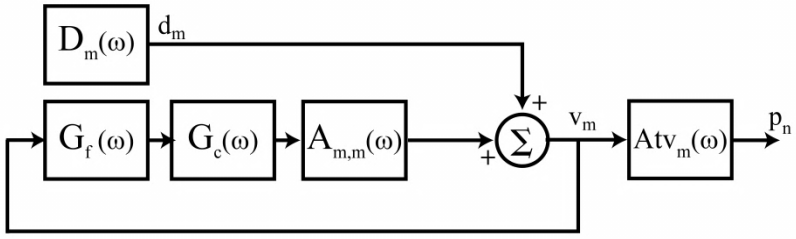

Figure 4.2.a Block-diagram for the closed-loop frequency response analysis for the sensor/actuator node

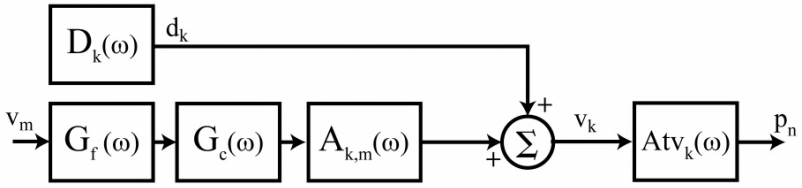

Figure 4.3.b Block-diagram for the closed-loop frequency response analysis for the other nodes (excluding the sensor/actuator node) of the structure

The controller generates excitation at the degree of freedom where the sensor/actuator pair is positioned additional to the external disturbance. But the structure is a continuous body; as a result, generated control action at the sensor/actuator location also results in excitation at the other degrees of freedom on the structure. Therefore, the block diagram of the system is divided into two parts: The first part (Fig.4.2.a) is used to simulate the generated sound pressure due the collocated sensor/actuator degree of freedom and the second part (Fig.4.2.b) is utilized for the simulation of the generated sound pressure due other degrees of freedom on the complex structure. In these diagrams, $\mathbf{D}_k(\omega)$ is the disturbance frequency response and using Eq.4.8 and Eq.4.9, response of the complex panel in the presence of structural disturbance is obtained as

$$\mathbf{D}_k(\omega) = \mathbf{H}_{k,j}(\omega)\mathbf{F}_j{}^e(\omega) \tag{4.13}$$

The disturbance matrix $\mathbf{D}_k(\omega)$ holds the open-loop response for each degree of freedom k on the complex panel. In Eq.4.13, k is the output degrees of freedom on complex panel for global behavior and the force vector $\mathbf{F}_j{}^e(\omega)$ is applied to the degree of freedoms on the structure j where j is the degrees of freedom where external disturbances are applied. On the complex panel, in addition to the external disturbance, actuator also generates loading effect. In Fig.4.2.a and 4.2.b, $\mathbf{A}_{k,m}(\omega)$ is the actuator transfer function. Response of the k^{th} degree of freedom with respect to actuator input to the degree of freedom m on the structure is derived as

$$\mathbf{A}_{k,m}(\omega) = \mathbf{H}_{k,j}(\omega)\mathbf{F}_m{}^a(\omega) \tag{4.14}$$

In Eq.4.14, k is the output degree of freedom on complex panel for global behavior and m is the degree of freedom where sensor/actuator pair is positioned and $\mathbf{F}_m{}^a(\omega)$ is the actuator force vector. To obtain actuator transfer function, $\mathbf{F}_m{}^a(\omega)$ is set to unity and

transfer function between applied unit forces to complex panel excitation in the form of panel velocities at the sensor point can be obtained. $\mathbf{A_{k,m}}(\omega)$ is the notation for the response of complex panel at the output location k with respect to the actuator positioned at the sensor/actuator location m $(k \neq m)$ and $\mathbf{A_{m,m}}(\omega)$ is the notation used for the collocated actuator/sensor case where $k = m$. In Figures 4.2.a and 4.2.b $\mathbf{P_n}$ is the resultant sound pressure at the acoustic degree of freedom n in response to the normal velocity at the structural degree of freedom k.

Using system representation in Fig.4.2 the closed-loop frequency response of vibro-acoustic system including complex panel response and acoustic response, $\mathbf{P_n}(\omega)$ can be obtained as:

$$\mathbf{P}_{n,k}(\omega) = \begin{cases} \left(\dfrac{\mathbf{D_m}(\omega)\mathbf{ATV_{n,m}}(\omega)}{1 + \mathbf{G_c}(\omega)\mathbf{G_f}(\omega)\mathbf{A_{m,m}}(\omega)} \right) & \text{k = m} \\ \left(\mathbf{D_k}(\omega) + \mathrm{v_m}\mathbf{G_c}(\omega)\mathbf{G_f}(\omega)\mathbf{A_{k,m}}(\omega) \right)\mathbf{ATV_{n,k}}(\omega) & \text{k} \neq \text{m} \end{cases} \quad \textbf{(4.15)}$$

In Eq.4.15 subscript m denotes to the degree of freedom on the complex panel where the sensor/actuator pair is positioned, k denotes to the output degrees of freedom for global behavior. $\mathbf{P}_{n,k}(\omega)$ is the closed- loop frequency response of the vibro-acoustic system. By utilizing Eq.4.15 the resultant sound pressure level at the acoustic degree of freedom n due to the structural vibrations of the degree of freedom k can be obtained. But when acoustics is considered all structural degrees of freedom on the complex panel surface contributes to the sound pressure levels. Therefore, resultant sound pressure level inside an acoustic enclosure due to the radiation from a set of structural degrees of freedom on complex panel can be obtained by summing the partial contributions of each degree of freedom to sound pressure levels as

$$\widehat{\mathbf{P}}_{\mathbf{n}}(\omega) = \sum_{k=1}^{d} \mathbf{P}_{\boldsymbol{n,k}}(\omega) \tag{4.16}$$

Using Eq.4.16, the resultant sound pressure levels at the acoustic degree of freedom n can be predicted in closed-loop cases. In order to achieve noise reduction inside the acoustic cavity, global vibration suppression of the vibrating structure is required. Therefore, both collocated sensor/actuator node's ($k = m$) and other nodes' ($k \neq m$) closed-loop vibration responses should be minimized. The optimum noise reduction can be achieved by placing the collocated sensor/actuator pair at the optimum location and parameter tuning of the controller by defining performance indices.

4.4.2. Optimization of Actuator/Sensor Location and Controller Parameters for Noise Suppression

In this section, the optimization methodology for acoustic suppression is presented. For the optimal noise suppression, the difference between the open-loop and closed-loop frequency response of sound pressure levels for a particular frequency is important. For the optimal case, the sensor/actuator pair and controller parameters should be optimized while considering global behavior of the controlled structure and coupled behavior of the fluid/structure domains. The optimization objective of acoustic suppression is to reduce sound pressure levels for a defined frequency band without causing any augmentation outside this frequency band. To guarantee optimality and increase control performance, three frequency bands are defined and their properties are presented on a representative frequency response function in Fig.4.3.

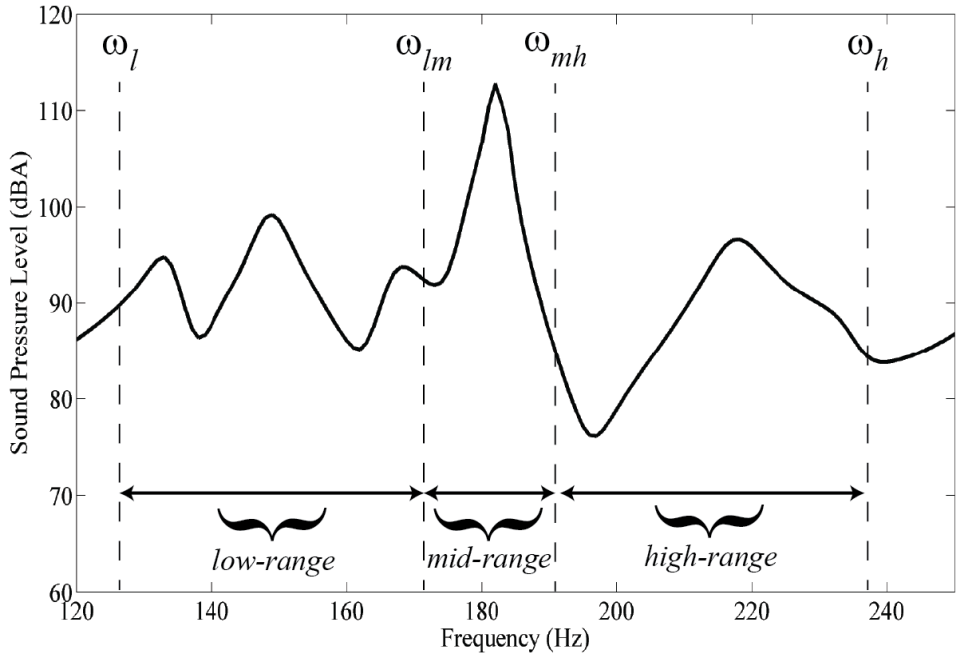

Figure 4.4 Representative sound pressure level frequency response, showing the defined frequency notations and optimization bands

The defined frequency bands in the frequency order are denoted as *low-range, mid-range*, and *high-range.* The frequency limits $\omega_l, \omega_{lm}, \omega_{mh}$ *and* ω_h are selected based on the frequency of interests. In the representative frequency response, *mid-range*s selected around the highest response and controller optimization is performed to increase suppression performance at this band. *Low-range* covers the frequencies lower than the frequency band of interest and *high-range* covers the higher frequencies. In the optimization study, each frequency band is considered. The H_2 norm of each band's open and closed loop frequency responses for the acoustic degree of freedom *n* is derived to obtain response characteristics of the vibro-acoustic system and for each band control performance is evaluated:

$$\boldsymbol{\alpha_{n,low}} = \left\|\boldsymbol{P_n}(\omega_p)\right\|_2^2 = \left(\frac{1}{2\pi}\right)\int_{-\infty}^{\infty}\left|\boldsymbol{P_n}(\omega_p)\right|^2 d\omega \qquad \omega_p = \{\omega_l, .. \omega_{lm}\}$$

$$\boldsymbol{\alpha_{n,mid}} = \left\|\boldsymbol{P_n}(\omega_p)\right\|_2^2 \qquad \omega_p = \{\omega_{lm}, .. \omega_{mh}\} \tag{4.17}$$

$$\boldsymbol{\alpha_{n,high}} = \left\|\boldsymbol{P_n}(\omega_p)\right\|_2^2 \qquad \omega_p = \{\omega_{mh}, .. \omega_h\}$$

$\boldsymbol{\alpha_{n,low}}$, $\boldsymbol{\alpha_{n,mid}}$ and $\boldsymbol{\alpha_{n,high}}$ are the H_2 norm of the open-loop frequency response of the system at the n^{th} acoustic degree of freedom for three frequency bands and includes characteristics of the measured response of the vibro-acoustic system under the influence of external disturbance.

$$\boldsymbol{\gamma_{n,low}} = \left\|\widehat{\boldsymbol{P}}_{\boldsymbol{cl,n}}(\omega_p)\right\|_2^2 = \left(\frac{1}{2\pi}\right)\int_{-\infty}^{\infty}\left|\widehat{\boldsymbol{P}}_{\boldsymbol{cl,n}}(\omega_p)\right|^2 d\omega \qquad \omega_p = \{\omega_l, .. \omega_{lm}\}$$

$$\boldsymbol{\gamma_{n,mid}} = \left\|\widehat{\boldsymbol{P}}_{\boldsymbol{cl,n}}(\omega_p)\right\|_2^2 \qquad \omega_p = \{\omega_{lm}, .. \omega_{mh}\} \tag{4.18}$$

$$\boldsymbol{\gamma_{n,high}} = \left\|\widehat{\boldsymbol{P}}_{\boldsymbol{cl,n}}(\omega_p)\right\|_2^2 \qquad \omega_p = \{\omega_{mh}, .. \omega_h\}$$

$\boldsymbol{\gamma_{n,low}}$, $\boldsymbol{\gamma_{n,mid}}$ and $\boldsymbol{\gamma_{n,high}}$ are the H_2 norms of the closed-loop frequency response of the system measured at n^{th} acoustic degree of freedom for three frequency bands and includes characteristics of the controlled response of the vibro-acoustic system. By taking differences of the open and closed-loop norms, controller performance are evaluated for each specific frequency band ω_p

$$\Gamma_{low} = \boldsymbol{\alpha_{n,low} - \gamma_{n,low}}$$

$$\Gamma_{mid} = \boldsymbol{\alpha_{n,mid} - \gamma_{n,mid}} \quad \textbf{(4.19)}$$

$$\Gamma_{high} = \boldsymbol{\alpha_{n,high} - \gamma_{n,high}}$$

In Eq.4.21, Γ_{low}, Γ_{mid} and Γ_{high} are the norm differences for the three frequency bands. To maximize and to find an optimal value for the vibro-acoustic system for the open loop and closed-loop cases norm differences are evaluated and based on the differences we define a performance index β as follows:

$$\forall \{K_p, K_i, m \in N_p\} \;\; Satisfying$$

$$\Gamma_{mid} > 0 \;\cap\; \Gamma_{low} > 0 \;\cap\; \Gamma_{high} > 0 \quad \textbf{(4.20)}$$

$$find \qquad \max\{\beta(K_p, K_i, m)\}$$

$$where \qquad \beta = \frac{\alpha_{n,mid} - \gamma_{n,mid}}{\max(\alpha_{n,mid} - \gamma_{n,mid})}$$

The closed-loop response of the panel is dependent on sensor/actuator location *m* (refer to section 4.3.1) and controller parameters K_p and K_i. With the performance index β and defined constraints, noise suppression is guaranteed at the frequency band, *mid-range* without any augmentation at the frequency bands, *low-range* and *high-range.* Also, the maximization of performance index β gives the optimal sensor/actuator location and settings of the controller. The optimization procedure is summarized with a flow chart in Fig.4.4. In the algorithm, first all Γ_{mid}, Γ_{low} and Γ_{high} values are obtained, then the best

solution satisfying the optimality condition in Eq.4.20 is obtained with corresponding actuator/sensor location and controller settings. In Fig.4.4 $\boldsymbol{N_p}$ is the vector of output degrees of freedom on complex panel considered for global behavior.

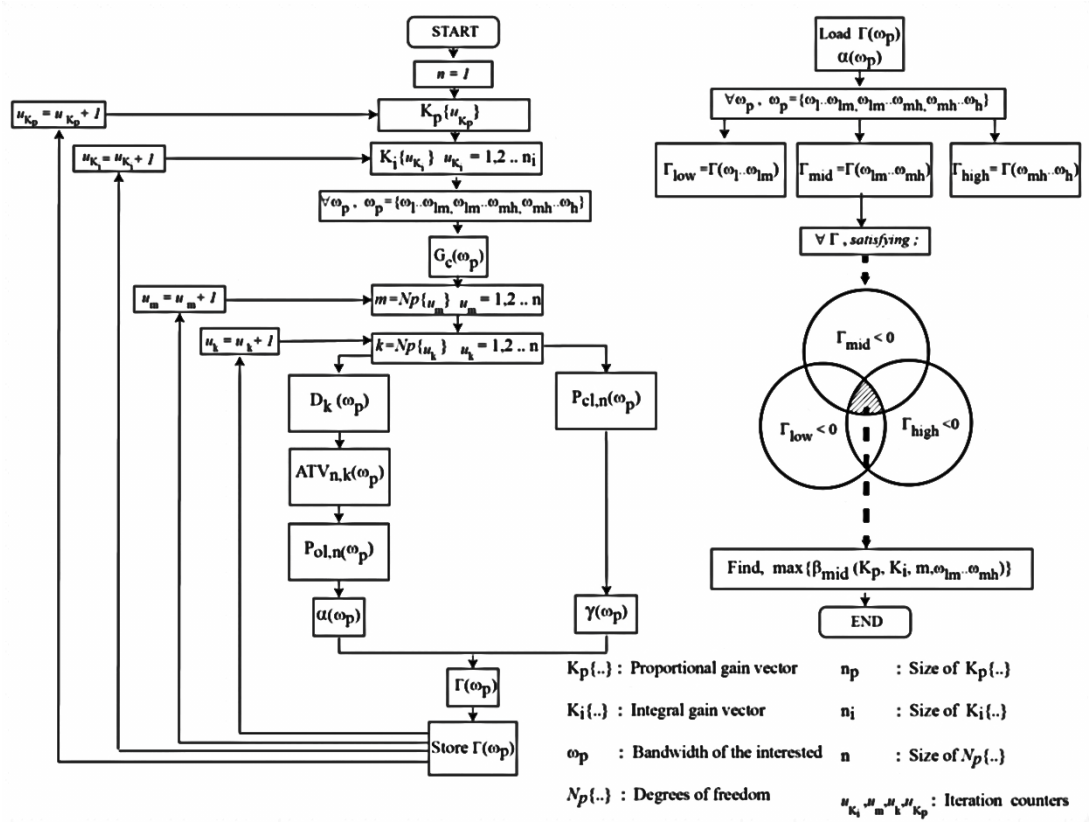

Figure 4.5 Flow-chart for determination of the control gains and sensor/actuator location for ASAC

4.5. Active Noise Suppression Case Study

In this study, a vehicle's vibro-acoustic model is used for implementation of the active structural acoustic control system and demonstration of the developed methodology.

4.5.1. Structural FE Model

The structural model of the vehicle enclosing the passenger cavity is shown in Fig.3a. The holes in the structural model are filled to obtain an acoustic enclosure for the vibro-acoustic analysis. The vehicle structure is modeled with shell elements with various thicknesses. The engine mount extensions at the front side of the vehicle (see Fig.5.b) are modeled with solid elements. These mounts are connected to the main body by rigid connections. The modal analysis of the structure is conducted with NASTRAN solver between 0-160 Hz range for the first fifty modes. The resultant file of modal analysis is used for vibro-acoustic analysis in LMS Virtual lab.

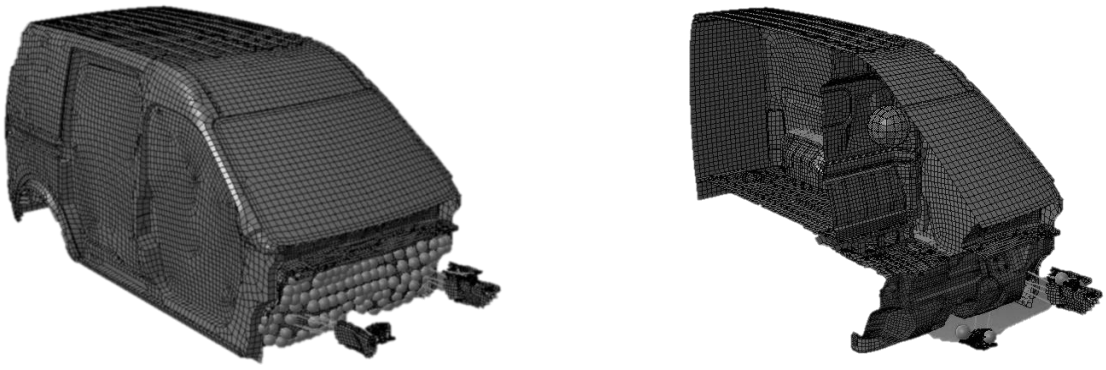

(a) **(b)**

Figure 4.6 a) Finite element model of the vehicle. b) Finite element model of the vehicle with centerline cut plane, showing right, left and transmission engine mounts and driver's head position (inside the passenger cabin)

For vibro-acoustic analysis, *FEM / FEM* approach is used to obtain sound pressure levels due to engine loading and additionally "panel acoustic contribution analysis" is performed to determine the contribution of each radiating panel to the interior noise level.

4.5.2. Acoustic Cavity FE Model

Vibro-acoustic analysis is performed to obtain pressure levels at driver's head position shown in Fig.5.b and to conduct panel contribution analysis for determination of the highest contributing panel to the sound pressure levels. The cavity (acoustic volume) is meshed such that the vibration from the structure can be transferred to the cavity across the coupled degrees of freedom (See Fig.6.a). Fig.6.b shows the panels selected for the panel acoustic contribution analysis (PACA).

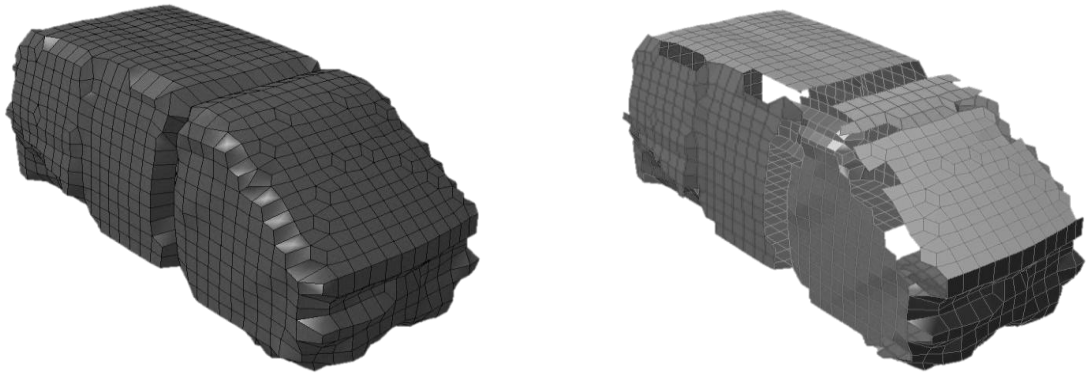

(a) (b)

Figure 4.7 a) Acoustic cavity mesh b) Panel set prepared on acoustic mesh for Panel Acoustic contribution analysis

4.5.3. External Disturbance Model

The vibration of the complex structure is caused by the disturbance loads generated by the engine. The representative engine forces are transferred to the complex structure through the engine mount extensions and the structure vibrates at its resonance frequencies.

Each engine mount (right, left and transmission) disturbance is modeled with three degrees of freedom (x, y, and z) where amplitudes of these forces vary with frequency.

4.5.4. Vibro-Acoustic Simulation and Panel Acoustic Contribution Results

For panel-acoustic contribution analysis, the frequency range is selected between *60* and *110* Hz range. As sensor location in acoustic cavity, driver's right ear position is selected. During simulations damping value for acoustic fluid is taken as 0.1 % and surrounding panels' acoustic absorption is neglected. Experimental engine excitation data in x, y and z directions is simultaneously applied to engine mounts of the vibro-acoustic model. Results for obtained sound pressure levels are presented in Fig.4.7 ($\mathbf{P}_n(\omega), refer\ to\ section$ 2.1) . Peak value for sound pressure level is obtained 116 dBA around 60-80 Hz band, which is also very distinctive in Fig.4.7. The acoustic system is coupled with the structural system and this result suggests that structural panels' vibration modes including 60-80 Hz frequency band are highly dominant on acoustic response of the system. In the presence of this information panel acoustic contribution analysis is performed and highly contributing panel at this frequency range is considered for ASAC application.

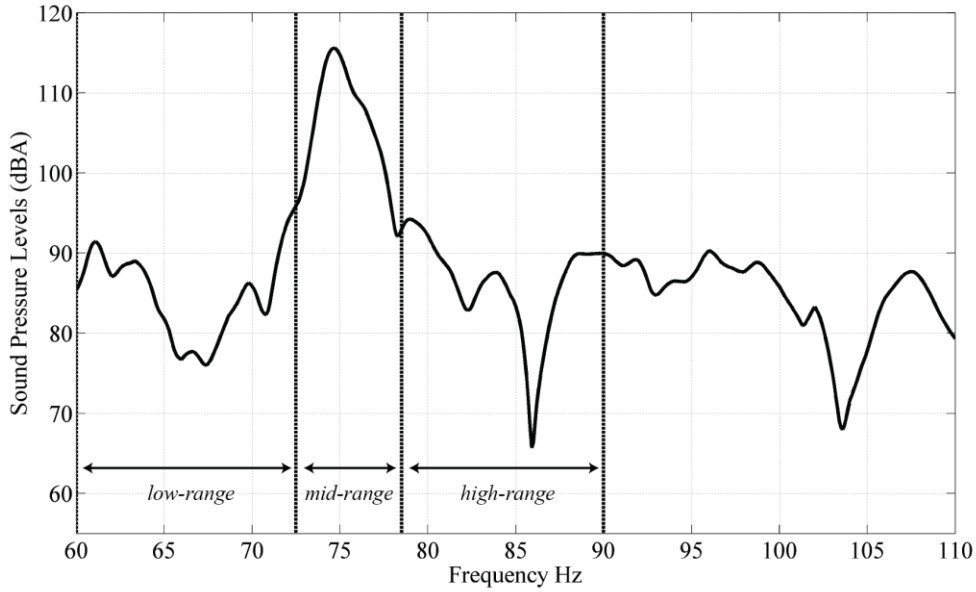

Figure 4.8 Sound pressure levels due engine disturbance at the driver's right ear position. ($\mathbf{P}_{ol,n}(\omega)$) and selected ranges for three frequency bands for optimization

With vibro-acoustic simulations, the frequency range for the highest sound pressure levels is determined. The solution of vibro-acoustic analysis is used to conduct panel contribution analysis (PACA) to determine the most contributing structural component to sound pressure levels. Panel contribution analysis is conducted between 60 to 110 Hz range to be consistent with the vibro-acoustic analysis and obtained results are shown in Fig.4.8. In Fig.4.8 the x-axis shows the frequency in Hz. The y-axis is divided into segments to show the contribution of each panel to the sound pressure levels. Red colored parts represent high contribution and blue colored parts represent low contribution to the overall sound pressure.

Among the analyzed panels, front panel has the highest contribution to sound pressure in the all frequency range. Particularly around 70 to 80 Hz front panel contribution is very distinctive, which is also the frequency of the highest sound pressure levels obtained from

vibro-acoustic simulations. These results indicate that noise suppression inside the cavity can be achieved by reducing structural vibrations occurring on this panel. Therefore, the controller implementation is carried out on the front panel and structural vibrations of this panel are reduced to attenuate high sound pressure levels. For controller design and optimization analysis, structural simulations are conducted on the front panel to obtain panel's open loop frequency response under influence of the external disturbance.

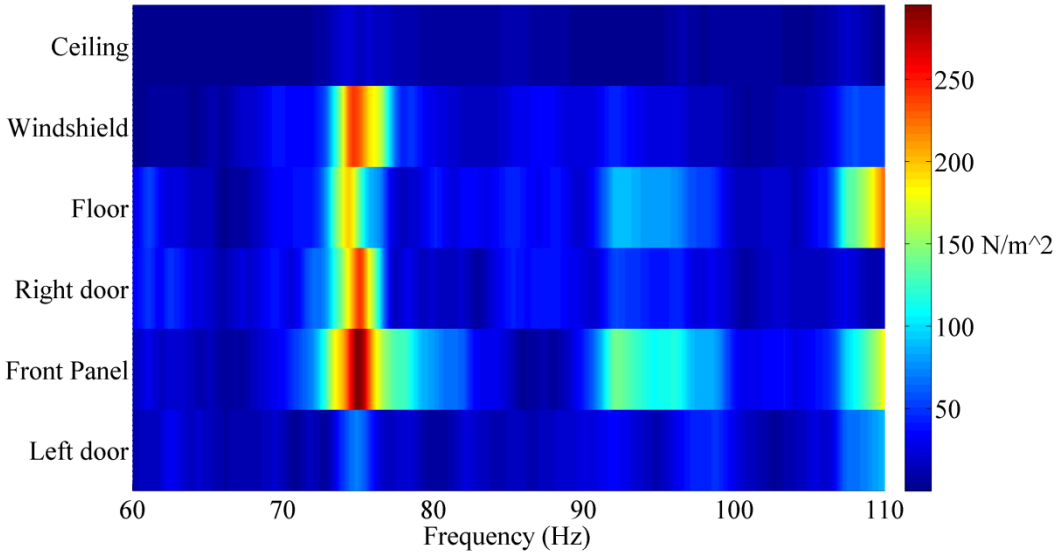

Figure 4.9 Panel acoustic contribution (PACA) for vibro-acoustic response at driver's right ear position

The distributed array with a two-dimensional grid (19 X 7 points) is utilized to obtain spatial response and sound radiation characteristic of complex panel in Figure 4.9.

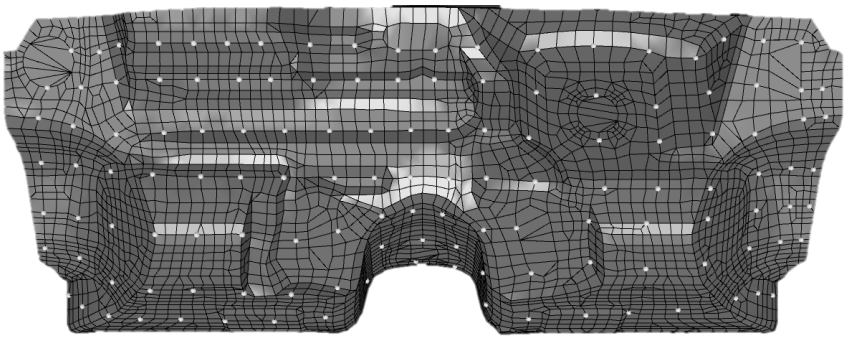

Figure 4.10.a Corresponding position of considered degrees of freedom on the complex structure

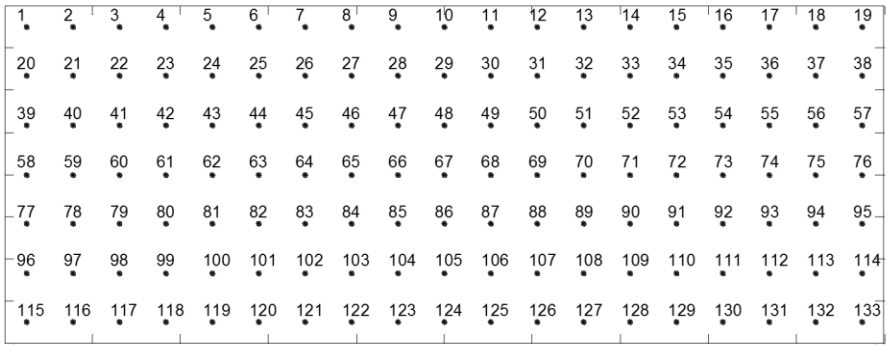

Figure 4.11.b Labeling of the set of considered degrees of freedom selected on the complex structure for the case study

In Fig.4.10, the obtained frequency responses for four different nodes are given. By utilizing the structural response of the panel with the corresponding acoustic response ($\mathbf{P_n}(\omega)$) , using Eq.4.11, Acoustic transfer vector ($\mathbf{ATV_{n,k}}(\omega)$) for the system is obtained.

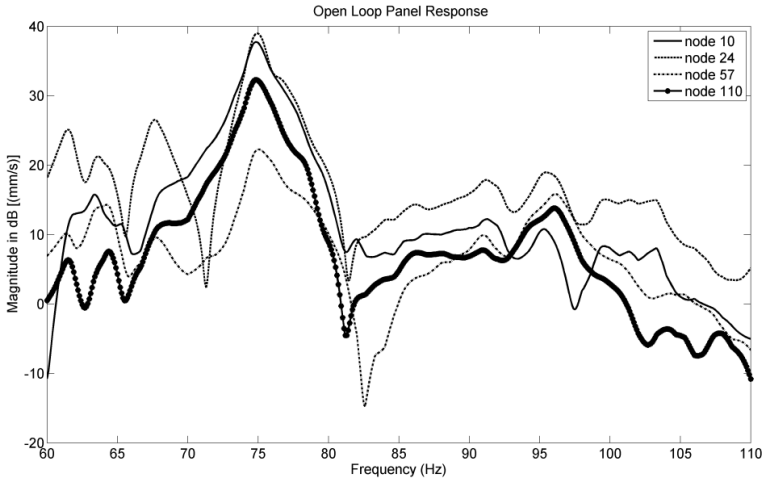

Figure 4.12 Open-loop frequency response at different nodes of the complex structure in the presence of external disturbance ($D_{k,j}(\omega)$)

4.5.5. Design Study for Active Structural Acoustic Controller

The motivation of the methodology is to optimize the sensor/actuator position and controller parameters for the maximization of noise suppression. To achieve this objective, the performance index (Eq.4.22) is maximized. This can be accomplished via the optimal location of the collocated sensor/actuator pair and optimal parameter settings of the controller. For this purpose, defined performance index β is calculated and optimized for various controller parameters and sensor/actuator locations. As described in Section 4.4.4, the vibro-acoustic system has the highest sound pressure levels at *75* Hz, so in performance index calculation, the particular frequency ranges for optimization bands, *low-range, mid-range* and *high-range* are selected as; *60-73, 73-80* and *80-90* Hz (Fig.4.8). Then, for each output degree of freedom on the structure, closed-loop vibration response of complex panel and contribution to sound pressure levels using the frequency response analysis (*refer to sec.3*) is obtained. For each output degree of freedom acoustic contribution is calculated via ATV and resultant closed-loop sound pressure level inside the cavity is obtained for the vibro-acoustic system. Then the performance index is obtained by evaluating defined

frequency bands. At the end of the optimization procedure, the maximum value of the performance index β is achieved for node 28 with proportional gain 120 and integral gain 10000. In Fig.4.11.a, the performance index variation with respect to the proportional and integral gains is presented.

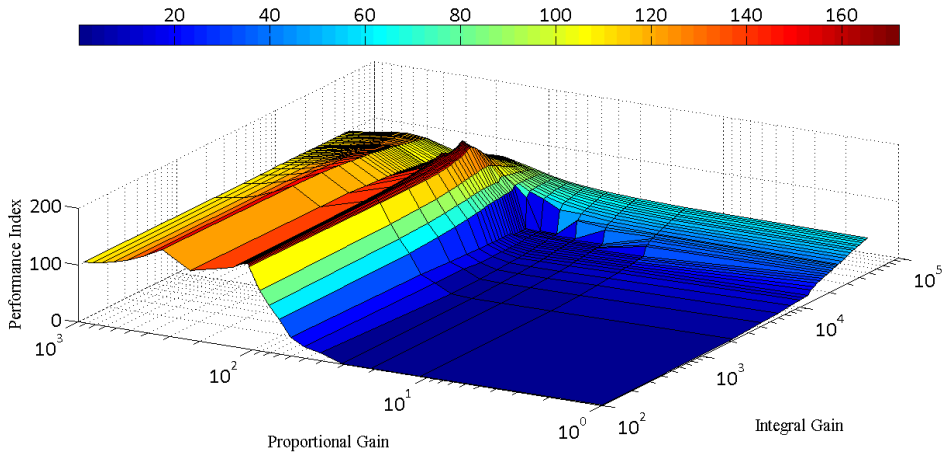

Figure 4.13 Variation of performance index with respect to the controller gains and actuator location

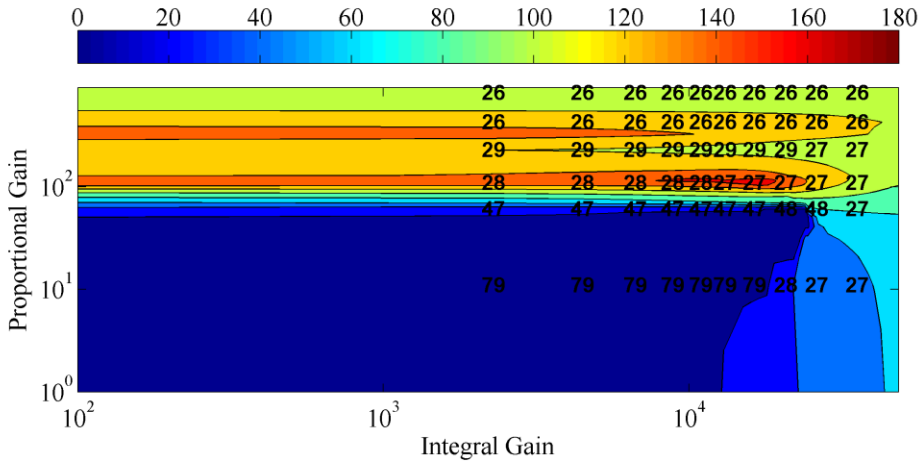

Figure 4.14 Variation of optimal actuator location with respect to the controller gains and performance index

The performance indices are considered for different controller parameters and sensor/actuator positions by the optimization algorithm. By conducting analysis, the

optimal location and optimal controller parameters for the highest performance index is determined. The performance index values versus controller parameters for the optimal actuator locations are shown in Fig.4.11.a. The optimization algorithm also computes best actuator position corresponding to the obtained performance indexes for each proportional and integral gain. The calculated optimal actuator locations corresponding to the proportional and integral gains are presented in Fig.4.11.b.

In Fig.4.12, an obtained sound pressure level for open and closed-loop cases is presented. By using optimized parameters for the controller and actuator location, the highest sound pressure level in 70-80 Hz band is suppressed around 23 dB without any augmentation at the other frequencies over the selected frequency bands. This shows that the design methodology and defined performance indexes is an efficient tool to optimize the location of controller sensor/actuator pair and control parameters for effective noise suppression.

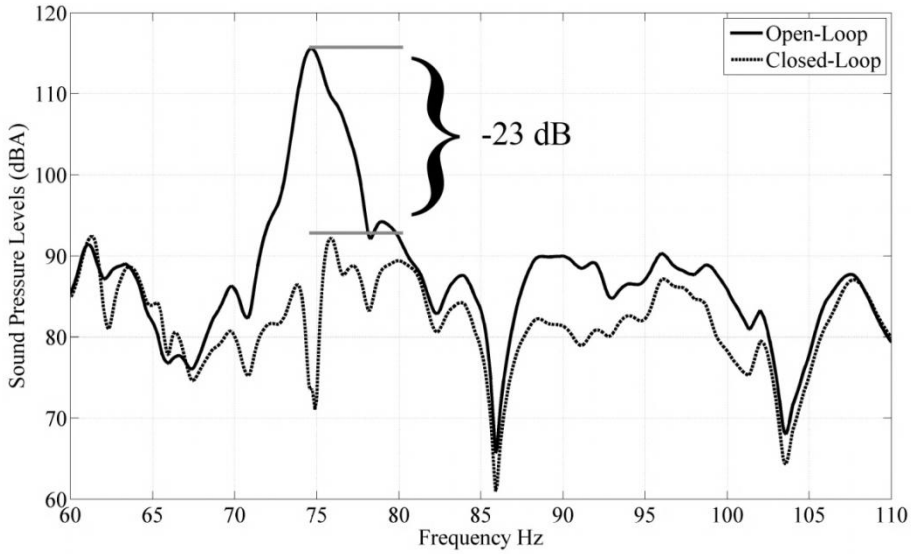

Figure 4.15 Open loop (solid line) and closed-loop (dashed line) sound pressure levels for the vibro-acoustic system

In other words, the total kinetic energy of the complex structure is reduced spatially by the designed controller; so that radiated vibration energy to the fluid medium is attenuated. The formula for the calculation of total kinetic energy density of the complex structure is

$$\boldsymbol{\eta_{oL}(\omega_p)_k = \frac{1}{2}\rho \sum_{k=1}^{n} \left[D_k(\omega_p)\right]^2}$$

$$\boldsymbol{\eta_{cL}(\omega_p)_k = \frac{1}{2}\rho \sum_{k=1}^{n} \left[\frac{P_{cl,n}(\omega_p)}{ATV_{n,k}(\omega_p)}\right]^2} \quad \textbf{(4.21)}$$

In this equation, $\boldsymbol{\eta}$ is the total kinetic energy density, k is the degree of freedom on the structure, ω_p is the particular frequency range selected for the suppression study and $\mathbf{D_k(\omega_p)}$ is the open loop velocities of the structure and closed loop surface velocities are obtained by dividing resultant sound pressure levels to the ATV. Eq.4.17 is used for calculation of the closed-loop vibration response at the sensor/actuator node ($k = m$), and at the other nodes ($k \neq m$) on the complex panel. Utilizing Eq.4.21, the total kinetic energy density of the complex structure is calculated for open-loop and closed-loop cases in the frequency range *60* Hz to *110* Hz. Fig.4.13 presents the kinetic energy densities. As can be seen from the figure, the total kinetic energy density is reduced by an amount of *48%* at the *70 – 80* Hz band without exciting any higher structural modes.

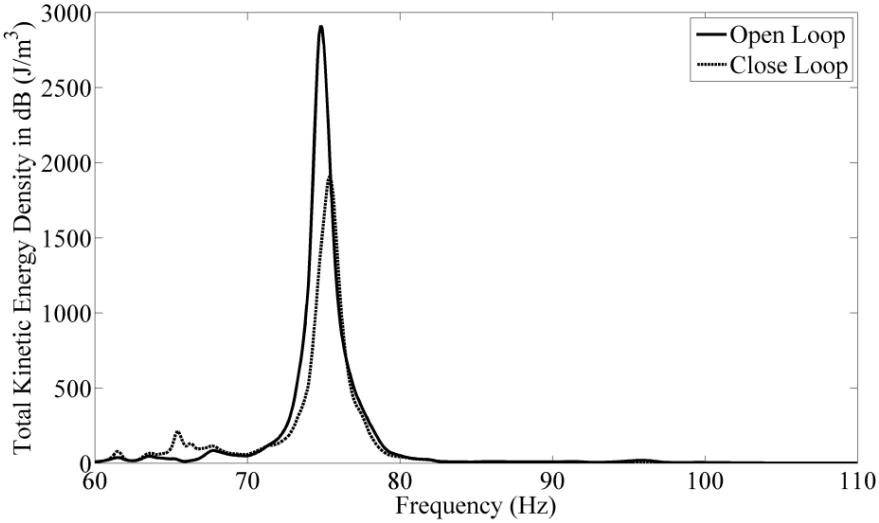

Figure 4.16 Open loop (solid line) and closed-loop (dashed line) total kinetic energy of the complex structure

To evaluate acoustic control effect over the entire complex panel structure, the distribution of change in noise radiations levels are evaluated at the output degrees of freedom *k*. Using Eq.4.15 and Eq.4.17, open and closed loop vibration responses for the each node are obtained and multiplied with corresponding ATV for noise radiation distribution on the panel. In Fig.4.14.a, for open-loop case, distribution of noise radiation from complex panel is presented for the frequency where highest sound pressure level is obtained. In Fig.4.14.b, radiation distribution for closed-loop case is presented for the same frequency. By implementing spatial considerations into the optimization algorithm, controller authority over the complex panel is maintained and therefore, sound pressure levels are suppressed (Fig.4.12)

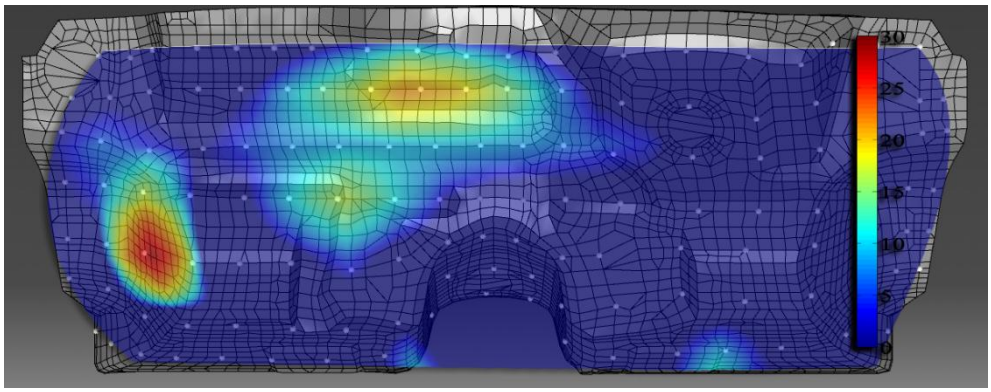

Figure 4.17 Noise radiation from panel surface for the open-loop case for the frequency of highest sound pressure level

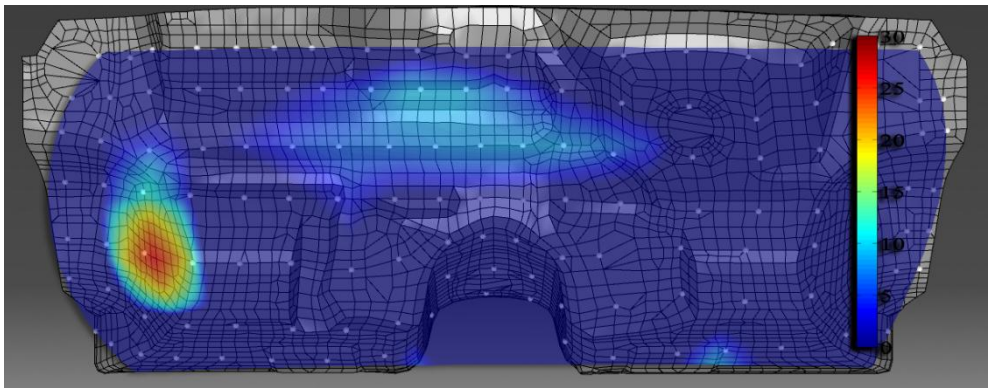

Figure 4.18 Noise radiation from panel surface for the closed-loop case for the frequency of highest sound pressure level

4.6. Conclusion

In this study, a novel methodology is developed for optimal placement of sensors/actuators and parameter tuning of the controllers. The applicability and effectiveness of the methodology is demonstrated with a vibro-acoustic system involving a complex structure which is a part of a vehicle model. The vibro-acoustic model of the structure is used for obtaining the acoustic and structural frequency response. In order to achieve effective acoustic suppression performance indices are defined for different frequency bands and used simultaneously for the optimization of the sensor/actuator position as well as the controller parameters. By implementing controller architecture in finite element simulations, the vibration of the complex structure is suppresses spatially. By comparing controller active and inactive cases, the acoustic suppression performance of the controller and the effectiveness of the developed methodology is also presented.

Chapter 5

DISCUSSION & CONCLUSION

Shell structures are commonly used in the automotive, aerospace and marine applications and vibrations of these structures can cause malfunction of the whole system or failure of certain components. In this thesis, new design methodologies for local and global vibration control and active structural acoustic control are developed for 3D shell structures. The methodology is developed on a simple plate-like structure then it is developed to make the methodology applicable on complex 3D structures with complex boundary conditions.

The main conclusions of this thesis can be summarized as follows; in chapter 2, finite element models of the flexible plate and the piezoelectric actuator patch are built together and verified experimentally. Then, the optimal location of collocated piezoelectric actuator and velocity sensor on the smart plate is investigated using the modal controllability measure (see Figures 2.10-2.11). After placing the disturbance and actuator patch on the smart plate, the velocity feedback controller is designed and implemented numerically and experimentally. Finally, the simulation and experimental results are compared for vibration suppression of the smart plate and it is shown that the simulated closed-loop model accurately estimates vibration attenuation levels obtained in experiments. Although the controller was designed for the first resonance frequency, it was observed that the sixth mode of the smart plate was also suppressed as it was predicted by the modal controllability measure. Furthermore, the controller didn’t excite the higher resonance frequency modes of the smart plate.. Based on the knowledge and experience obtained in

this section, vibration suppression system design for complex structures with complex boundary conditions is studied in the following sections.

In chapter 3, we developed a novel methodology for optimal placement of sensors/actuators and parameter tuning of the controller for a complex 3D geometry structure. The optimization studies are carried out to increase controller performance considering local and global panel vibrations. The objective of the local vibration control is to reduce vibration energy at the sensor location whereas the objective of the global vibration control is to reduce vibration over the entire structure. In order to achieve effective vibration suppression of the structure, local and global performance indices are defined and used for the optimization of sensor/actuator position as well as the controller parameters. A vehicle panel is used to demonstrate the developed methodologies. The finite element model of the structure is used for frequency response analysis. Then, local and global optimization studies are carried out for positioning the sensor/actuator pair and parameter tuning of the controller. By comparing controller active and inactive cases, the vibration suppression performance of the controller is demonstrated locally and globally. Optimal placement locations are presented with contour plots on the panel surface (Fig.3.11, Fig.3.14). For the local vibration control case, upper mid-section and right mount weld location are obtained as optimal locations for suppressing high amplitude vibrations around 75 Hz. For the global vibration control case, same regions are obtained as possible placement locations but the applicable region in global case is obtained in a more narrow area then the local case. Also at the top left section of the panel, for global case, negative performance index for optimization is obtained indicating amplification instead of suppression. These differences are expected due to additional global considerations into optimization algorithm. By utilizing the developed optimization algorithm (Fig.3.5), global panel vibration energy is also reduced around 91% (Fig.3.13). For the same frequency, for optimal case, panel vibration energy only reduced around 10% for local case. This result is

also presented in Fig.3.15 with a color bar plot. With the obtained results, it can be concluded that for effective vibration suppression, considering only local sensor information is not sufficient. The structure should be considered globally to obtain effective vibration suppression. Also obtained results indicate that the developed optimization method is an effective tool for the design of a spatial active structural control system and is applicable to complex 3D shaped structures with complex boundary conditions.

In chapter 4, the developed methodology for global optimization is used to develop a design methodology for an active structural acoustic controller (ASAC) on a complex 3D geometry. The reduction of noise radiation from vibrating surfaces requires spatial control, since all wetted areas contribute energy transfer from structure to fluid medium. In previous chapter, it is shown that on a complex 3D surface, a well -placed collocated sensor and actuator pair with optimized tuning can suppress the vibration spatially on a complex shaped panel. Therefore, by reducing panel vibrations, noise radiation into acoustic medium can be reduced. For acoustic controller, generated noise due panel vibrations inside an acoustic cavity is considered in the global optimization algorithm. The actuator/sensor position and control parameters are optimized based on the performance indices that include noise suppression performance inside an enclosed cavity. Position and controller parameter optimization are based on the noise reduction levels for three different frequency bands. A vibro-acoustic model of a vehicle is used to demonstrate the developed methodology. Vibro-acoustic analyses are conducted and the most influential panel for the sound pressure level inside the passenger cabin is identified. This panel's frequency responses are obtained from the FE model and optimization algorithm is used to determine effective actuator/sensor location on the panel and controller gains (Fig.4.10). By utilizing the algorithm, panel vibration energy is reduced around 48% (Fig.4.13) and sound pressure levels inside the passenger cabin is reduced 23 dBA (Fig.4.12). Also noise radiation from complex panel is reduced considerably with control implementation (Fig.4.14). With the

obtained results it can be concluded that the proposed methodology can be successfully applied for the structures that have complex shape and boundary conditions for noise suppression.

As a future topic, multiple input multiple output (MIMO) controller optimization can be studied. With MIMO approach more control authority over the entire structure could be increased. However, consideration of MIMO system will require a different approach for estimation of the closed-loop dynamics of the system since frequency response of system under multiple actuators should be considered in the design.

Another future study would be to adapt developed methodology to an experimental system. With an experimental demonstration, it is possible to see the efficiency of the developed methodologies in real life applications. Instabilities in frequency responses and uncertainties in systems and measurements are the issues that should be considered which may affect the applicability of the proposed methodologies.

For the optimization procedure, different algorithms like neural-network can be used to increase the optimization procedure, performance and decrease convergence time. Adaptive controllers may be also considered instead of the P-I controller which may further increase suppression performance of the controller.

BIBLIOGRAPHY

1. Kozek, M., et al., *Vibration damping of a flexible car body structure using piezo-stack actuators.* Control Engineering Practice, 2011. **19**(3): p. 298-310.
2. Bohn, C., et al., *Active control of engine-induced vibrations in automotive vehicles using disturbance observer gain scheduling.* Control Engineering Practice, 2004. **12**(8): p. 1029-1039.
3. Song, C.K., et al., *Active vibration control for structural–acoustic coupling system of a 3-D vehicle cabin model.* Journal of Sound and Vibration, 2003. **267**(4): p. 851-865.
4. de Oliveira, L.P.R., et al., *Concurrent mechatronic design approach for active control of cavity noise.* Journal of Sound and Vibration, 2008. **314**(3–5): p. 507-525.
5. Gonzalez, A., et al., *Sound quality of low-frequency and car engine noises after active noise control.* Journal of Sound and Vibration, 2003. **265**(3): p. 663-679.
6. Alkhatib, R. and M.F. Golnaraghi, *Active Structural Vibration Control : A Review.* The Shock And Vibration Digest, 2008.
7. Gupta, V., M. Sharma, and N. Thakur, *Optimization Criteria for Optimal Placement of Piezoelectric Sensors and Actuators on a Smart Structure: A Technical Review.* Journal of Intelligent Material Systems and Structures, 2010. **21**(12): p. 1227-1243.
8. Hamdan, a.M.a. and a.H. Nayfeh, *Measures of modal controllability and observability for first- and second-order linear systems.* Journal of Guidance, Control, and Dynamics, 1989. **12**(3): p. 421-428.
9. Bin, L., et al., *Maximal Modal Force Rule for Optimal Placement of Point Piezoelectric Actuators for Plates.* Journal of Intelligent Material Systems and Structures, 2000. **11**(7): p. 512-515.

10. Jingjun, Z., et al. *Study of the Optimal Location and Size of Piezoelectric Actuator in Smart Structures*. in *Informatics in Control, Automation and Robotics, 2009. CAR '09. International Asia Conference on*. 2009.
11. Quek, S.T., S.Y. Wang, and K.K. Ang, *Vibration Control of Composite Plates via Optimal Placement of Piezoelectric Patches.* Journal of Intelligent Material Systems and Structures, 2003. **14**(4-5): p. 229-245.
12. Halim, D. and S.O. Reza Moheimani, *An optimization approach to optimal placement of collocated piezoelectric actuators and sensors on a thin plate.* Mechatronics, 2003. **13**(1): p. 27-47.
13. Yaowen, Y. and Z. Lei, *Optimal excitation of a rectangular plate resting on an elastic foundation by a piezoelectric actuator*. Smart Materials and Structures, 2006. **15**(4): p. 1063.
14. Demetriou, M.A. *A numerical algorithm for the optimal placement of actuators and sensors for flexible structures*. in *American Control Conference, 2000. Proceedings of the 2000*. 2000.
15. Fahroo, F. and W. Yun. *Optimal location of piezoceramic actuators for vibration suppression of a flexible structure*. in *Decision and Control, 1997., Proceedings of the 36th IEEE Conference on*. 1997.
16. Li, Y., J. Onoda, and K. Minesugi, *SIMULTANEOUS OPTIMIZATION OF PIEZOELECTRIC ACTUATOR PLACEMENT AND FEEDBACK FOR VIBRATION SUPPRESSION.* Acta Astronautica, 2002. **50**(6): p. 335-341.
17. Tae-Woo, K. and K. Ji-Hwan, *Optimal distribution of an active layer for transient vibration control of a flexible plate.* Smart Materials and Structures, 2005. **14**(5): p. 904.

18. Kumar, K.R. and S. Narayanan, *Active vibration control of beams with optimal placement of piezoelectric sensor/actuator pairs.* Smart Materials and Structures, 2008. **17**(5): p. 055008.
19. Aoki, Y., P. Gardonio, and S.J. Elliott, *Modelling of a piezoceramic patch actuator for velocity feedback control.* Smart Materials and Structures, 2008. **17**(1): p. 015052.
20. Baudry, M., P. Micheau, and A. Berry, *Decentralized harmonic active vibration control of a flexible plate using piezoelectric actuator-sensor pairs.* The Journal of the Acoustical Society of America, 2006. **119**(1): p. 262-277.
21. Preumont, A. and K. Seto, *Active Control of Structures*. 2008: John Wiley & Sons.
22. Preumont, A., *Mechatronics: Dynamics of Electromechanical And Piezoelectric Systems*. 2006: Springer.
23. Behrens, S., A.J. Fleming, and S.O.R. Moheimani, *A broadband controller for shunt piezoelectric damping of structural vibration.* Smart Materials and Structures, 2003. **12**(1): p. 18.
24. Buaka, P., P. Masson, and P. Micheau. *Experimental validation of a semi-active friction control device*. 2004. San Diego, CA, USA: SPIE.
25. Gu, Y., et al., *Experiments on Active Control of Plate Vibration Using Piezoelectric Actuators and Polyvinylidene Fluoride (PVDF) Modal Sensors.* Journal of Vibration and Acoustics, 1994. **116**(3): p. 303-308.
26. Donadon, L.V., et al., *Comparing a filtered-X LMS and an H2 controller for the attenuation of the sound radiated by a panel.* Proc. of the ISMA. Leuven., 2006.
27. Sohn, J.W., S.-B. Choi, and H.S. Kim, *Vibration control of smart hull structure with optimally placed piezoelectric composite actuators.* International Journal of Mechanical Sciences, 2011. **53**(8): p. 647-659.

28. Mahmoodi, S.N., M.R. Aagaah, and M. Ahmadian. *Active vibration control of aerospace structures using a modified Positive Position Feedback method*. in *American Control Conference, 2009. ACC '09.* 2009.
29. Chantalakhana, C. and R. Stanway, *Active constrained layer damping of plate vibrations: a numerical and experimental study of modal controllers.* Smart Materials and Structures, 2000. **9**(6): p. 940.
30. Boudaoud, H., et al., *Damping analysis of beams submitted to passive and active control.* Engineering Structures, 2009. **31**(2): p. 322-331.
31. Hau, L.C. and E.H.K. Fung, *Effect of ACLD treatment configuration on damping performance of a flexible beam.* Journal of Sound and Vibration, 2004. **269**(3–5): p. 549-567.
32. Moon, S.H. and S.J. Kim, *Suppression of nonlinear composite panel flutter with active/passive hybrid piezoelectric networks using finite element method.* Composite Structures, 2003. **59**(4): p. 525-533.
33. Makihara, K., J. Onoda, and K. Minesugi, *Comprehensive Assessment of Semi-Active Vibration Suppression Including Energy Analysis.* Journal of Vibration and Acoustics, 2007. **129**(1): p. 84-93.
34. Yonghui Zhao, *Vibration Suppression of a Quadrilateral Plate Using Hybrid Piezoelectric Circuits.* Journal of Vibration and Control, 2010. **16**(5): p. 701-720.
35. Qiu, J. and M. Haraguchi, *Vibration Control of a Plate using a Self-sensing Piezoelectric Actuator and an Adaptive Control Approach.* Journal of Intelligent Material Systems and Structures, 2006. **17**(8-9): p. 661-669.
36. Young-Hun, L., *Finite-element simulation of closed loop vibration control of a smart plate under transient loading.* Smart Materials and Structures, 2003. **12**(2): p. 272.

37. Dozio, L. and G.L. Ghiringhelli, *Experiments on active vibration and noise reduction of a panel using predictive techniques.* Structural Control and Health Monitoring, 2008. **15**(1): p. 1-19.

38. Elliott, S.J., et al., *Active vibroacoustic control with multiple local feedback loops.* The Journal of the Acoustical Society of America, 2002. **111**(2): p. 908-915.

39. Bianchi, E., P. Gardonio, and S.J. Elliott, *Smart panel with multiple decentralized units for the control of sound transmission. Part III: control system implementation.* Journal of Sound and Vibration, 2004. **274**(1–2): p. 215-232.

40. Ma, K. and J. Melcher, *Adaptive Control of Structural Acoustics using Intelligent Structures with Embedded Piezoelectric Patches.* Journal of Vibration and Control, 2003. **9**(11): p. 1285-1302.

41. de Oliveira, L.P.R., et al., *Active sound quality control of engine induced cavity noise.* Mechanical Systems and Signal Processing, 2009. **23**(2): p. 476-488.

42. Gardonio, P., E. Bianchi, and S.J. Elliott, *Smart panel with multiple decentralized units for the control of sound transmission. Part II: design of the decentralized control units.* Journal of Sound and Vibration, 2004. **274**(1–2): p. 193-213.

43. Gardonio, P., E. Bianchi, and S.J. Elliott, *Smart panel with multiple decentralized units for the control of sound transmission. Part I: theoretical predictions.* Journal of Sound and Vibration, 2004. **274**(1–2): p. 163-192.

44. Hurlebaus, S., U. Stöbener, and L. Gaul, *Vibration reduction of curved panels by active modal control.* Computers & Structures, 2008. **86**(3–5): p. 251-257.

45. Mauro, C., *Active control of sound radiated by a submarine in bending vibration.* Journal of Sound and Vibration, 2011. **330**(4): p. 615-624.

46. StÖBener, U.W.E. and L. Gaul, *ACTIVE VIBRATION CONTROL OF A CAR BODY BASED ON EXPERIMENTALLY EVALUATED MODAL PARAMETERS.* Mechanical Systems and Signal Processing, 2001. **15**(1): p. 173-188.

47. Boz, U., et al., *Analog Velocity Feedback Controller for Effective Vibration Suppression and Sound Attenuation*, in *Conference On Smart Materials, Adaptive Structures And Intelligent Systems, SMASIS 2011*. 2011: Phoenix, Arizona.

48. Zilletti, M., S.J. Elliott, and P. Gardonio, *Self-tuning control systems of decentralised velocity feedback.* Journal of Sound and Vibration, 2010. **329**(14): p. 2738-2750.

49. Zilletti, M., et al., *Experimental implementation of a self-tuning control system for decentralised velocity feedback.* Journal of Sound and Vibration, 2012. **331**(1): p. 1-14.

50. Barrault, G., D. Halim, and C. Hansen, *High frequency spatial vibration control using method.* Mechanical Systems and Signal Processing, 2007. **21**(4): p. 1541-1560.

51. Barrault, G., et al., *High frequency spatial vibration control for complex structures.* Applied Acoustics, 2008. **69**(11): p. 933-944.

52. Barrault, G., et al., *Optimal truncated model for vibration control design within a specified bandwidth.* International Journal of Solids and Structures, 2007. **44**(14–15): p. 4673-4689.

53. Dunant, H., *Structural vibration control with spatially varied disturbance input using a spatial method.* Mechanical Systems and Signal Processing, 2007. **21**(6): p. 2496-2514.

54. Bein, T., et al., *Smart interfaces and semi-active vibration absorber for noise reduction in vehicle structures.* Aerospace Science and Technology, 2008. **12**(1): p. 62-73.

55. de Oliveira, L.P.R., et al., *NEX-LMS: A novel adaptive control scheme for harmonic sound quality control.* Mechanical Systems and Signal Processing, 2010. **24**(6): p. 1727-1738.

56. Misol, M., S. Algermissen, and H.P. Monner, *Experimental investigation of different active noise control concepts applied to a passenger car equipped with an active windshield.* Journal of Sound and Vibration, 2012. **331**(10): p. 2209-2219.
57. Halim, D., G. Barrault, and B.S. Cazzolato, *Active control experiments on a panel structure using a spatially weighted objective method with multiple sensors.* Journal of Sound and Vibration, 2008. **315**(1–2): p. 1-21.
58. Fenik, S. and L. Starek, *Optimal PI Controller with Position Feedback for Vibration Suppression.* Journal of Vibration and Control, 2010. **16**(13): p. 2023-2034.
59. Ikeda, T., *Fundamentals of Piezoelectricity*. 1996: Oxford University Press.
60. *IEEE Standard on Piezoelectricity.* ANSI/IEEE Std 176-1987, 1988: p. 0_1.
61. Vincent, P., *Finite Element Modelling of Piezoelectric Active Structures*, in *Faculty of Applied Sciences,Department of Mechanical Engineering and Robotics,*. 2000-2001, Universite Libre de Bruxelles: Bruxelles. p. 125.
62. Noliac-Ceramics. 2011 [cited 2012 25 April]; Available from: http://www.noliac.com/Material_characteristics_-143.aspx.
63. Emery, J. (1997) *Piezoelectricity*. 71.
64. ISO, *Quantities and units* in *Part 6: Electromagnetism*. 2008. p. 58.
65. Physik-Instrumente(PI)GmbH&Co. 1996-2012 [cited 2012 10 May]; Available from: http://www.physikinstrumente.com/en/index.php.
66. Polytech. 2012 [cited 2012 05 May]; Available from: http://www.polytec.com/us/products/vibration-sensors/single-point-vibrometers/complete-systems/pdv-100-portable-digital-vibrometer/.
67. O1dB-metravib. 2012 [cited 2012 10 May]; Available from: http://www.01db-metravib.com/nvh-instruments.477/pro-120-real-time-analyser-4-channels-netdb-daq-solution.511/?L=1.

68. Physik-Instrumente(PI)GmbH&Co. 2012 [cited 2012 10 May]; Available from: http://www.physikinstrumente.com/en/products/prdetail.php?sortnr=602050.

69. National-Instruments-Corporation. 2012 [cited 2012 10 May]; Available from: http://sine.ni.com/nips/cds/view/p/lang/en/nid/14136.

70. Ewins, D.J., *Modal testing: theory, practice, and application*. 2000: Research Studies Press.

71. Fuller, C.R., S.J. Elliott, and P.A. Nelson, *Active Control of Vibration*. 1997: Academic Press.

72. Sumeet, S.A., J.F. Andrew, and S.O.R. Moheimani, *Integral resonant control of collocated smart structures.* Smart Materials and Structures, 2007. **16**(2): p. 439.

73. Desmet, W. and D. Vandepitte, *Finite Element Modeling for Acoustics*, in *LMS Numerical Acoustics Theoretical Manual*. p. 37-85.

74. Tournour, M., *ATV Concept and ATV based applications*, in *LMS Numerical Acoustics Theoretical Manual*. p. 127-139.

75. Citarella, R., L. Federico, and A. Cicatiello, *Modal acoustic transfer vector approach in a FEM–BEM vibro-acoustic analysis.* Engineering Analysis with Boundary Elements, 2007. **31**(3): p. 248-258.